STATISTICAL ENERGY ANALYSIS FOR DESIGNERS

PART II. THE ENGINEERING APPLICATION

CAMBRIDGE COLLABORATIVE

PREPARED FOR
AIR FORCE FLIGHT DYNAMICS LABORATORY

SEPTEMBER 1974

NOTICE

When Government drawings, specifications, or other data are
for any purpose other than in connection with a definitely
ted Government procurement operation, the United States
rnment thereby incurs no responsibility nor any obligation
soever; and the fact that the government may have formulated,
ished, or in any way supplied the said drawings, specifications,
ther data, is not to be regarded by implication or otherwise
n any manner licensing the holder or any other person or
oration, or conveying any rights or permission to manufacture,
or sell any patented invention that may in any way be related
to.

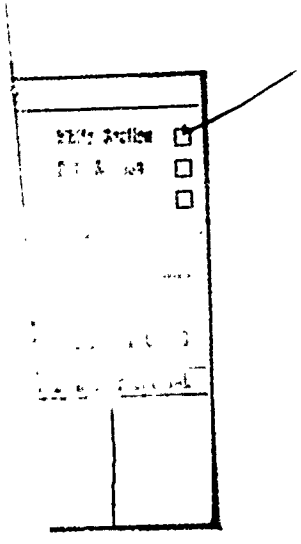

s of this report should not be returned unless return
d by security considerations, contractual obligations,
on a specific document.

21 January 1975 — 150

UNCLASSIFIED
Security Classification

AD A006414

DOCUMENT CONTROL DATA - R & D

(Security classification of title, body of abstract and indexing annotation must be entered when the overall report is classified)

1. ORIGINATING ACTIVITY (Corporate author)	2a. REPORT SECURITY CLASSIFICATION
Cambridge Collaborative Cambridge, Massachusetts	UNCLASSIFIED
	2b. GROUP N/A

3. REPORT TITLE

STATISTICAL ENERGY ANALYSIS FOR DESIGNERS
PART II. The Engineering Application

4. DESCRIPTIVE NOTES (Type of report and inclusive dates)

Final Report - April 1972 to December 1973

5. AUTHOR(S) (First name, middle initial, last name)

Richard H. Lyon and Huw G. Davies

6. REPORT DATE	7a. TOTAL NO. OF PAGES	7b. NO. OF REFS
September 1974	~~207~~ 212	43

8a. CONTRACT OR GRANT NO	9a. ORIGINATOR'S REPORT NUMBER(S)
F33615-72-C-1196 b. PROJECT NO. 1370 c. Task No. 137002 d.	Cambridge Collaborative 7351 9b. OTHER REPORT NO(S) (Any other numbers that may be assigned this report) AFFDL-TR-74-56 , Part II

10. DISTRIBUTION STATEMENT

Approved for public release; distribution unlimited.

11. SUPPLEMENTARY NOTES	12. SPONSORING MILITARY ACTIVITY
	Air Force Flight Dynamics Laboratory Wright-Patterson AFB, Ohio 45433

13. ABSTRACT

This report is concerned with the practical applications of Statistical Energy Analysis (SEA) to the prediction of vibration in high speed flight vehicles. The procedures of estimation, based on the theory presented in Part I, are presented in Section I of this Part II of the report. We describe how energy estimates are used to infer stress, displacement, or other dynamical variables. Obtaining the energy estimates is described next, and the SEA parameters - mode count, loss factor, and coupling loss factor are introduced. A discussion of SEA modeling completes Section I. Experimental and analytical procedures for evaluating the SEA parameters are presented in Section II. In Section III, an example of the use of SEA to predict the vibration of an equipment shelf in a reentry vehicle is described in some detail.

DD FORM 1 NOV 65 1473

UNCLASSIFIED
Security Classification

14. KEY WORDS	LINK A		LINK B		LINK C	
	ROLE	WT	ROLE	WT	ROLE	WT
Response Prediction, Statistical Energy Analysis, Preliminary Design, Environmental Estimation						

*U.S.Government Printing Office: 1974 — 657-017/338

STATISTICAL ENERGY ANALYSIS FOR DESIGNERS

PART II. THE ENGINEERING APPLICATION

Richard H. Lyon
Huw G. Davies
Cambridge Collaborative

FOREWORD

The research described in this report was performed by Cambridge Collaborative, Cambridge, Massachusetts for the Aerospace Dynamics Branch, Vehicle Dynamics Division, Air Force Flight Dynamics Laboratory, Wright-Patterson Air Force Base, Ohio under Contract F33615-72-C-1196, Project No. 1370, "Dynamic Problems in Flight Vehicles," and Task No. 137002 "Flight Vehicle Vibration Control." Mr. A. R. Basso and later Mr. J. D. Willenborg were the Project Engineers at the Air Force Flight Dynamics Laboratory.

Part I of this report covers the basic theory of statistical energy analysis methods while Part II covers the application of statistical energy analysis.

The report covers work conducted from April 1972 to December 1973. Cambridge Collaborative report number is 73-1.

This report was released by the author in December 1973.

This technical report has been reviewed and approved.

WALTER J. MYKYTOW
Asst. for Research & Technology
Vehicle Dynamics Division

ABSTRACT

This report is concerned with the practical applications of Statistical Energy Analysis (SEA) to the prediction of vibration in high speed flight vehicles. The procedures of estimation, based on the theory presented in Part I, are presented in Section I of this Part II of the report. We describe how energy estimates are used to infer stress, displacement, or other dynamical variables. Obtaining the energy estimates is described next, and the SEA parameters - mode count, loss factor, and coupling loss factor are introduced. A discussion of SEA modeling completes Section I. Experimental and analytical procedures for evaluating the SEA parameters are presented in Section II. In Section III, an example of the use of SEA to predict the vibration of an equipment shelf in a reentry vehicle is described in some detail.

TABLE OF CONTENTS

		Page
INTRODUCTION		1
SECTION I - THE USE OF SEA IN PRELIMINARY DESIGN		3
CHAPTER 5.	RESPONSE ESTIMATION DURING PRELIMINARY DESIGN	3
CHAPTER 6.	PROCEDURES OF STATISTICAL ENERGY ANALYSIS	5
	6.0. Introduction	5
	6.1. Modeling the System	5
	6.2. Evaluating the Parameters	6
	6.3. Solving for the Energy Distribution	8
	6.4. Evaluating Response from Energy Estimate	9
CHAPTER 7.	ESTIMATION OF DYNAMICAL RESPONSE	13
	7.0. Introduction	13
	7.1. Representations of the Energy Estimate	13
	7.2. Conversion from Energy to Other Variables	15
	7.3. Response Concentration Factors	20
	7.4. Variance in Estimation Intervals	24
	7.5. Using Variance to Calculate Safety Factors	27
CHAPTER 8.	ESTIMATING THE ENERGY OF VIBRATION	37
	8.0. Introduction	37

TABLE OF CONTENTS (CONTINUED)

		Page
8.1.	How the Overall System is Described	37
8.2.	Alternative Form of the Energy Equations	44
8.3.	Parameter Evaluation Using the Energy Equations	45
8.4.	Useful Approximations and Simplifications	46
8.5.	Conclusions	49
CHAPTER 9.	THE MEANING AND USE OF SEA PARAMETERS	53
9.0.	Introduction	53
9.1.	Dissipation Parameters	53
9.2.	Power Transfer Parameters	55
9.3.	Modal Count of Subsystems	58
9.4.	Input Power Prediction	61
9.5.	Conclusion	64
CHAPTER 10.	MODELING THE SYSTEM	67
10.0.	Introduction	67
10.1.	Principles of SEA Modeling - Definition of Subsystems	67
10.2.	Identifying and Evaluating the Coupling Between Subsystems	69
10.3.	Subsystems Within a Section of the System	71
10.4.	Discussion	72

TABLE OF CONTENTS (CONTINUED)

		Page
SECTION II -	EVALUATION OF SEA PARAMETERS.....	79
CHAPTER 11.	PARAMETER EVALUATION - THE ENGINEERING BASE OF SEA.....	79
11.0.	Introduction.....	79
11.1.	What Are the SEA Parameters.....	80
11.2.	How Accurately Can (Must) We Know SEA Parameters?.....	81
11.3.	How To Use This Part Of The Report.....	82
CHAPTER 12.	THE DAMPING PARAMETER.....	83
12.0.	Introduction.....	83
12.1.	Measurement of Damping.....	84
12.2.	Damping Values for Materials.....	86
12.3.	Damping of Built-Up Structures....	89
12.4.	The Damping of Add-On Systems.....	91
CHAPTER 13.	EVALUATING THE MODE COUNT.....	111
13.0.	Introduction.....	111
13.1.	Experimental Procedures for Determining Mode Count.....	112
13.2.	Mode Counts of Acoustical Subsystems.....	113
13.3.	Flat Structures.....	114
13.4.	Mode Count of Curve Structures....	116
13.5.	One-Dimensional Structures.....	121

TABLE OF CONTENTS (CONTINUED)

		Page
CHAPTER 14.	EVALUATING COUPLING LOSS FACTORS.....	127
14.0.	Introduction.....	127
14.1.	Coupling Between Acoustical Spaces.....	128
14.2.	Coupling Between Structures and Acoustical Spaces.....	132
14.3.	Coupling Between Structural Subsystems.....	136
SECTION III -	EXAMPLE OF RESPONSE ESTIMATION.....	151
CHAPTER 15.	VIBRATION OF A REENTRY VEHICLE	151
15.0.	Introduction.....	151
15.1.	Modeling the Vehicle.....	151
15.2.	Modal Density.....	153
15.3.	Coupling Loss Factor.....	157
15.4.	Prediction of the Vehicle Skin Vibration Levels.....	168
15.5.	Vibration Levels of the Instrument Shelf.....	174
15.6.	Confidence Limits.....	178
REFERENCES.....		199

LIST OF ILLUSTRATIONS

Figure		Page
6.1	An SEA Model of the System.....	11
7.1.	Interpretation of Energy in Frequency Band as Area Under Spectral Density Curve.....	29
7.2.	Standard Center Frequencies for One-Third and Full Octave Bands.....	29
7.3.	Typical Band Levels Spectrum of Vibrational Energy.....	30
7.4.	Comparisons of Band Level Response Spectra for Different Variables.....	30
7.5.	Nomograph for Conversion of Displacement Related Vehicles.....	31
7.6.	Spatial Distribution of Displacement Assumed in Bolotin "Dynamic Edge Effect" Model.....	32
7.7.	Regions of Edge and Interior Stress Dominance In Plates with Rotationally "Clamped-Like" Edges ($\alpha_r > \alpha_1$).....	33
7.8.	Regions of Edge and Interior Stress Dominance In Plates with Rotationally "Free-Like" Edges ($\alpha_r > \alpha_1$).....	34
7.9.	Effect of Excitation Bandwidth of Response Variance.....	35
7.10.	Form of Response Probability Density.....	35
7.11.	Graph of"Safety Factor"r Against Normalized Variance.....	36
7.12.	Graph of Bracketing Interval.....	36

LIST OF ILLUSTRATIONS (CONTINUED)

Figure		Page
8.1.	An SEA Model of System Containing N Subsystems.....	51
8.2.	SEA Model of Circuit Board in Computer Frame with Parameters for the 250 Hz Octave Band.....	52
9.1.	Various Forms of Applied Damping.....	65
9.2.	Equipment Shelf Made from 3/16 in. Aluminum Plate.....	65
9.3.	The Impedance of the Structure and the Internal Impedance of the Exciter are shown in (a). The apparent force spectrum based on the input current and shaker characteristics are shown in (b). Also in (b) are shown the actual force spectrum and its "flat" equivalent based on the impedance diagrams in (a).....	66
10.1.	Diagram of Airborne Computer Assembly.....	75
10.2.	Major Sections of the System Shown in Figure 10.1.....	75
10.3.	System of Figure 10.2. with Power Transfer through Interfaces Shown.....	76
10.4.	Modifications in Diagram of Figure 10.3. Due to Non Resonant Motions of Frame and Shell.....	76
10.5.	The SEA Model of the System of Figure 10.1. with a Greater Number of Modal Groups and Interactions Represented.....	77

LIST OF ILLUSTRATIONS (CONTINUED)

Figure		Page
12.1.	Experimental Arrangement for Measuring Frequency Response of a Structure.....	97
12.2.	Response Curve for a Single Mode.....	97
12.3.	Response Curve for a System with High Modal Overlap.....	98
12.4.	Arrangement for Determining Damping from Input Power and Average Response.....	98
12.5.	Arrangement for Measuring Decay Rate of Structural Vibrations.....	99
12.6.	Simultaneous Decay of Two Modes Having Slightly Different Natural Frequencies.....	99
12.7.	Loss Factors and Elastic Moduli for Various Classes of Materials (Adapted from Ref. 3).....	100
12.8.	Effects of Temperature and Frequency in the Transition Region on the Storage Modulus and Loss Coefficient of Buna N Rubber.....	100
12.9.	Dependence of Loss Factor on Ratio of Gap Between Plate and Beam to Viscous Boundary Layer Thickness.....	101
12.10.	Dependence of Air Pumping Loss Factor on Air Pressure and Frequency: Gap thickness 5×10^{-3} cm.....	102
12.11.	Typical Free-Layer Configurations.....	103
12.12a.	Composite loss factor vs. frequency for Spaced Damping and Conventional Damping, applied to a 12' x 2" x0.25" Solid Steel. Damping materials and coverage the same in both cases.....	104

LIST OF ILLUSTRATIONS (CONTINUED)

Figure		Page
12.12b.	Composite Loss Factor Vs. Frequency for Spaced Damping and Conventional Damping, Applied to a 0" x 1/8" Square Tubular Beam. Damping materials and coverage the same in both cases.....	104
12.13.	Systems with Viscoelastic Layers.....	105
12.14.	Composite Loss Factor of Constrained Damping Layer on Base Structure.....	106
12.15.	Configuration of Constrained Layer Composite.....	106
12.16.	Typical Values of Structural Parameter.....	107
12.17.	Maximum Damping of Constrained Layers Vs. Material Loss Factor.....	108
12.18.	Comparison of Free and Constrained-Layer Treatments on Steel Plates. Subscripts 1 and 2 Refer to Plate and Damping Materials Respectively.....	109
13.1.	Arrangement for Finding Mode Count by Sine Sweep Technique.....	123
13.2.	Acoustical Subsystem; 1-Dimensional Cylinder.....	123
13.3.	Acoustical Subsystem; 2-Dimensional Cavity.....	124
13.4.	Acoustical Subsystem; 3-Dimensional.....	125
13.5.	Anisotropic Plate: Phase Speed c_1 in One-Direction, c_2 in Two-Direction.....	125

LIST OF ILLUSTRATIONS (CONTINUED)

Figure		Page
13.6.	Modal Density of Cylinder.....	126
13.7.	Section of a Torus, a Shell with Two Constant Radii of Curvature.....	126
14.1.	Set up for Measuring Acoustical Transmissibility of an Aerospace Structure.....	143
14.2.	Transmission Loss of Steel Sheet.....	144
14.3.	Noise Reduction of Cylindrical Structure; Theory and Experiment.....	145
14.4.	Effect on Radiation Resistance of Finite Mass of Beam on a Panel.....	146
14.5.	Experimental Determination of η_{12} (and τ) for Two Connected Plates.....	146
14.6.	Experimental Determination of Transmissibility of a Beam on a Plate.....	147
14.7.	Two Plates, Rigidly Connected Along a Linear Junction.....	147
14.8.	Beam Cantilevered to a Plate.....	148
14.9.	Beam Connected to Edge of a Plate.....	148
14.10.	Coupling Loss Factors for a Beam Connected to the Edge of a Plate: Theory and Experiment.....	149
15.1	Reentry Vehicle.....	181
15.2.	A Truncated Conical Shell Showing (a) Geometry with Equivalent Cylinder Section and (b) Wavenumbers and Mode Shapes for Various Cases.....	182

LIST OF ILLUSTRATIONS (CONTINUED)

Figure		Page
15.3	Modal Density of Circular Cylinder.....	183
15.4	Cylindrical Shell Test Fixture.....	184
15.5	Variation of Vibration Level in Reverberant Field of Fixture.....	185
15.6	Variation of Vibration Level on Ring Connector.....	186
15.7	Transmissibility from the Test Fixture to the Instrument Shelf.....	187
15.8	Lumped Parameter Model of Shelf.....	188
15.9	Comparison of Predictions of η_{12}	189
15.10	Representation in the Wavenumber of the TBL Pressure Field.....	190
15.11	Estimated TBL Pressure Spectrum at the Mid-Section of the Conical Shell.....	191
15.12	Estimated Response of the Conical Shell to TBL Pressure Field.....	192
15.13	Alternate Estimates of Response of the Conical Shell to TBL Pressure Field	193
15.14	Franken Prediction Scheme (From Ref. 41).....	194
15.15	Prediction of Vehicle Shelf Vibration Level.....	195

LIST OF ILLUSTRATIONS (CONTINUED)

FIGURE		PAGE
15.16.	Variance of $\langle a_2^2 \rangle$	196
15.17.	80% Confidence Limits for Mean of $\langle a_2^2 \rangle$..	197

LIST OF TABLES

7.1.	Relations Between Dynamical Variables and Levels.....	19
12.1.	Comparison of Commonly Used Damping Measures.....	95
15.1.	Mode Counts for Shell and Shelf Structures.....	161
15.2.	Values of Coupling Loss Factor.....	162

INTRODUCTION

This Part II of the report of Statistical Energy Analysis for Designers describes the engineering application of statistical energy analysis to the prediction of the vibration of flight vehicles and their subsystems. The procedures are based upon the theoretical discussion presented in Part I of the report, but are intended to be independent from the theoretical background. Therefore, if one is willing to accept the basic formulas as presented, the estimates can be performed without reference to Part I.

Many of the parameters introduced in Section I of Part II represent information about the system that is not commonly evaluated in vibration analysis in the preliminary design stage. The quantification of these parameters either by theoretical or experimental procedures is covered in Section II.

The emphasis in the prediction methods presented in Section I is on the average value of response, but we have also included some information regarding the variability or uncertainty in the response estimate. An understanding of the potential uncertainty in the response estimate can be quite important in interpreting departures from the predicted values of response. A consistent departure from the prediction of several frequency bands is a signal that some aspect of the SEA model is inadequate and probably should be modified, whereas a scatter in the data around the predicted average that is within the calculated uncertainty is an indication that the model cannot be improved upon easily.

Section II of Part II of the report is concerned with evaluating the SEA parameters; loss factor, mode count, and coupling loss factor. Methods of evaluating parameters are empirical, experimental and theoretical. All of these methods are described for evaluating the parameters. In practical situations, it may be necessary to use a mix of procedures to get all the desired values. Mode counts, for example, tend to be easy to calculate and difficult to measure, whereas damping is simpler to measure and more difficult to calculate.

We have tried to preserve an engineering applications - oriented approach to the formulas and techniques, and in the notation in which the results are presented. In many cases,

the formulas are presented in slightly modified form from that of the original source, if the change simplifies the computation required, with little sacrifice in accuracy. Also, for example, we use cyclic frequency (in hertz) rather than radian frequency since this is the quantity that one tends to use experimentally. This preference is not faithfully followed in all instances, but generally we try to adhere to it.

One cannot cover all cases of interest that will arise in design work in a report such as this. This is partly because of space limitation, but also because all the important cases of interest have not yet been worked out. We have tried to indicate sufficient sources for additional background information, so that the reader has access to the information needed to extend the information in this report as needed.

In Section III, we give an example of the use of SEA in the prediction of vibratory response in a high speed flight vehicle and the transmission of that vibration to an internally mounted equipment shelf. As the reader will note, a combination of models, techniques, and analyses are required to cover the frequency range and subsystem behavior. In the final analysis, there is still room for improvement of the model, but the procedures point the direction for the improvements and leave it to the designer whether the next step is worthwile or whether the estimate "will do" as it stands.

This example should be looked upon as an indication that hard estimation problems can be solved with reasonable effort, rather than a formula for success in other estimation efforts. The various approaches to evaluating mode counts, injected powers and coupling loss factors may be of little direct value in the next estimation problem that has to be solved, but a willingness to look at several different models and to use experiment when a calculation can't resolve an issue are lessons of great value.

This part of the handbook does not close the door on SEA developments, but rather opens it up. As SEA becomes more widely used by designers, the data on parameters, the models that have been analyzed, and the correlation of predictions with data will grow. Thus, in using SEA designers are not only availing themselves of a new tool, but they are contributing directly to the growth in the usefulness of that tool.

SECTION I - THE USE OF SEA IN PRELIMINARY DESIGN

CHAPTER 5. RESPONSE ESTIMATION DURING PRELIMINARY DESIGN

In the early stages of design of a high speed flight vehicle, it is often necessary to develop estimates for vibration amplitudes and spectra of major sections of the vehicle. This may be to anticipate possible fatigue problems as a result of the mission profiles and their mix for the aircraft, or to provide data to the environmental specialists in the development of proper test specifications. [1]

This requirement for response estimation will usually first arise during a fairly early stage of the vehicle development. At this point, only some mission parameters and major structural geometry may be known, but details of construction, fastening, etc. may well not be known. Nevertheless, it is necessary that one make the vibration estimates in the face of this uncertainty and do it as well as possible in order to avoid overdesign and its attendant extra expense, or conversely, underdesign and the potential for malfunction or failure.

It is perhaps worth commenting on three procedures for estimating response that have been used. They are the Mahaffey-Smith procedure [2], the Franken method [3], and the Eldred procedure [4]. Of these, the Mahaffey-Smith procedure has been the most widely used because it is quite simple to apply and provides results in a form that is directly usable by the engineer. It suffers from a complete lack of inclusion of acoustical or structural parameters, meaning that the estimate cannot be improved as more becomes known about the vehicle.

The Eldred procedure improves on the Mahaffey-Smith method by incorporating structural damping as a parameter. This is done by making an analogy with the response of a simple 1 dof system to noi se excitation as described in Chapter 2 of Part I. We should note, however, that the damping of different built-up aerospace structures is not very different so that the inclusion of this parameter does not greatly strengthen our hand in developing response estimates. The Franken method does not include damping, but does include surface mass density of the structure and its radius of curvature. We can look therefore for certain changes in response as we vary the structure. Thus, although the basis of the Franken method is empirical, the data normalization used allows its application to quite a variety of structures.

The major advantages of SEA is that the degree of parameterization of the prediction problem can be varied as more structural and loads information becomes available. Thus, it is possible to continually refine our response estimates as the design becomes

more fixed. An important consequence of this is that we can see the effect of various design alternatives in changing noise and vibration levels. When SEA is used, there is no "discontinuity" between the empirical procedures used in the preliminary phase and the much more detailed analyses that may be used at later stages of design.

In Part I of this report, we followed a pedagogical approach in which the theory and applications of SEA were developed along a "conventional" path. We began with the model and then worked out its consequences. In this Section I of Part II, we take a rather different approach. The SEA procedure is described as a complete process in Chapter 6. The steps involved are itemized and explained as an engineering procedure rather than as a conceptual development as was done in Part I. We first focus on the output of the procedure - the response estimate. Generally, the SEA calculation gives results in terms of energy of vibration, which must then be converted to stress, or some other dynamical variable. We then proceed to determine how that energy estimate was arrived at. The use of energy estimates to develop estimates for oth er response variables is discussed in Chapter 7.

The calculation of the energy estimate itself requires use of the SEA model for energy flow. As discussed in Part I and reviewed in Chapter 8, this model contains energy storage, loss and transfer parameters - which are the modal density, loss factor and coupling los s factor, respectively. In addition, we must know the input power injected into the structure by the environment. Chapter 8 shows how the energy estimate is developed from knowledge of these parameters when they are expressed in either analytical or graphical form.

The SEA parameters that are important in determining the energy for the actual system under design must then be evaluated. Chapter 9 shows how this is done by using experimental methods, theoretical predictions and empirical values. Two kinds of coupling factors are discussed: those appropriate for blocked energies, and those for actual system energies. Modal densities are discussed in both theoretical and experimental terms. Input and junction impedances are introduced for the purposes of evaluating coupling loss factors and input power.

The final chapter of Section I deals with the construction of system models. This is one of the most important steps in SEA. The general model configuration is likely to be fairly similar for various detailed designs of a given system. Thus, a particular class of high speed vehicles are all likely to have similar system models, so that once defined, only relatively minor changes to the model will be necessary.

CHAPTER 6. PROCEDURES OF STATISTICAL ENERGY ANALYSIS

6.0 Introduction

In this Chapter, we survey the entire SEA estimation procedure as an engineering process, as contrasted with the theoretical approach taken in Part I. The process consists of (1) model definition, (2) parameter evaluation, (3) calculating energy distributions and (4) response estimation. In general, it will not be necessary to repeat all parts of this process for every new situation, but only the latter parts may have to be revised. For that reason, in Chapters 3 through 6, we have reversed the order of presentation, discussing the latter stages of the process first since they are more directly connected with what the engineer wants to know and are also the parts of the procedure that are most likely to change with each new situation.

In this Chapter, however, we follow the more customary sequence in which we start with the modeling discussion and end up with response estimation. We try to indicate as well as we can just what the real engineering considerations are at each step. In the later chapters, more detailed discussion of the procedures will be presented.

6.1 Modeling the System

As an example of a system that we might wish to model, consider an aircraft and its attached equipment pod shown in Figure 6.1. Such a system will have its dominant response determined by "resonant", that is, damping controlled vibration and, hence is a candidate for SEA prediction. We also assume that whatever nonlinear effects there are may be neglected for the purposes of estimating response at this stage.

Modeling this physical system requires that we identify the following features of energy flow and storage in the system:

(1) Sources of input power and mode groups (subsystems) on which they directly act. In the case of Fig. 6.1, these would be the acoustical noise field and turbulent boundary layer acting on both the aircraft and the pod.

(2) Groups of "similar" and "significant" modes that store energy and result in response that affects the estimates we wish to make. In the case of Fig. 6.1, we might make a first try by grouping all flexural modes of the aircraft panels together, and flexural modes of the pod together. If it turned out later that some group of modes originally ignored was important, then one would have to add it to the diagram.

(3) It is automatically assumed that every group of energy-storing modes will have a finite amount of damping. Thus, the identification of the dissipation of energy represents no additional task.

(4) The junctions through which appreciable energy may flow from one mode group to another. In the case of Fig. 6.1, this is the pair of connecting spars between the aircraft and the pod. The energy flow links are usually identifiable by a direct interface between the energy storage boxes or mode groups.

When all of the energy storage and power input, dissipation and transfer processes are defined, the SEA modeling is essentially complete and results in a diagram like that shown in Fig. 6.1 (but is generally more complicated!). At this point, the SEA parameters that we need to solve for the energy values will be evident. In the next section, we review briefly the procedures by which the parameter evaluation is made.

6.2 Evaluating the Parameters

The parameters that define the four processes of paragraph 6.1 are:

(1) the input conductance (for input power),

(2) modal densities (or mode count) to determine the number of modes in a "box",

(3) the dissipation loss factor that relates energy stored to power dissipated,

(4) the coupling loss factor that relates differences of modal energy of subsystems to the power flow.

In this section, we give a brief overview of the parameter evaluation process which we shall cover more fully in Chapter 9.

If the environmental excitation produces a force on a system, then the parameter governing the input power resulting from that force is in the form of an input "conductance". If the load is a prescribed motion (such as the injection of volume velocity into an acoustical space), then the proper parameter is an input resistance of the system. These parameters which collectively are known as "immittance" functions [5] are known for structural excitation by some environmental loads, such as shakers, turbulent boundary layers, sound fields, and separated flows on vehicles. In any particular situation, however, a measurement or new calculation of the appropriate immittance may be necessary.

Modal densities are known for many of the elements that make up the systems that interest us. Modal density is usually written n(f), meaning the average number of modes that resonate in a 1 Hz band around the frequency f. Elements for which modal densities are known include flat plates (isotropic and anisotropic), curved plates, acoustical spaces, strings and beams. [6] Since modal densities of combined systems are additive, any sytem that is composed of these elements also has a known modal density. Modal densities can be measured by counting resonances as the excitation frequency is varied, but considerable care is necessary to avoid missing a sizable number of them in the count.

Care must also be taken to use the proper modal density for the kinds of modes that are important for the purpose at hand. For example, in Fig. 6.1 the modes of the aircraft that contain the most energy and are best coupled to the turbulence and noise are those of panel flexure. Thus, even though torsional or in-plane motion modes of the fuselage may resonate in the frequency range of interest, we would very likely ignore these non-flexural modes. It turns out that a 10% error in the mode count is only about 1 dB uncertainty in the response estimate, so that it is not necessary to have great precision in the modal density.

The damping of the mode group is expressed in SEA work by the loss factor. This quantity is the reciprocal of the electrical engineer's Q or quality factor and is twice the mechanical engineer's critical damping ratio. Calculation of the damping from first principles is generally quite unreliable so that one usually relies on measurements to predict

loss factor as a function of frequency. Typical values for the loss factor are in the range 0.1 to 0.001.

A damping measurement is usually accurate enough to determine loss factor to two significant figures, but not much more than that. Two commonly employed ways of measuring damping are a free decay of the system, or a measurement of modal response bandwidth when the excitation is a pure tone. The bandwidth technique is a bit more accurate when it works, but it must be done on a mode-by-mode basis, and it fails when the modal density is high and the modes get too close to each other along the frequency axis. Occasionally, one can also measure damping by injecting a known amount of power into the system and observing the steady-state response.

The transfer of power between mode groups is determined by the coupling loss factor. This parameter, in turn, is related to or determined by other parameters that are probably more familiar to engineers who work with the systems involved. For example, the coupling loss factor for power flow between two rooms can be readily related to the transmission loss of the wall, which is a familiar parameter to workers in building acoustics. Similarly, the coupling loss factor governing the interaction of a panel and a sound field may be related to the radiation damping (or mechanical radiation resistance) of the panel, a quantity that is known to structural vibration engineers. Thus, although the coupling loss factor itself is not a well known parameter, in particular situations it is often relatable to other parameters that are more familiar. Since these other parameters have been calculated or tabulated in many instances, the coupling loss factor can also be evaluated.

6.3 Solving for the Energy Distribution

The SEA model allows one to calculate the equilibrium energy of each mode group from a knowledge of the parameters involved. The simultaneous equations for the energy are linear, algebraic and the solutions give each energy in terms of all the input powers to the system and the various loss and coupling loss factors. Normally, the input power to each mode group and the parameters such as modal density and coupling and dissipative loss factors are assumed to be known. One then solves for the energy values.

It is also possible in principle to use the energy equilibrium equations to try to evaluate all of the SEA parameters, and the coupling loss factors in particular.

In this instance one tries to control the input power and to measure the energy equilibrium values as well as possible. The equations are then solved for the coupling loss factors. This is not a totally satisfactory way of determining these parameters, however, since the solutions seem to be quite sensitive to rather small errors in the measured energy values. Nevertheless, this approach has been used with limited success in a few situations. [7,8]

The result of the energy calculation is the total energy of resonant vibration (or oscillation) in a frequency band Δf wide for each "box" of the system. This information is then used to predict the actual dynamical response that is of direct interest.

6.4 Evaluating Response from Energy Estimate

In Chapter 7, we will develop the procedures used in converting the energy found from the calculations just discussed into useful estimates of vibration, pressure, strain or some other appropriate response variable. In this section, we merely summarize the procedure, which has two major estimation outputs: the mean energy or rms response and, where appropriate, an estimation interval.

The mean value estimate of energy gives the mean square acceleration in some frequency band (an octave band, for example). This mean square response is also a spatial average, so that it applies to a region of the structure. For example, an energy estimate might be found for the aircraft fuselage to be 10 joules (watt-seconds) in the 1 kHz octave band. If the total mass of the fuselage were 1000 Kg, then one estimate of the m.s. velocity in the band would be 10^{-2} $(m/sec)^2$ and the rms acceleration would be approximately 60 g's. This average result is both a spatial average and an ensemble average, i.e., it applies to a hypothetical group of structures, similarly constructed, of which our structure is a representative sample.

An important modification of this average estimate is to take account of "response concentration", that is, to recognize that particular regions of the structure will have a time mean square response that is greater than the spatial average. For example, the m.s. pressure near the wall of a room is twice the space average value. As another example, the m.s. velocity at the free tip of a beam is just four times the spatial m.s. velocity of the beam as a whole. For other boundary conditions on panel type structures, Ungar and Le[illegible] have evaluated several of these "response concentration" values [9].

Since we admit to variation, we must have a procedure for making estimates that incorporate this uncertainty in a useful and realistic way. This is done by forming an estimation interval. Such an interval is a familiar idea. It is frequently seen in cases in which vertical bars are placed on a mean value measurement to either indicate the range of observed data or the mean, plus or minus the standard deviation. We can be more definitive than this in our use of estimation intervals in Chapter 7. We calculate the range of values of response that are expected to "capture" the observations, say 95% of the time. This form of estimate is of value when applying SEA to reliability analyses since the probability of levels occurring that exceed a particular value may be quite important.

The estimation intervals are derived from a calculation of the standard deviation of the m.s. response. We have explained in Part I that the theory in support of this calculation is not so well established as it is for the mean value theory. Nevertheless, the importance of this aspect of estimation is great enough that we must use the limited results that are available to calculate the standard deviation for the purposes of interval estimation.

The result of the estimation then is to say that, for example, the rms value of fuselage acceleration in the 1 kHz band is 60 g's. In addition, if we bracket this mean value with a range from 20 to 200 g's (± 10 dB), we would expect to have 95% of all observations of response fall within this interval. Such an estimate can then be used to compute fatigue accumulation or some other response related failure rate.

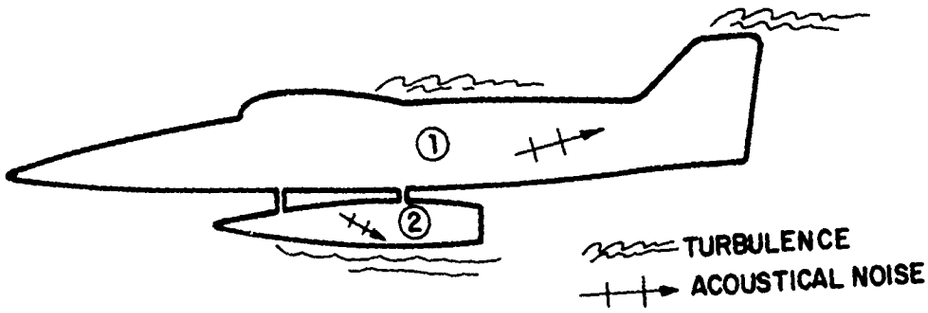

THE SYSTEM

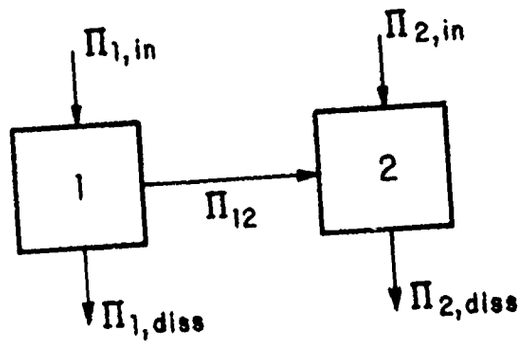

FIG. 6.1

AN SEA MODEL OF THE SYSTEM

CHAPTER 7 ESTIMATION OF DYNAMICAL RESPONSE

7.0 Introduction

This chapter is concerned with the estimation of the dynamical response of a system in terms of such variables as stress, acceleration, pressure, etc. The starting point is the knowledge of system vibrational energy, typically in the standard frequency bands. The goal is a prediction of mean square response for the same frequency bands. We include uncertainty in the estimate by using estimation intervals, and response concentration effects due to boundaries or impedance variations in the system.

The energy is assumed to be known, it will have been found previously according to the methods of Chapter 8. However, the discussion of this chapter is sufficient in itself to allow one to make many useful conversions from one response variable to another. For example, the average energy of vibration of a system may be determined by measurements of acceleration. The methods of this chapter allow one to convert this acceleration measurement to an estimate of stress. Further, one could estimate the increase in variance due to restricting the bandwidth of measurement. Much of the data manipulation that is useful in particular instances has its basis in the discussions of this chapter, quite apart from their broader usefulness in SEA.

7.1 Representations of the Energy Estimate

In engineering usage, the "power spectral density" (psd) of the energy of vibration may be denoted by $\mathcal{E}(f)$, and the energy of vibration associated with a frequency band Δf in the range $f_1 < f < f_2$ would simply be

$$E_{\Delta f} = \int_{f_1}^{f_2} \mathcal{E}(f)\, df. \qquad (7.1.1)$$

This integration is shown graphically as the hatched area in Fig. 7.1. If $f_2-f_1=1$ Hz, then the integral is plotted as the energy psd, which is $\mathcal{E}(f)$ in Fig. 7.1. Other

"constant frequency bandwidth" presentations of data in aerospace applications are typically 10 Hz or 50 Hz.

It is also common practice to present data or the results of calculations in terms of "constant percentage bandwidths". In this instance, the nominal "center frequency" of the band is the geometric mean of the limits:

$$f_c = \sqrt{f_1 f_2}$$

and the bandwidth $\Delta f = f_2 - f_1$ is always a constant fraction r of the center frequency: $\Delta f = r f_c$. If $r = 1/\sqrt{2}$, then $f_2 = 2f_1$ and we have "octave bands". If r=0.26, then the bands are called "1/3 octave bands". A table of the center frequencies for the standardized octave and 1/3 octave bands is shown in Fig. 7.2.

The mks unit for energy is the joule (or watt-second) which is the amount of work involved when a force of 1 newton acts along a distance of 1 meter. The unit for the psd of energy $\mathcal{E}(f)$ is joule-sec, since the unit of frequency is cycles per second or hertz (Hz).* Since the energy in a band $E_{\Delta f}$ is the integration of $\mathcal{E}(f)$ over frequency, the band energy unit is also the joule.

We may also express the energy E as a "level" defined by

$$L_E \equiv 10 \log E/E_{ref}, \text{ dB} \qquad (7.1.2)$$

The standard reference for energy is 10^{-12} joules. A band energy of 0.1 joule, therefore, would correspond to a band energy level of 110 dB, normally written

*Clarity of presentation would insist that there is no difference between the unit "Hz" and $(\text{second})^{-1}$, but engineering usage of Hz is widespread.

$$L_E = 110 \text{ dB re } 10^{-12} \text{ joules}$$

In Fig. 7.3, we show how the octave and 1/3 octave band levels of energy might be graphed in a typical situation. The 1/3 octave band levels will generally be of the order of 5 dB lower than the octave band levels since the response of three adjacent 1/3 octave bands must be combined to account for the response in a single octave band. Also, note that only the band values have significance, the connecting lines between the points are only an aid to seeing the overall trend of the data as a function of frequency.

7.2 Conversion From Energy to Other Variables

The relation between vibratory energy and the space-time mean square velocity of the structure or sound field is

$$E = M \langle v^2 \rangle = M v_{rms}^2 \qquad (7.2.1)$$

where M is the structural mass in kilograms.

By taking 10 log of this expression, we can express this as a relation between energy levels and velocity levels,

$$L_E = 10 \log E/E_{ref} = 10 \log M + L_V + 120 \qquad (7.2.2)$$

where $L_V \equiv 20 \log v_{rms}/v_{ref}$, and $v_{ref} = 1$ m/sec. Thus, for example if a structure has a mass of 10 kg, and the band level of energy is 97 dB, (the 125 Hz octave band level of Fig. 7.3) then the velocity level is

$$L_V = 97 - 10 \log 10 - 120 = -3 \text{ dB re } 1 \text{ m/sec} \qquad (7.2.3)$$

We can develop a velocity spectrum for this structure using Eq. (7.2.2). This spectrum is presented in Fig. 7.4 and corresponds to the octave band spectrum of energy shown in Fig. 7.3. Note that a velocity level of -40 dB corresponds to an rms velocity of 1 cm/sec.

The displacement or acceleration spectra are readily derived from the velocity spectrum, simply by noting that for each band having a center frequency f,

$$\langle a^2 \rangle = 4\pi f^2 \quad \langle v^2 \rangle; \quad \langle d^2 \rangle = \langle v^2 \rangle / 4\pi^2 f^2 \qquad (7.2.4)$$

If we define

$$\left.\begin{aligned} L_a &= 20 \log a_{rms}/a_{ref} \\ L_d &= 20 \log d_{rms}/d_{ref} \end{aligned}\right\} \qquad (7.2.5)$$

in which $a_{ref} = 10$ m/sec^2 ($\approx$1g) and $d_{ref} = 1$ m, then

$$L_a = 10 \log 4\pi^2 + 20 \log f + 20 \log v - 20 \log 10$$

$$= L_v + 20 \log f - 4, \text{ dB re 1 g}$$

and

$$L_d = L_v - 20 \log f - 16, \text{ dB re 1 m.}$$

As an example, these are also graphed in Fig. 7.4 for the velocity spectrum shown there. Of course, the relative numerical values of the band levels depend on the reference value chosen, but the comparative shapes of the spectra are not. Note that the displacement spectra tend to be large at low frequencies and the acceleration spectra are higher at high frequencies. A conversion nomograph between levels is shown in Fig. 7.5.

The mean square velocity we have been dealing with has been called the "kinetic velocity", [10] a velocity defined in terms of the kinetic energy of the system. If the structure is fairly homogeneous (beams, cylinders, plates and sound fields meet this requirement), the kinetic velocity is also equal to the space-time mean square velocity of the system.

In addition, these systems also allow us to use a simple relationship between the mean square velocity and the strain in the structure. One can readily show that for a variety of mechanical motions (flexure, torsion, compression, etc.) the mean square strain $\langle\varepsilon^2\rangle$ is simply related to the kinetic velocity. [11, 12]

$$\langle\varepsilon^2\rangle = K \langle v^2\rangle / c_\ell^2 \qquad (7.2.6)$$

in which the constant K depends on the type of motion and system geometry but varies over a small range near unity. For estimation purposes we can set K = 1.

A useful reference strain is $\varepsilon_{ref} = 10^{-6}$, or "1 microstrain". Defining the strain level as

$$L_\varepsilon = 10 \log \langle\varepsilon^2\rangle / \varepsilon_{ref}^2$$

one has

$$L_\varepsilon = L_v - 20 \log c_\ell + 120 \qquad [\text{dB re } 10^{-6}, \text{ or 1 microstrain}]$$

$$= L_E - 10 \log M - 20 \log c_\ell \qquad (7.2.7)$$

Thus, if L_v = - 30 dB re 1/msec and if c_ℓ = 5000 m/sec, L_ε = - 30 - 74 + 120 or 16 dB re 1 microstrain, corresponding to an rms strain of 6.5×10^{-6} .

We can also relate the velocity to stress τ by noting that the strain times stiffness modulus is stress. For most structures the appropriate stiffness is the Young's modulus Y_o,

$$\langle \tau^2 \rangle = Y_0^2 \langle \varepsilon^2 \rangle \qquad (7.2.8)$$

The stress level is defined as

$$L_\tau \equiv 10 \log \langle \tau^2 \rangle / \tau_{ref}^2 . \qquad (7.2.9)$$

Any convenient reference stress τ_{ref} can be used. If we use $\tau_{ref} = 10^6$ newtons/meter^2 then

$$L_\tau = 20 \log Y_o - 120 + L_\varepsilon$$

$$= L_v + 20 \log Y_o - 20 \log c_\ell$$

$$= L_v + 20 \log \rho c_\ell \qquad (7.2.10)$$

using $Y_o = \rho c_\ell^2$ where ρ is the density and c_ℓ is the longitudinal wave speed. Thus, the form of the velocity spectrum also determines the form of the strain and stress spectra. In Table 7.1, we summarize the relations between the variables discussed and the level defined in the preceding paragraphs. These relations as a group allow us to

Variable	Relation	Level	Formula	Reference
energy E	1	$L_E \doteq 10 \log E/E_{ref}$	$L_E = 10 \log E + 120$	$E_{ref}=10^{-12}$
velocity v	$\langle v^2 \rangle = E/M$	$L_v = 10 \log \langle v^2 \rangle / v_{ref}^2$	$L_v = L_E - \log M - 120$	$v_{ref}=1$ m/sec
displacement d	$\langle d^2 \rangle = \langle v^2 \rangle / \omega^2$	$L_d = 10 \log \langle d^2 \rangle / d_{ref}^2$	$L_d = L_v - 20 \log f - 16$	$d_{ref} = 1$ mm
acceleration a	$\langle a^2 \rangle = \omega^2 \langle v^2 \rangle$	$L_a = 10 \log \langle a^2 \rangle / a_{ref}^2$	$L_a = L_v + 20 \log f - 4$	$a_{ref} = 10 \frac{m}{sec^2}$
strain ε	$\langle \varepsilon^2 \rangle = k \langle v^2 \rangle / c_\ell^2$	$L_\varepsilon = 10 \log \langle \varepsilon^2 \rangle / \varepsilon_{ref}^2$	$L_\varepsilon = L_v - 20 \log c_\ell + 120$	$\varepsilon_{ref}=10^{-6}$
stress τ	$\langle \tau^2 \rangle = Y_0^2 \langle \varepsilon^2 \rangle$	$L_\tau = \log \langle \tau^2 \rangle / \tau_{ref}^2$	$L_\tau = L_v + 20 \log \rho c_\ell$	$\tau_{ref}=10^6 \frac{newtons}{m^2}$

[Y_0 = Young's modulus in newt/m^2, c_ℓ = longitudinal wave speed in m/sec M = mass in kg, $\omega \triangleq$ radian frequency, f = cyclic frequency, k = constant of order unity, ρ = mass density in kg/m^3]

TABLE 7.1

RELATIONS BETWEEN DYNAMICAL VARIABLES AND LEVELS

generate average (meaning space-time square) response of the system if the average energy of vibration or any of the other variables are known.

7.3 Response Concentration Factors

The average response values are useful as a first step in estimation of vehicle vibration, but there are at least two reasons that we have to modify the average estimates for engineering purposes. The first reason is that of "response concentration", which is well known in the case of the stress concentration factors commonly used in structural design. Such response concentrations are tabulated and available for various common configurations. [13]

The second kind of concentration factor or effect is the local maximum of response due to coherence effects between modes which many modes are excited simultaneously. This coherence may be spatial or temporal. The variation of and peaks in local rms response due to coherence between modes was discussed in Chapter 4 (of Part I). In this chapter, we merely use some of those formulas to estimate extreme values of response that result.

Modal Stress Concentration

We can estimate the spatial mean square of stress for example, according to Eq. (7.2.8) and its antecedents. We can also estimate the effect of edge fixation on the stress of the boundary of a plate by methods reported by Ungar and Lee [9]. These authors use the "dynamic edge effect" method of Bolotin to calculate stresses in situations for which there are no exact solutions to the thin-plate equations.

We imagine a modal vibration pattern like that sketched in Fig. 7.6. The displacement w near the boundary defined by x_2 = constant is written

$$w(x_1,x_2)=\sin k_1x_1[\sin k_2x_2+B_1 \cos k_2x_2+B_2 e^{-k_2'x_2}] \tag{7.3.1}$$

where

$$k_2' = \sqrt{2k_1^2+k_2^2}$$

and

$$k_1^2+k_2^2 = \omega^2/c_b^2 = k_b^2$$

where

$$c_b = \sqrt{\omega\kappa c_\ell}$$

is the free bending wave speed.

The maximum response of a single 2-dimensional mode in the "interior" is

$$\langle v^2_{max} \rangle = 4 \langle v^2 \rangle \qquad (7.3.2)$$

since the mode shape function is

$$\psi_m = 2 \sin k_{m_1} x_1 \sin k_{m_2} x_2 \qquad (7.3.3)$$

Thus, we have a concentration factor of 2 built into a single mode response. The major interest in the edge effect is whether the constraint due to the edge causes stress concentration there that are greater than the interior values.

The analysis by Ungar and Lee [9] is rather detailed and lengthy, but they find that the ratio R of edge to interior stress can be simply stated in two important cases

(A) "clamped-like" edges

$$R = \frac{4\alpha_r G\,[2\alpha_t G^3 - H J]}{M\{[4\alpha_r G(\alpha_t G - H) + J - 2G^2]^2 + \Delta^2\}^{\frac{1}{2}}}; \quad (a_r > a_l) \tag{7.3.4}$$

(B) "free-like" edges

$$R = \frac{2G}{M}\ \frac{(\nu+\beta^2)(2\alpha_r H + G) - \nu G(4\alpha_r\alpha_t G^2 + J)}{\{\Delta^2 + [4\alpha_r G(\alpha_t G - H) + J - G^2]^2\}^{\frac{1}{2}}}; \quad (a_r < a_l) \tag{7.3.5}$$

In these expressions

$$\alpha_r = K_r/2D\,k_p \qquad G = \sqrt{1+\beta^2}$$

$$\alpha_t = K_t/2D\,k_p^3 \qquad H = \sqrt{1+2\beta^2}$$

$$\beta = k_1/k_2 \qquad J = 1 + \nu\beta^2$$

$$\Delta = J\,H - 4\alpha_t G^2(G + \alpha_r H)$$

$$k_p^2 = k_1^2 + k_2^2 = G^2 k_y^2 \qquad M = \max\,[J, \nu + \beta^2]$$

The elastic supports are defined by a rotational stiffness K_r and a translational stiffness K_t per unit length. The plate has a Poisson's ratio ν and a bending rigidity $D = \rho_s \kappa^2 c_\ell^2$.

The surfaces R = 1 for these two conditions are shown in Figs. 7.7 and 7.8 which was adapted from the report by Ungar and Lee [9]. The region within the surface represents conditions in the parameter space for which the stresses along

the edge are greater than at interior locations. The actual stress ratio for any situation may, of course, be found from Eqs. (7.3, 7.4, and 7.5). For example, if we find the stress ratio due to a "normally incident" ($\beta=0$) mode on the $x_2=0$ edge (shown in Fig. 7.6) when the edge is clamped ($\alpha_r,\alpha_t\to\infty$), we find R=2. Thus, the simple clamped edge produces a stress concentration factor of 2 above the peak stresses that occur in the interior of the plate due to the normal mode shape. This same stress concentration also occurs for "grazing modes" ($\beta\to\infty$) in which the waves are travelling parallel to the edge of the panel.

Multi-Modal Stress Concentration. In Chapter 4 (of Part I) we discussed the effect of coherence between modes in multi-modal response. We found that it was possible to obtain that we called "statistical response concentrations" of significant value when many modes are coherently excited. Such a situation can arise when structures are excited by a pure tone at a frequency well above the lowest panel resonances. The expression for the response concentration for this situation is [see Eq. (4.4.12)]

$$\frac{w_{max}}{w_{rms}} = \psi_{max}\sqrt{N}$$

which is $2\sqrt{N}$ for 2-dimensional modes.

As an example of the application of Eq. (7.3.6), consider the aircraft shown in Fig. 6.1 excited by the pure tone from a bypass engine fan at 2.5 kHz. Assume the structural loss factor is 10^{-2}, so that an equivalent modal bandwidth is approximately 40 Hz. If the fuselage has an area of 50 m^2 and an average thickness of 2 mm, the average spacing between modes is $\delta f = 0.12$ Hz. Thus, at 500 modes will be excited by this tone and the statistical concentration factor is

$$R_{stat} = 2\sqrt{500} \simeq 45, \qquad \text{(pure tone)} \qquad (7.3.7)$$

quite a large concentration factor. Detailed analysis shows that this concentration has a nearly unity probability of occurring, but that its position will shift depending on the frequency of the excitation. Thus, if the tone frequency varies at all, this concentration point will wander over the structure.

When the system excitation is broad band, the statistical response concentration is almost never important. The response concentration in the case of excitation by a band Δf is given by

$$R_{stat} = \left[\frac{(\frac{\pi}{2}\eta f)^2}{\delta f \, \Delta f} \psi^2_{max} + (1 - \frac{\pi}{2}\frac{\eta f}{\Delta f}) \right]^{\frac{1}{2}} \qquad (\Delta f > \eta f) \tag{7.3.8}$$

Applying this to our example, we get $R_{stat} = 10$ when $\Delta f = 600$ Hz (the bandwidth of the 2.5 kHz third octave band). Thus, the "statistical response concentration" is a function of the bandwidth of the vibration, decreasing as the noise bandwidth increases.

We have shown how we can estimate extreme values of response for single and multi-modal response situations. Such extreme values are of particular interest when "exceedance" type failures, such as fracture, plastic deformation, or collisions are considered. We now turn to procedures for forming estimation intervals which are useful in amplitude related damage estimates.

7.4 Variance and Estimation Intervals

Variance is a measure of the likely departure of any single measurement of response from the average value. Since the shapes and the resonance frequencies of the modes will vary from one structure to another and the details of location of excitation and response measurement will also vary, we may think of the output of a particular experiment as a statistical sampling of a distribution of possible response values. We present here some formulas for the standard deviation to be expected in cases in which one system is excited directly by a point source and for the case in which a second system is excited by its attachment to the directly excited system.

Single System Response. As explained earlier, the energy estimate provides us with a prediction of m.s. response (velocity, say) which we write as $\langle v^2 \rangle$. When a single system is excited by a point source, the theoretical relation for the variance (square of the standard deviation σ) is as follows [10]

$$\frac{\sigma^2_{v^2}}{\langle v^2 \rangle^2} = \frac{2F(Q)}{Q} \left\{ 1 + \frac{1}{2M} \frac{\langle \psi^4 \rangle^2}{\langle \psi^2 \rangle^4} \right\} \qquad (7.4.1)$$

where $Q = 2\Delta f/\pi f\eta$, $M = \pi f\eta/2\delta f$, and ψ is the mode shape. Also Δf is the bandwidth of the noise excitation, η is the loss factor, and δf is the average frequency spacing between modes. The parameters η and δf are discussed further to Chapter 9. The function $F(Q)$ is graphed in Fig. 7.9. The modal shape factor has the following values:

$$\begin{aligned} \langle \psi^4 \rangle / \langle \psi^2 \rangle^2 &= 3/2 \quad \text{(one-dimensional systems)} \\ &= 9/4 \quad \text{(two-dimensional systems)} \\ &= 27/8 \quad \text{(three-dimensional systems)} \end{aligned} \qquad (7.4.2)$$

The parameter M is the modal overlap, the ratio of effective modal bandwidth to average frequency spacing between the modes. The parameter Q is a ratio of excitation bandwidth to modal bandwidth. If we divide our interest between cases of narrow and broad excitation bandwidths and small and large degrees of modal overlap, we get the following simplified formulas for the "normalized variance" [10]

$$\frac{\sigma^2_{v^2}}{\langle v^2 \rangle^2} = \frac{\delta f}{\pi \eta f} \frac{\langle \psi^4 \rangle^2}{\langle \psi^2 \rangle^4} \quad \begin{array}{l} \text{narrow band } (Q<<1) \\ \text{no overlap } (M<<1) \end{array}$$

$$= 1 \quad \begin{array}{l} \text{narrow band } (Q<<1) \\ \text{high overlap } (M>>1) \end{array}$$

$$= \frac{\delta f}{\Delta f} \frac{\langle \psi^4 \rangle^2}{\langle \psi^2 \rangle^4} \qquad \text{band of noise } (Q>>1) \text{ little overlap } (M<<1)$$

$$= 2 \frac{\pi f \eta/2}{\Delta f} \qquad \text{band of noise } (Q>>1) \text{ high overlap } (M>>1) \qquad (7.4.3)$$

The quantities evaluated by Eqs. (7.4.3) will turn out to be quite important for determining estimation intervals or "safety factors" for response prediction.

Coupled System Response. When two systems are joined together and only one system is directly excited by an external source, then the mean value of energy is estimated by methods to be discussed in Chapter 8. The variance in response has also been derived for this situation for the simple case of point excitation, point connection between systems, and point observation. Such a calculation is thought to represent an upper bound on the variance to be encountered in other situations. Thus, the estimates of confidence that we discuss later are likely to be on the conservative side.

From Chapter 4 of Part I, the normalized variance for an indirectly excited system is [see Eq. (4.2.13)];

$$\frac{\sigma^2_{v^2}}{\langle v^2 \rangle^2} \frac{\langle \psi_1^4 \rangle^a}{\langle \psi_1^2 \rangle^{2a}} \frac{\langle \psi_2^4 \rangle^b}{\langle \psi_2^2 \rangle 2b} \frac{\delta f_1 \, \delta f_2}{\Delta f \, \frac{1}{2} \pi f (\eta_1 + \eta_2)} \qquad (7.4.4)$$

In this expression, ψ_1 is a mode shape for the directly excited system, ψ_2 a mode shape for the indirectly excited system. The average frequency separations for modes in the two systems are δf_1 and δf_2. The excitation and analysis bandwidths are Δf, and the loss factor for systems 1 and 2 are η_1 and η_2 respectively. If one of the systems has a single mode in the band, then set $\delta f = \Delta f$ for that system.

The exponents a and b in Eq. (7.4.4) are concerned with the nature of the excitation and observation locations. If these are "average" interior locations on the structures (or sound fields) then a = b = 2. In some instances we can sense the response so that all resonant modes contribute equally to the response. Examples include measurement of motion at the free end of a beam or sound pressure at the corner of a rectangular room. If such a location is picked for the excitation, then a = 1, and if such a location is picked for the observation of response, then b = 1.

We see from Eqs. (7.4.1) and (7.4.4) that the variance is generally reduced as the modes get more dense (and, therefore, δf is reduced) and as the excitation bandwidth Δf is increased. From Eq. (7.4.2), systems of higher dimensionality have a greater contribution to the variance by this spatial factor, whereas the usually higher modal density of such a system is usually sufficient to offset this effect. In balance, one-dimensional systems such as ring frames and beams have higher variance than do plates, cylinders or acoustical spaces.

7.5 Using Variance to Calculate Safety Factors

The variance of response has two applications that are of interest to the structural designer. The first is as a simple metric to judge the scatter of data in response simulation experiments. The second is the setting of estimation levels that represent a reasonable bound to the expected response in a variety of situations. Usually such a bound will be several times the estimate of average response so that the observed response may be reasonably expected to fall within the bound. We may interpret such a bound, therefore, as a "safety factor" on the mean value estimate.

In order to calculate estimation intervals, we need the probability of the response variables, $\langle v^2 \rangle_t$, $\langle \tau^2 \rangle_t$, $\langle p^2 \rangle_t$, etc. We let any of these positive variables to represented by the variable θ. The probability density of response is denoted $\phi(\theta)$, which will have the general form sketched in Fig. 7.10. The probability that the measured response θ will lie in the interval $\theta_1 < \theta < \theta_2$ is called the confidence coefficient, CC, and is graphically represented as the hatched area shown in Fig. 7.11.

A very convenient form for the probabilty density is the so-called gamma density. If we assume that θ is distributed according to this density, then we can relate the confidence coefficient directly to the estimation interval for a given normalized variance as determined either by Eq. (7.4.1) or (7.4.4). For example, if we define an upper limit $\theta_2 = r\langle\theta\rangle$ where r is a positive number greater than unity and a lower limit $\theta_1 = 0$ for the estimation interval, we obtain the relationship shown in Fig. 7.11. Thus, for example, assume that we want to be 99% sure of not exceeding the response estimate θ_2, where $\theta_2 = r\langle\theta\rangle$. If, for example, $\sigma_\theta^2/\langle\theta^2\rangle = 0.3$ and if $r = 2.5$, then we can be 99% confident of not exceeding a response of $\theta_2 = 2.5\langle\theta\rangle$. We can think of the factor r, therefore, as a kind of safety factor; the greater r is, the less chance we have of exceeding the estimate.

A second kind of estimation interval, which is of greater importance in experimental studies, may be termed a "bracketing estimate". In this case, we set $\theta_2 = r\langle\theta\rangle$ as before, and also set $\theta_1 = \langle\theta\rangle/r$. Since the ratio of the limit to the mean is fixed, we can refer to the estimate in this case as the mean plus or minus 10 log r(dB). This is a convenient and natural form for the estimation interval, particularly if the response has been expressed in logarithmic terms (as a level.) Again, using the gamma density for $\phi(\theta)$, the relation between CC, r, and $\sigma^2/\langle\theta^2\rangle$ for the "bracketing interval" is shown in Fig. 7.12. The use of this graph to define an estimation interval is identical to the procedure described in the preceding paragraph.

Summary. Starting with the estimate of expected vibrational energy in a band Δf, we have shown how to reinterpret this estimate in terms of variables of more direct interest. We have also discussed the effects that may cause extreme values of response at particular locations. In addition, we have shown how to develop estimation intervals for use in those cases in which the expected variation leads to too much uncertainty for the use of the mean value as an estimate. In the next chapter, we discuss the way in which we obtain the energy estimate from the SEA model.

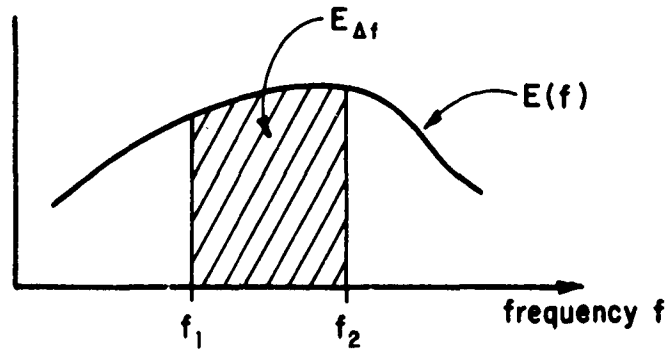

FIG. 7.1

INTERPRETATION OF ENERGY IN FREQUENCY BAND AS AREA UNDER SPECTRAL DENSITY CURVE

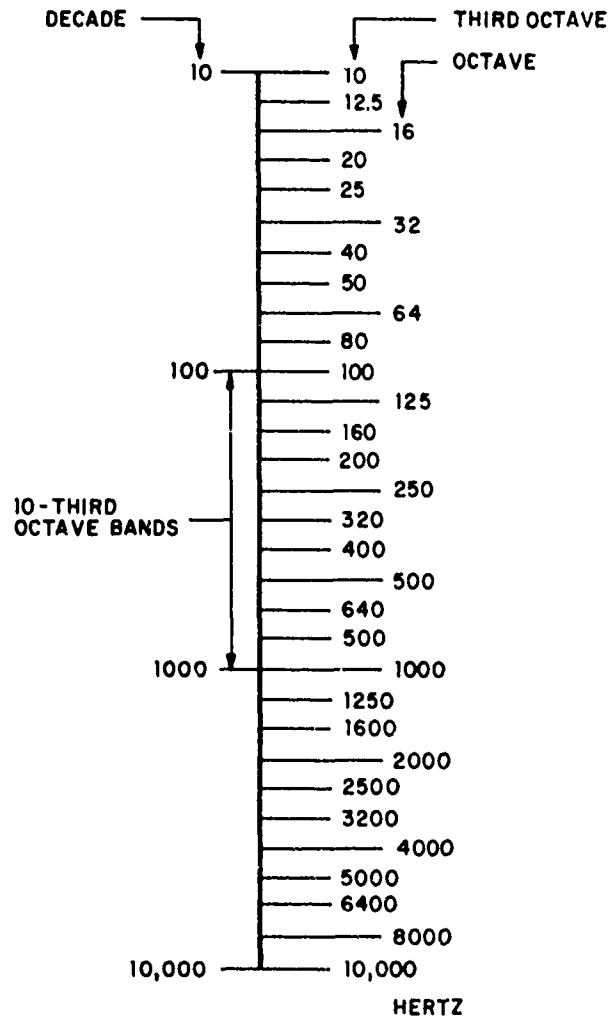

FIG. 7.2

STANDARD CENTER FREQUENCIES FOR ONE-THIRD AND FULL OCTAVE BANDS

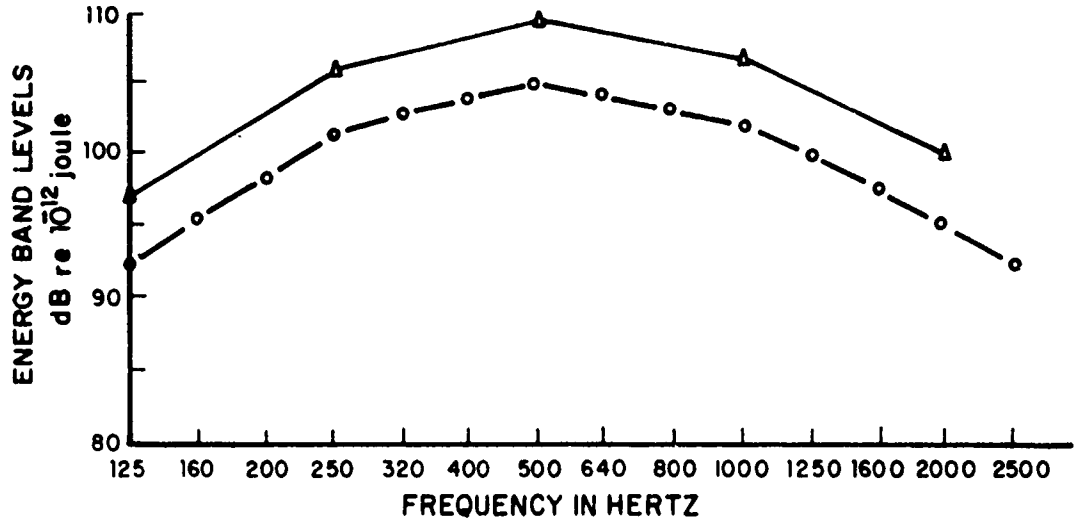

FIG. 7.3

TYPICAL BAND LEVELS SPECTRUM OF VIBRATIONAL ENERGY

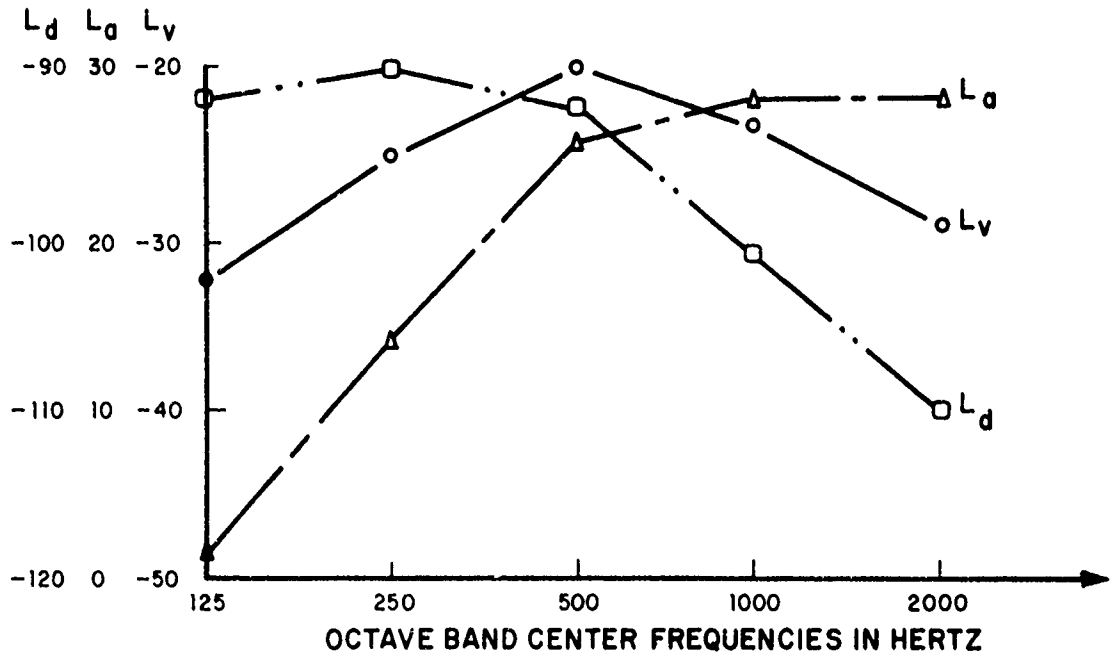

FIG. 7.4

COMPARISONS OF BAND LEVEL RESPONSE SPECTRA FOR DIFFERENT VARIABLES

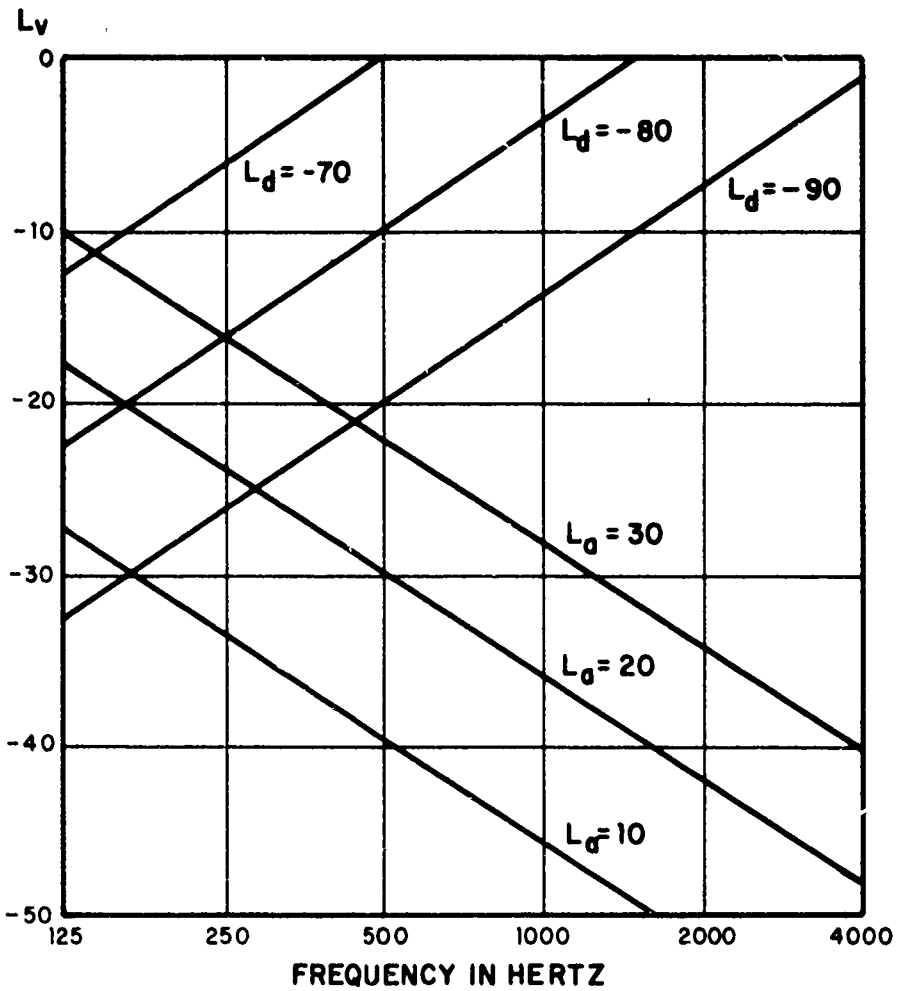

FIG. 7.5

NOMOGRAPH FOR CONVERSION OF DISPLACEMENT RELATED VARIABLES

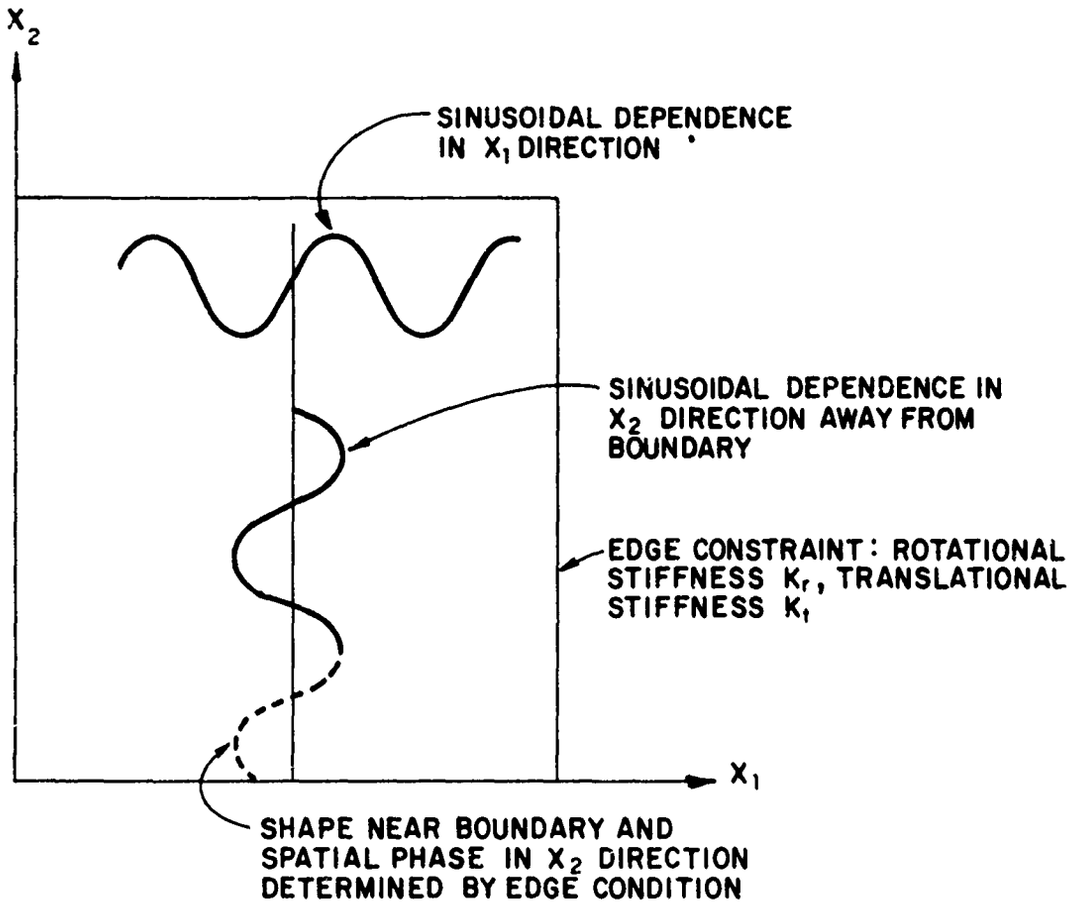

FIG. 7.6

SPATIAL DISTRIBUTION OF DISPLACEMENT ASSUMED IN BOLOTIN "DYNAMIC EDGE EFFECT" MODEL

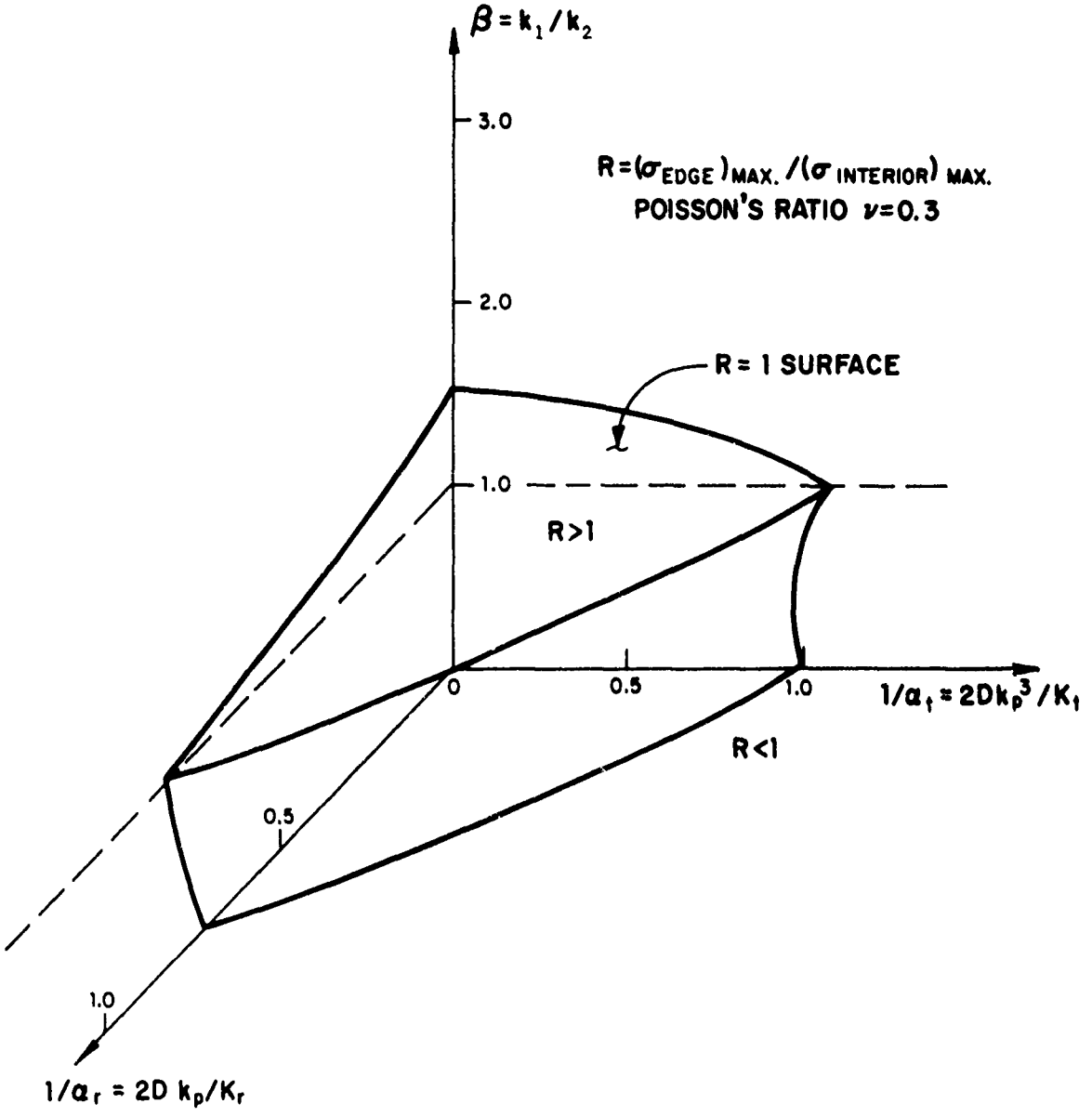

FIG. 7.7

REGIONS OF EDGE AND INTERIOR STRESS DOMINANCE IN PLATES WITH ROTATIONALLY "CLAMPED-LIKE" EDGES ($\alpha_r > \alpha_t$)

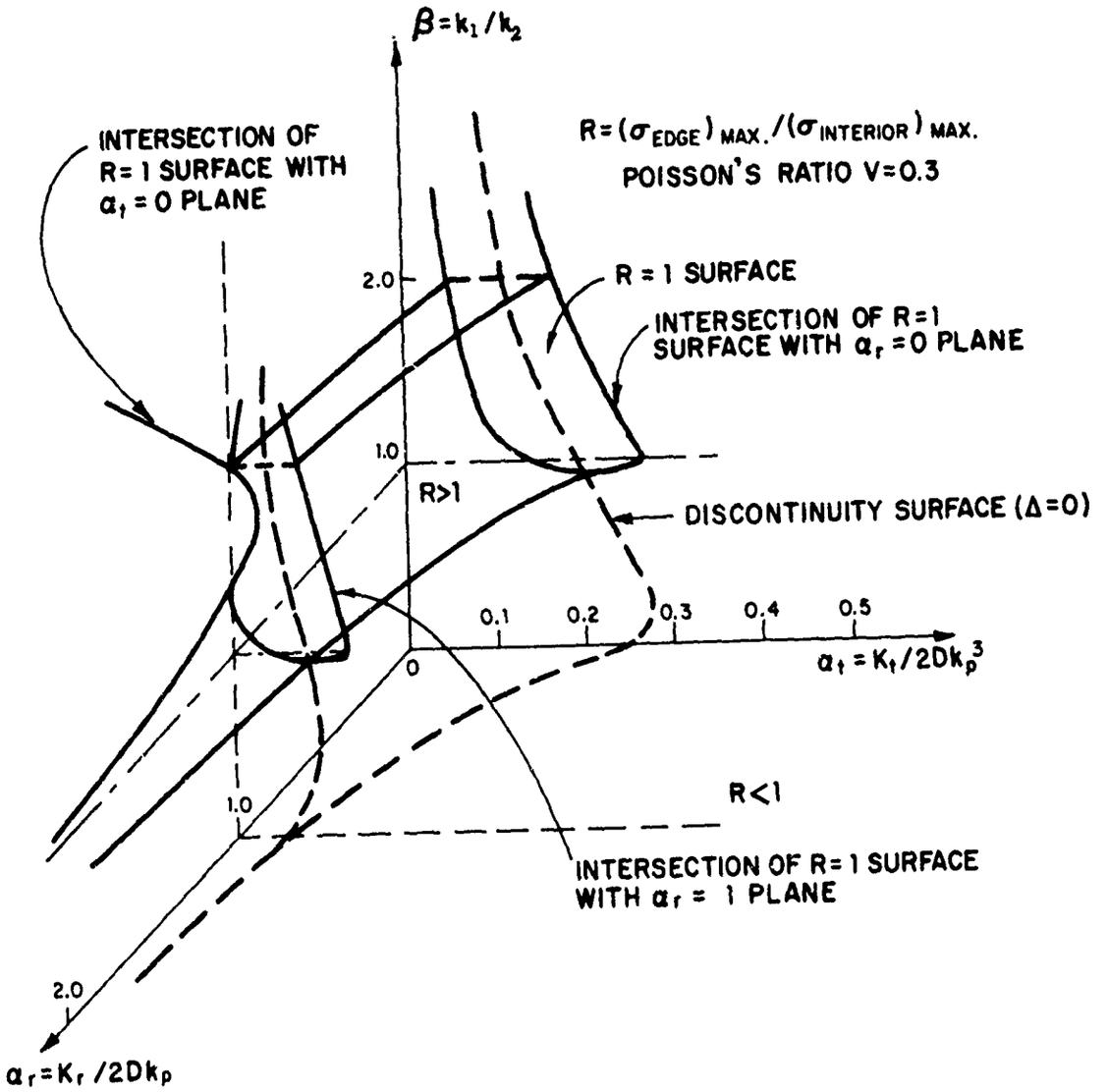

FIG. 7.8

REGIONS OF EDGE AND INTERIOR STRESS DOMINANCE IN PLATES WITH ROTATIONALLY "FREE – LIKE" EDGES ($\alpha_r < \alpha_t$)

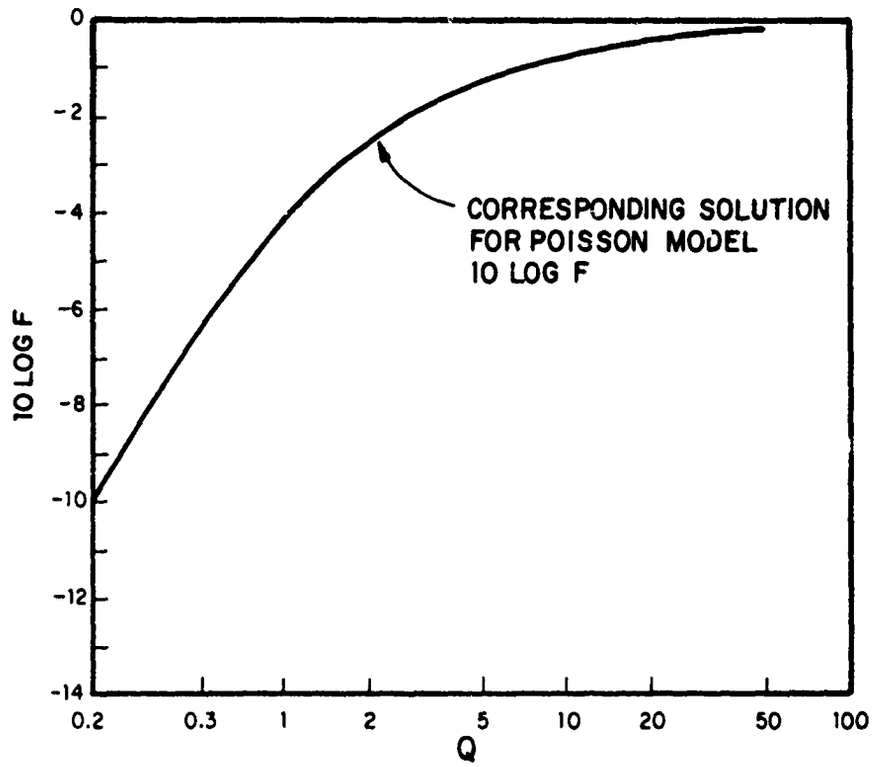

FIG. 7.9

EFFECT OF EXCITATION BANDWIDTH OF RESPONSE VARIANCE

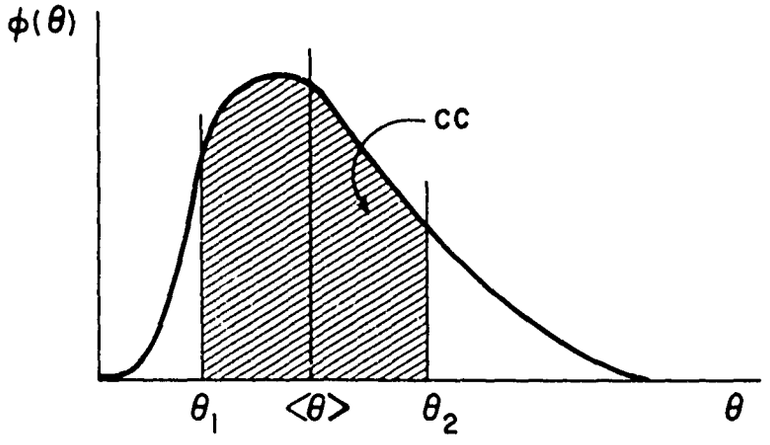

FIG. 7.10

FORM OF RESPONSE PROBABILITY DENSITY

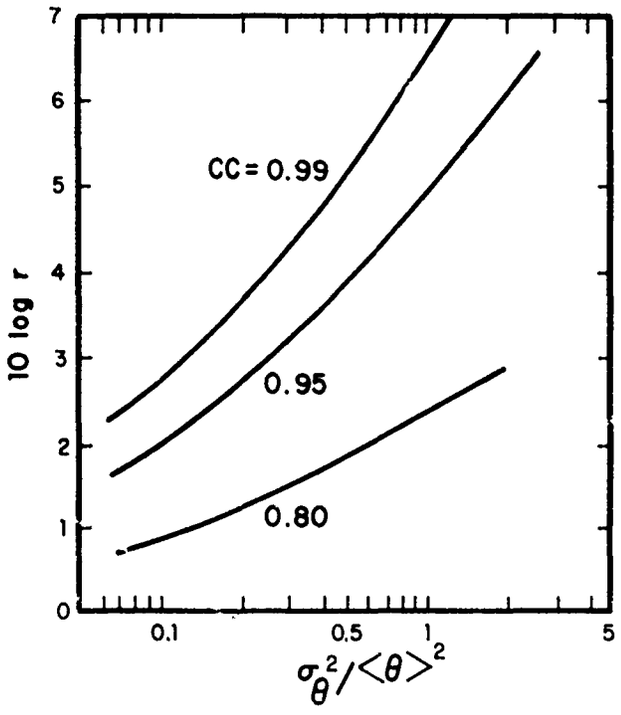

FIG. 7.11
GRAPH OF "SAFETY FACTOR" r AGAINST NORMALIZED VARIANCE

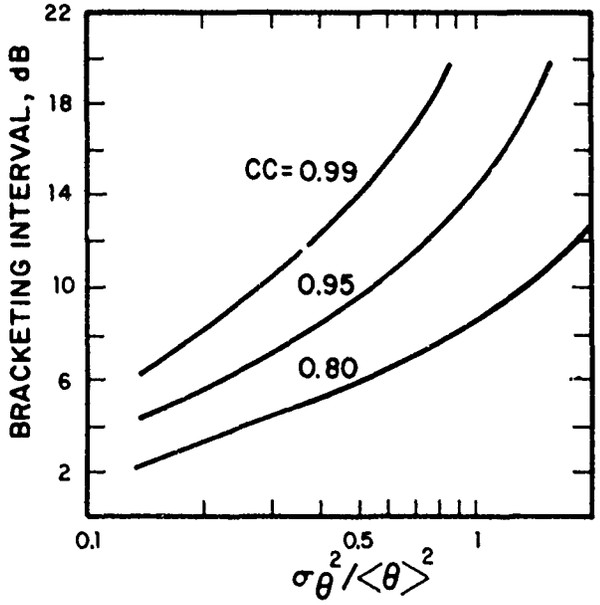

FIG. 7.12
GRAPH OF BRACKETING INTERVAL

CHAPTER 8. ESTIMATING THE ENERGY OF VIBRATION

8.0 Introduction

This chapter is concerned with describing how one obtains an estimate of average system energy from the SEA model and a knowledge of its parameters. In this chapter, the model and its parameter values are assumed to be given. In Chapter 10 we will describe how the model is defined. Parameter values are discussed in Chapter 9. In practical situations, however, in which one deals with effects of minor changes in structural configuration or connections in an overall system that is the same from one situation to the next, then with each modified calculation of system energy, one is basically starting at the point where this chapter commences.

The energy that we solve for is the vibrational energy in the frequency band Δf of each "subsystem". This energy is found as a result of a set of linear simultaneous algebraic equations in which the energy of certain systems and input power to other systems are the known quantities. The unknown energies of the remaining systems are solved for in terms of these known quantities and the system parameters. The system parameters include the number N_i of resonant modes in the frequency band, Δf, of each system, the system damping as measured by the loss factor η, and the coupling loss factor, which we have discussed in Chapter 3 (of Part I) and will discuss further in Chapter 9.

Since this Part II of the report is concerned with engineering procedures, we do not derive the relationships that we use. The derivations of the basic relations were made in Part I. Here, the emphasis is on explaining what must be known to carry out the estimates, and how one applies that information to interpret the estimates.

8.1 How the Overall System is Described

A fairly general SEA model is depicted in Fig. 8.1. It consists of N subsystems, each of which may receive power Π_{in} from an external source (unspecified) and dissipate power Π_{diss} due to the damping of the subsystem.

In addition, power Π_{ij} is transferred between subsystems by the action of coupling forces at the junctions between these subsystems. Finally, the energy of each subsystem is denoted by E_{tot}, and it is this set of energy values that we solve for. Since the energy E_{tot} is the vibrational energy of the subsystem in a frequency band Δf, it is the energy that we began with to make our subsystem response estimates in Chapter 3.

The fundamental relation that we use is that of the conservation of energy for each subsystem, or a balance between power in and out of the subsystem. For the i^{th} subsystem in Fig. 8.1, therefore, we have:

$$\Pi_{i,in} = \Pi_{i,diss} + \sum_{j=1}^{N'} \Pi_{ij} \qquad (8.1.1)$$

where the prime on the sum means that j=1 is excluded. We are able to solve for the system energies because both the dissipated power and transfer power can be related to subsystem energies. The dissipation relation is

$$\Pi_{i,diss} = \omega \eta_i E_{i,tot} \qquad (8.1.2)$$

where η_i is the loss factor previously introduced and $\omega=2\pi f$, where f is the center frequency of the band of interest.

The power transferred from subsystem i to subsystem j was found in Part I to be [see Eq. (3.2.11)]:

$$\Pi_{ij} = \omega \eta_{ij} E_{i,tot} - \omega \eta_{ji} E_{j,tot} \qquad (8.1.3)$$

where the quantities η_{ij} are called coupling loss factors. They are not all independent because they must satisfy the consistency relation

$$N_i \eta_{ij} = N_j \eta_{ji} \tag{8.1.4}$$

where N_i, N_j are the numbers of resonant modes of subsystems i,j in the band Δf.

Placing Eqs. (8.1.2) and (8.1.3) into Eq. (8.1.1) results in the following set of equations:

$$\begin{aligned}
\Pi_{1,in}/\omega &= (\eta_1 + \Sigma_j' \eta_{1j}) E_{1,tot} - \Sigma_j' \eta_{j1} E_{j,tot} \\
\Pi_{2,in}/\omega &= (\eta_2 + \Sigma_j' \eta_{2j}) E_{2,tot} - \Sigma_j' \eta_{j2} E_{j,tot} \\
&\vdots \\
\Pi_{N,in}/\omega &= (\eta_N + \Sigma_j' \eta_{Nj}) E_{N,tot} - \Sigma_j' \eta_{jN} E_{j,tot}
\end{aligned} \tag{8.1.5}$$

The solutions for these simultaneous equations is found in the conventional way. We can, if we wish, express these equations in matrix form:

$$\begin{bmatrix}
\eta_{1,tot} & -\eta_{21} & -\eta_{31} & \cdots & -\eta_{N1} \\
-\eta_{12} & \eta_{2,tot} & -\eta_{3,2} & & -\eta_{N,2} \\
-\eta_{13} & -\eta_{2,3} & \eta_{3,tot} & & -\eta_{N,3} \\
\vdots & \vdots & \vdots & & \vdots \\
-\eta_{1N} & -\eta_{2N} & -\eta_{3N} & & \eta_{N,tot}
\end{bmatrix}
\begin{Bmatrix}
E_{1,tot} \\ E_{2,tot} \\ E_{3,tot} \\ \vdots \\ E_{N,tot}
\end{Bmatrix}
=
\begin{Bmatrix}
\Pi_{1,in}/\omega \\ \Pi_{2,in}/\omega \\ \Pi_{3,in}/\omega \\ \vdots \\ \Pi_{N,in}/\omega
\end{Bmatrix} \tag{8.1.6}$$

This set of N simultaneous equations is appropriate if only values of input power are known. If, however, the energy $E_{i,tot}$ of any subsystem is known by measurement or some other means, then the energy balance equation (8.1.1) for that subsystem is removed, reducing the order of the set of equations and the known energy becomes a "source" term in each equation and is moved to the right hand side of the new set of simultaneous equations.

The diagonal terms of the coefficient matrix $\eta_{i,tot}=\eta_i+\Sigma_j\eta_{ij}$ may be thought of as total loss factors for each subsystem. This total loss factor includes not only dissipative losses, but also the effects of transfer losses to other subsystems. Of course, whether or not the loss to other subsystems actually occurs will depend on the energy that they contain.

If we call the coefficient matrix in Eq. (8.1.6) N, then it may be written

$$N \cdot \vec{E}_t = \vec{\Pi}_{in}/\omega \qquad (8.1.7)$$

where $\vec{E}_t$ and $\vec{\Pi}_{in}$ are N-dimensional vectors having components $E_{i,tot}$ and $\Pi_{i,in}$ respectively, found by operating on Eq. (8.1.7) from the left with the inverse of N, defined as N^{-1};

$$N^{-1} \cdot N \cdot \vec{E}_t = I \cdot \vec{E}_t = \vec{E}_t = N^{-1} \cdot \vec{\Pi}_{in}/\omega \qquad (8.1.8)$$

The elements of the inverse of N are $(-)^{i+j}M_{ij}/\Delta$, where M_{ij} is the minor determinant formed by eliminating the i^{th} row and j^{th} column of the transpose of the matrix N, and Δ is the determinant of N. The identity matrix I operating on the vector $\vec{E}_t$ leaves it unchanged.

The calculations involved in finding N^{-1} and, consequently, $\vec{E}_t$ must be carried out for each frequency band Δf of interest. Since the parameters such as Π_{in}, η_i, and η_{ij} will generally vary with frequency, even the set of

algebraic calculations involved in solving Eq. (8.1.6) can get quite cumbersome. There are computer routines available, however, that can reduce this effort considerably if the number of subsystems N is large. When N is less than 4, however, the saving of effort is usually not worthwhile and formal algebraic solution is adequate.

Example: 2 Subsystems

The case in which there are only two subsystems applies to very many situations of practical interest; the situation depicted in Fig. 6.1, for example. Equations (8.1.6) in this case are

$$\begin{Bmatrix} \eta_1+\eta_{12} & -\eta_{21} \\ -\eta_{12} & \eta_2+\eta_{21} \end{Bmatrix} \begin{Bmatrix} E_{1,tot} \\ E_{2,tot} \end{Bmatrix} = \begin{Bmatrix} \Pi_{1,in}/\omega \\ \Pi_{2,in}/\omega \end{Bmatrix} \qquad (8.1.9)$$

The determinant of the coefficient matrix is

$$\begin{aligned} \Delta &= (\eta_1+\eta_{12})\ (\eta_2+\eta_{21}) - \eta_{12}\eta_{21} \\ &= \eta_1\eta_2+\eta_2\eta_{12}+\eta_1\eta_{21} \end{aligned} \qquad (8.1.10)$$

Thus, the expression for $E_{1,tot}$ is

$$E_{1,tot} = \left[\frac{\Pi_{1,in}}{\omega}\ (\eta_2+\eta_{21})+\frac{\Pi_{2,in}}{\omega}\ \eta_{21}\right]\Delta^{-1} \qquad (8.1.11a)$$

$$E_{2,tot} = \left[\frac{\Pi_{1,in}}{\omega}\eta_{12} + \frac{\Pi_{2,in}}{\omega}(\eta_1+\eta_{12}) \right] \Delta^{-1} \qquad (8.1.11b)$$

There is a simplification of this result that is very important from the point of view of estimation. Suppose that only system 1 has external excitation. Then $\Pi_{2,in}=0$ and

$$E_{1,tot} = \frac{\Pi_{1,in}}{\omega} (\eta_2+\eta_{21})(\eta_1\eta_2+\eta_2\eta_{12}+\eta_1\eta_{21})^{-1}$$

and, therefore,

$$E_{2,tot} = E_{1,tot} \frac{\eta_{12}}{\eta_2+\eta_{21}} \qquad (8.1.12)$$

This relation allows us to estimate $E_{2,tot}$ if $E_{1,tot}$ is known (by calculation of the response to the environment or by measurements on a similar system.) Only one coupling loss factor need be known since the consistency relation Eq. (8.14) allows the other to be calculated if the mode counts in the band (or average frequency separation of the modes for each system) are known.

Example: 3 Subsystems

Three element systems usually arise when a resonant element (such as a wall) intervenes between two resonant systems of interest. The general equations for this case are

$$\begin{Bmatrix} \eta_1+\eta_{12}+\eta_{13} & -\eta_{21} & -\eta_{31} \\ -\eta_{12} & \eta_2+\eta_{21}+\eta_{23} & -\eta_{32} \\ -\eta_{13} & -\eta_{23} & \eta_3+\eta_{32}+\eta_{31} \end{Bmatrix} \begin{Bmatrix} E_{1,tot} \\ E_{2,tot} \\ E_{3,tot} \end{Bmatrix} = \begin{Bmatrix} \Pi_{1,in}/\omega \\ \Pi_{2,in}/\omega \\ \Pi_{3,in}/\omega \end{Bmatrix} \qquad (8.1.13)$$

The determinant Δ of the N-matrix is quite complicated and will not be written out here. The matrix inverse to N is found to be

$$N^{-1}=\frac{1}{\Delta}\begin{Bmatrix} \eta_{2t}\eta_{3t}-\eta_{23}\eta_{32} & \eta_{21}\eta_{3t}+\eta_{23}\eta_{31} & \eta_{21}\eta_{32}+\eta_{31}\eta_{2t} \\ \eta_{12}\eta_{3t}+\eta_{13}\eta_{32} & \eta_{1t}\eta_{3t}-\eta_{13}\eta_{31} & \eta_{1t}\eta_{32}+\eta_{31}\eta_{12} \\ \eta_{12}\eta_{23}+\eta_{2t}\eta_{13} & \eta_{1t}\eta_{23}+\eta_{21}\eta_{13} & \eta_{1t}\eta_{2t}-\eta_{12}\eta_{21} \end{Bmatrix} \qquad (8.1.14)$$

where $\eta_{1t} \equiv \eta_1 + \eta_{12} + \eta_{13}$, etc.

To obtain a simple result that illustrates the procedure, but that is <u>not</u> representative of many situations of interest, first assume that only subsystem 1 is externally excited so that $\Pi_{2,in} = \Pi_{3,in} = 0$. Secondly, we set $\eta_{13}=\eta_{31}=0$ so that the three subsystems form a chain (1)→(2)→(3). With these assumptions

$$E_{1,tot} = \Pi_{i,in}(\eta_{2t}\eta_{3t}-\eta_{23}\eta_{32})/\omega\Delta \qquad (8.1.15)$$

$$E_{2,tot} = \Pi_{i,in}(\eta_{12}\eta_{3t}+\eta_{13}\eta_{32})/\omega\Delta = E_{1,tot}\,\frac{\eta_{12}\eta_{3t}}{\eta_{2t}\eta_{3t}-\eta_{23}\eta_{32}}$$

$$E_{3,tot} = \Pi_{i,in}(\eta_{12}\eta_{23}+\eta_{2t}\eta_{13})/\omega\Delta = E_{2,tot}\,\frac{\eta_{23}}{\eta_{3t}}$$

$$= E_{1,tot}\,\frac{\eta_{12}\eta_{23}}{\eta_{2t}\eta_{3t}-\eta_{23}\eta_{32}}$$

If we assume that $\eta_{23} << \eta_{2t}$ and $\eta_{32} << \eta_{3t}$, (coupling loss small compared to internal damping)

$$E_{3,tot} = E_{2,tot} \frac{\eta_{23}}{\eta_{3t}} = E_{1,tot} \frac{\eta_{12}}{\eta_{2t}} \cdot \frac{\eta_{23}}{\eta_{3t}} \qquad (8.1.16)$$

Clearly, the result in Eq. (8.1.16) is a product of two ratios of the kind shown in Eq. (8.1.12).

8.2 Alternative Form of the Energy Equations

In certain instances, we may know the energy of vibration of the subsystems in the absence of coupling. The uncoupled condition is obtained, as explained in Part I, by causing the response of all other subsystems to vanish. Thus, a boundary between subsystems in which motions are the response variable becomes "fixed". If force (pressure for example) is the response variable, then the boundary becomes "free" when the subsystems are decoupled or "blocked".

The power flow between two subsystems having total blocked energies

$$E_{1,tot}^{(b)} \quad \text{and} \quad E_{2,tot}^{(b)}$$

is given by

$$\Pi_{12} = \omega a_{12} E_{1,tot}^{(b)} - \omega a_{21} E_{2,tot}^{(b)} \qquad (8.2.1)$$

where the coefficients a_{ij} are different from the η_{ij}'s that appear in Eq. (4.1.3), but satisfy the same consistency relation,

$$N_1 a_{12} = N_2 a_{21} \quad . \qquad (8.2.2)$$

The "blocked energy" relation in this form can only be applied to two subsystem problems, so that if system 2 does not have external excitation, one has

$$E_{2,tot} = \frac{\Pi_{12}}{\omega\eta_2} = \frac{a_{12}}{\eta_2} E_{1,tot}^{(b)} \qquad (8.2.3)$$

since $E_{2,tot}^{(b)} = 0$ if there is not external excitation of system 2. The result in Eq. (8.2.3) is very near to that in Eq. (8.1.12). Evaluation of the coefficients a_{ij} is discussed in Chapter 9.

Fundamentally, the blocked energy of a subsystem is simply a measure of the input power, since

$$E_{tot}^{(b)} = \Pi_{in}/\omega\eta \ .$$

Thus, any of the relations in paragraph 8.1 that express actual energy of vibration in terms of input power may also be modified to express vibrational energy in terms of blocked energy.

8.3 Parameter Evaluation Using the Energy Equations

The energy equations can also be used in conjunction with experiments to calculate the parameters (coupling loss factors and loss factors) for a system. Eqs. (8.1.5) are linear in these parameters. Thus, if we measure the energy in each subsystem for a known set of input power values $\Pi_{i,in}$ we can generate a set of linear simultaneous equations for the η_i's and η_{ij}'s.

If we have N subsystems, then the total number of parameters in N^2 which consists of N loss factors and N(N-1) coupling loss factors. Of course, we could use the consistency relation Eq. (8.1.4) to reduce the number of required coupling loss factors to N(N-1)/2 and an equal number of mode count ratios could also be found.

Any one experiment (for example, setting $\Pi_{2,in} \neq 0$ and $\Pi_{1,in} = \Pi_{3,in} = \ldots = \Pi_{N,in} = 0$ and measuring all the $E_{j,tot}$ values) generates N simultaneous equations for the parameters. Therefore, we must perform N independent measurements (for example, sequentially injecting known power into each of the subsystems and measuring the resulting energies) to obtain the necessary N^2 equations. Of course, any parameter values we may know will reduce the number of measurements accordingly, although we may choose to build some redundancy into the parameter evaluation for greater accuracy or as a check on the procedures.

We should emphasize that the procedure for parameter evaluation just described is not an established method. There has been only partial success for it in the cases for which it has been tried. The difficulties have shown themselves in the form of negative values of parameters. This impossible answer is the result of small errors that occur in each set of measurements that mounts up as one proceeds through the calculations. There is no reported analysis of the sensitivity of the derived parameter values to small errors in measured energy and input power values. Such an analysis is needed to establish the use of the energy equilibrium equations as a useful technique for determining SEA parameter values.

8.4 Useful Approximations and Simplifications

In most SEA calculations, three or four interconnected subsystems may suffice to describe the overall system, but it can easily happen that more subsystems are required. Even though the equations introduced in paragraph 8.1 are readily solved for such numbers of unknowns, it is desirable in many cases to seek ways to abbreviate the calculations.

We may want to simplify the calculations in order to get a "quick look" answer to compare with the more detailed calculation. Or, we may know some of the parameter values only approximately and seek to make sure we are not spending effort on evaluating unneeded parameters. Also, it is sometimes easier to get a better idea of the energy flow process from the simpler calculations so that changes in vibration levels that would result from changing parameter values can be inferred.

The principles of simplification may be listed quite simply. They will not all be applicable or useful in any

particular system, but by using them it is usually possible to get answers that are of sufficient accuracy. The principles are as follows:

(1) Compute the approximate modal energies of the directly excited subsystems using $E_{tot}=\Pi_{in}/\omega\eta$. The subsystems with the high modal energies E_{tot}/N are usually those that will "drive" the other subsystems.

(2) Identify the path(s) from the most energetic subsystem to the subsystem of interest. Concentrate on those paths that would appear to be dominant based on the relative sizes of coupling and dissipation loss factors.

(3) When the loss factor of a subsystem is larger than the coupling loss factor connecting it to a more energetic system, ignore the coupling loss factors in the total damping η_{it}. When the loss factor is smaller than the coupling loss factor, assume the subsystem in question has the same modal energy as its more energetic neighbor.

(4) If a neighboring subsystem has less modal energy than the subsystem being studied and it is not "in line" to another subsystem of interest, ignore it or at most include the coupling loss factor to it as part of the subsystem damping.

The result of these approximations will generally lead to a "chain" sort of calculation as illustrated by the results in Eqs. (8.1.12) and (8.1.16). The energy of the adjoining subsystem is found by taking the product of the energy of the source subsystem times the ratio of coupling loss factor to damping for the receiving subsystem. This process is then repeated for all subsystems along the line.

To illustrate the application of this simplified approach, consider the diagram shown in Fig. 8.2 that models an airborne computer. The exterior panels and frame of the computer are excited directly by the environment, and we are interested in knowing the dominant path that the energy takes getting to the circuit boards and what the resulting vibration levels will be.

Suppose that the input power to the computer frame is known to be $\Pi_{1,in}=0.1$ watts in the 250 Hz octave band (we will describe ways of computing input power in the following chapter). Our first task is to compute the energy of system 1.

Noting that η_{12} and η_{14} are both small compared to η_1, we ignore the coupling and compute

$$E_{1,tot} = \Pi_{1,in}/\omega\eta_1 = 6.4x10^{-3} \text{ joules,} \qquad (8.4.1)$$

and a modal energy of

$$E_1 = E_{1,tot}/N_1 = 6.4x10^{-4} \text{ joules.} \qquad (8.4.2)$$

Using Eq. (8.1.12) and ignoring coupling losses compared to dissipation, we get

$$E_{2,tot} = E_{1,tot} \frac{\eta_{12}}{\eta_2} = 6.4x10^{-6} \text{ joules} \qquad (8.4.3)$$

and

$$E_{4,tot} = E_{1,tot} \frac{\eta_{14}}{\eta_4} = 6.4x10^{-4} \text{ joules,} \qquad (8.4.4)$$

corresponding to modal energies of E_2=6.4x10^{-8} and E_4 = 3.2x10^{-5} joules respectively.

The energy of the circuit boards due to the air path is given by

$$E^{(air)}_{3,tot} = E_{2,tot} \frac{\eta_{23}}{\eta_3} = 6.4x10^{-10} \qquad (8.4.5a)$$

while that due to the structural path is

$$E_{3,tot}^{(struct)} = E_{4,tot} \frac{\eta_{43}}{\eta_3} = 6.4x10^{-7} \qquad (8.4.5b)$$

Obviously, the structural path is more significant in this example. The modal energy of the circuit board is, therefore:

$$E_3 = E_{3,tot}/N_3 = 1.3x10^{-7} \text{ joules.} \qquad (8.4.6)$$

Since E_3 is greater than E_2, the actual energy flow will be from the circuit board to the air space. That is, the boards are radiating more energy to the air space than they receive from the surrounding air. Of course, this conclusion is dependent on the parameters arbitrarily chosen for the example, but the procedure shown here will usually supply results of sufficient accuracy and provide insight into the physical principles involved.

8.5 Summary

In this chapter, we have shown how energy estimates can be made from the equilibrium relations of SEA. These estimates must use values of SEA parameters, which will be discussed in the following chapter. The estimate is obviously also based on a model of the system. Nevertheless, the work in this chapter will be sufficient to tell us how the system might be changed to reduce the response to an acceptable level.

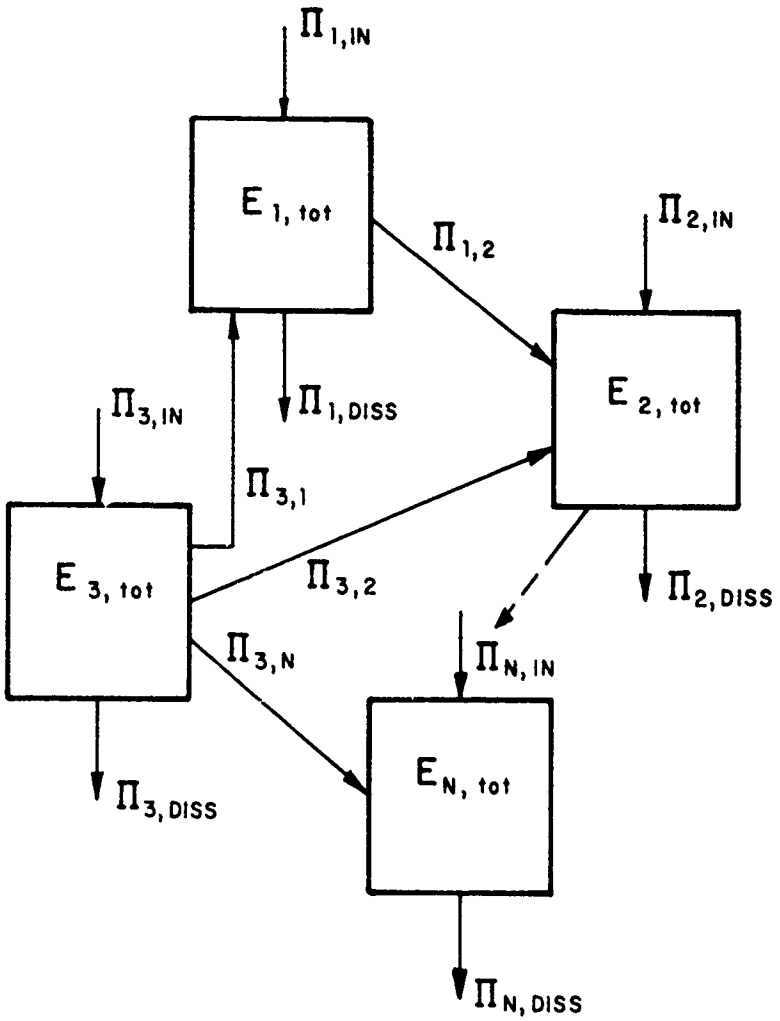

FIG. 8.1

AN SEA MODEL OF SYSTEM CONTAINING N SUBSYSTEMS

Preceding page blank

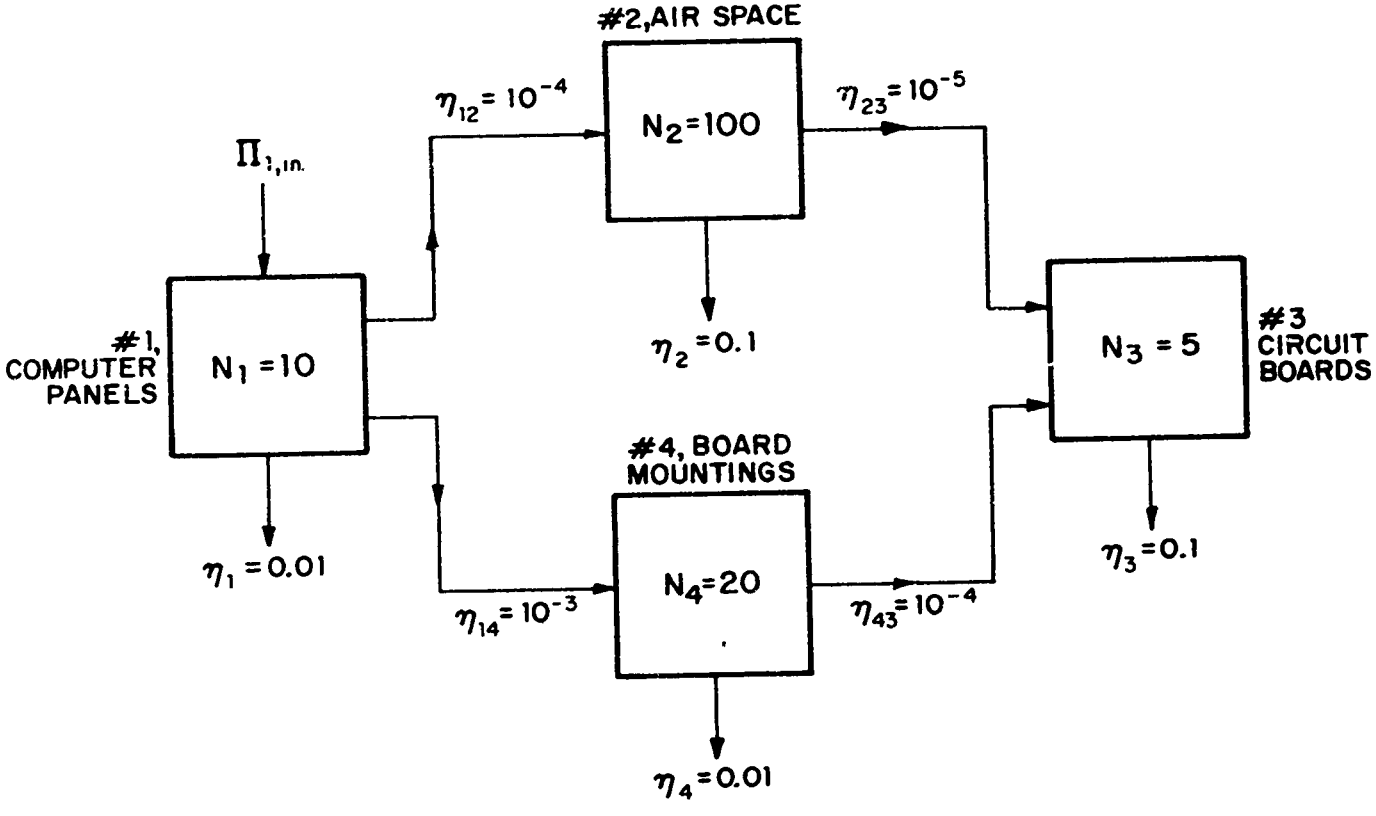

FIG. 8.2

SEA MODEL OF CIRCUIT BOARD IN COMPUTER FRAME WITH PARAMETERS FOR THE 250 Hz OCTAVE BAND

CHAPTER 9. THE MEANING AND USE OF SEA PARAMETERS

9.0 Introduction

In the preceding chapters we have shown how to interpret energy estimates in terms of dynamical response and how the energy estimate itself is computed in terms of the SEA model and its associated parameters. In this chapter we discuss the SEA parameters in more detail, describing what they are from a physical point of view and how one goes about getting values for them.

The parameters govern the power input to each subsystem, the dissipation of energy, energy storage, and energy transfer between subsystems. Section II of this report is a fairly extensive tabulation of SEA parameters, so that we shall not duplicate that work here. Rather, our emphasis is on explaining the parameters and how they are used in the calculations. To obtain formulas or values for the parameters, reference should be made to Section II.

9.1 Dissipation Parameters

The dissipation of stored energy in each subsystem is measured by the parameter η_i, termed the "loss factor." The loss factor is a measure of the ratio of energy dissipated per unit time (one second) to average energy stored

$$\eta = \frac{\Pi_{diss}}{2\pi f E_{stored}} \quad . \tag{9.1.1}$$

Defined in this way, the loss factor is the reciprocal of the "quality factor" Q used in electrical engineering: $\eta = 1/Q$. The damping parameter commonly used in mechanical engineering is ξ, the ratio of damping to critical damping, and $\eta = 2\xi$.

The loss factor η is occasionally introduced in structural vibration problems as the phase angle of a complex Young's modulus: $E \rightarrow E_o(1-i\eta)$. In other cases, the damping is introduced via a viscous element of value R, in which case, $\eta = R/\omega M$ where M is the subsystem mass. Of course, if the dis-

sipation is actually occurring at the joints or rivet points, neither of these damping descriptions is really descriptive of the physical dissipation process.

It is occasionally asserted that a loss factor description of damping implies a very particular mechanism of dissipation and that erroneous estimates will occur if the actual mechanism is not the assumed ones. In general, response estimates are slightly dependent on the mechanism of damping, but the differences are very small if the loss factor is in the range η=0.1 or less. Most structures have damping much less than this, so that we need not imply any specific damping mechanism by introducing the loss factor.

In acoustical systems, the dissipation is normally expressed by the rate of decay of sound level after the source of excitation has been turned off. This "decay rate", DR (in dB/sec), is given by

$$DR = 27.3\, f\eta$$

where f is the center frequency of the band Δf in which the data is taken. Typical values of decay rate for the small acoustical spaces associated with aircraft are of the order of 100 dB/sec or greater. It is often difficult to measure such rapid rates of decay with standard acoustical apparatus. In such a circumstance one may use an oscilloscope for the display.

Damping is probably the single most important parameter in establishing subsystem response because we are dealing with resonant modes. A 10% error in damping will result in a 1 dB error in the response estimate, and a 100% error in damping results in a 3 dB change in estimated response. When coupling factors are larger than the damping, the damping plays a less important role in setting response levels - there is then a tendency for energy equipartition with the adjacent subsystem (energy equipartition means equal modal energies of the subsystems connected by the "large" coupling loss factor).

Damping may be enhanced by addition of "applied damping" treatments. This might consist of a single layer of visco-elastic material adhered to the panel. Such a treatment is

a "free" or "unconstrained" layer, as diagrammed in Fig. 9.1a. A more complex damping treatment that does not have as large a weight penalty is the constrained layer, shown in Fig. 9.1b. An alternative that uses a stiff spacer amplifies the strain in the viscoelastic layer as shown in Fig. 9.1c. A variant of this design uses a constrained layer spaced away from the base panel. Finally, to reduce "drumming" vibration of a single mode, the damping element can employ resonance to amplify strain and provide a high degree of damping over a fairly narrow frequency range as shown in Fig. 9.1d.

9.2 Power Transfer Parameters

The power flow between subsystems may be described either in terms of the actual energies of vibration, or in terms of the energy of vibration that they would have in the absense of coupling. In the first case, the parameter of interest is the coupling loss factor, η_{ij}. There is no general name for the second parameter, but it has been denoted in Part I as a_{ij}. The formulas for power flow from subsystem i to subsystem j are as follows:

$$\Pi_{ij} = \omega\eta_{ij}E_{i,tot} - \omega\eta_{ji}E_{j,tot} \qquad (9.2.1a)$$

$$= \omega a_{ij}E^{(b)}_{i,tot} - \omega a_{ji}E^{(b)}_{j,tot} \qquad (9.2.1b)$$

Equation (9.2.1a) applies to any situation, but Eq. (9.2.1b) has only been demonstrated to apply to 2-subsystem situations.

The principle utility of a_{ij} is that it allows for a computational algorithm for η_{ij}. This relation was derived in Part I and will be used in Section II of the report. To illustrate how this works, however, suppose the two subsystems are joined at a point and that a point input impedance $Z_{i,in}$ can be defined for each at the attachment location. Then, the value of a_{ij} is

$$a_{ij} = \frac{2\Delta f}{\pi\omega N_i} \frac{R_{i,in}\,R_{j,in}}{|Z_{i,in} + Z_{j,in}|^2} \qquad (9.2.2)$$

A general relation between the coupling loss factor η_{ij} and the parameter a_{ij} may be found when the j^{th} system becomes "dense", i.e., $N_i f\eta_i/\Delta f \gg 1$. In this circumstance, as shown in Part I [Eq. (4.1.21)]

$$\eta_{ij} = a_{ij} \, (1-a_{ij}/\eta_i)^{-1} \tag{9.2.3}$$

In the case where subsystem i has a single mode, $N_i = 1$, then one can show that [Eq. (3.4.6)],

$$\eta_{ij} = R_{i,in}/\omega M_j \tag{9.2.4}$$

where M_j is the total mass of the j^{th} subsystem. When the i^{th} system has many modes, $N_i \gg 1$, one can show that $\eta_{ij} \to a_{ij}$. Thus, the evaluation of the coupling loss factor can be expressed entirely in terms of junction impedances.

The theoretical calculation of coupling loss factors can get quite complicated for one or more of the following reasons:

1. Neither system is "dense"; only a few modes of each of the two subsystems resonate in the band of interest.

2. The junction is not a point, but extends along a line or over an area. More complex impedance functions are necessary to describe the interaction in this case.

3. The actual interaction may not be "scalar", but "vectorial". This is particularly true when the interacting systems are structures, since a proper description of the interacting forces may include moments and shear and compressional forces. Our purpose in this chapter is to indicate the process by which one obtains the coupling parameter. The detailed methods and available results are covered in Section II of this Part of the report.

We have shown that the coupling loss factor can be related to the junction impedance. It can also be related to other parameters that are well known in certain specialized fields, such as sound transmission between rooms. In that field, the sound transmission is defined by a "transmissibility" τ, which is related to the well known "transmission loss" TL by

$$TL \equiv - 10 \log \tau. \tag{9.2.5}$$

The relation between coupling loss factor and τ is simply

$$\eta_{ij} = \frac{A_w c}{2\omega V_i} \tau \tag{9.2.6}$$

where A_w is the area of the wall through which the sound is "leaking", c is the speed of sound and V_i is the volume of room i. Thus, all the data available on TL for various wall constructions becomes a source of information of coupling loss factors between subsystems that are acoustical spaces.

The experimental determination of coupling parameters is usually approached along lines indicated in Chapter 8. A system has power injected into it in a simply way and the resulting response (or subsystem energy) is measured. From this data and a knowledge of the loss factors in the system, the coupling loss factor may be found. This is the manner in which the transmissibility between rooms is found. From Eq. (8.1.12), a measurement of the ratio

$$\frac{E_{2,tot}}{E_{1,tot}} = \frac{\eta_{12}}{\eta_2 + \eta_{21}} \tag{9.2.7}$$

is sufficient to determine η_{12} if η_2 is known and $\eta_{21} << \eta_2$. Thus, if the junction of interest is reproduced between two test structures, structure 1 is excited in some convenient way, and the damping of the receiving structure (#2) is

adjusted to satisfy $\eta_2 >> \eta_{21}$, then a simple measure of the vibrational energies of the two structures will determine η_{12}.

9.3 Modal Count of Subsystems

The modal count N_i of a subsystem is the number of modes of that subsystem that resonate in the band Δf under consideration. In some systems the number may be of the order of unity, in others (particularly acoustical subsystems at higher frequencies) the number may be in the thousands. Basically, the mode count is a measure of the number of modes available to accept and store energy.

In SEA work, the modal count is often expressed in terms of a modal density n so that

$$N_i = n_i \Delta f \ . \tag{9.3.1}$$

Since the modal count will vary from one band to another, we may indicate that the modal density will vary with f, the center frequency of the band, by writing it $n_i(f)$. Most subsystems have modal densities that vary with frequency.

In Chapter 7, we expressed the modal density $n_i(f)$ in terms of its reciprocal, the average frequency separation between resonant modes,

$$\delta f_i = 1/n_i(f) \tag{9.3.2}$$

One may also find the frequency separation expressed in terms of radian frequency

$$\delta \omega_i = 1/n_i(\omega) = 2\pi\delta f_i = 2\pi/n_i(f) \tag{9.3.3}$$

and, consequently, $n_i(\omega) = n_i(f)/2\pi$.

Most SEA formulas that are expressed in terms of modal density can be converted to modal count by using Eq. (9.3.1). This is particularly true in dealing with a system that only has one mode in the band of interest Δf. It also applies to cases in which the subsystem may have several modes, but we may wish to concentrate our interest on a single resonant mode. In this case, $N_i=1$ and $n_i(f)=1/\Delta f$ and <u>not</u> $1/\delta f_i$. Note that the fundamental quantity in all cases is the mode count N_i, and the modal density is a derivated quantity.

The modal count may be found by both experimental and computational procedures. We shall review both methods in Section II. Here we describe briefly these procedures as a way of determining the most appropriate method in the preliminary design process. Very often several of these alternatives will be possible ways of getting a modal count. One is not faced with this dilemma of choice very often with the other SEA parameters.

The only really verified way of measuring the modal count is to excite the subsystem with a pure tone and observe the response at a second location. The frequency is then swept slowly over the band Δf and the response peaks are counted. Of course, only modes that are non-vanishing at the excitation and observation points will show-up in the response. For this reason, one should select those locations carefully; either at a "corner" location for acoustical systems or along a free edge of a structure.

One will also miss modes if their average spacing δf_i becomes of the same order as their resonance bandwidth $f\eta_i$. The equality

$$\delta f_i = f\eta_i \tag{9.3.4}$$

is the condition of modal overlap and marks the frequency range in which one will begin missing modes because they are too close together to be resolved. It is this limitation that the second procedure, the "point conductance" method is proposed to avoid. This method relies on the result that a mean square force $\langle f^2 \rangle$ in the band Δf applied at an "average" point on the subsystem will result in an injected power [see Eq. (2.2.24)],

$$\Pi_{in} = \langle f^2 \rangle / 4M_i \delta f_i \ , \qquad (9.3.5)$$

and since the mass M_i is known and presumably $\langle f^2 \rangle$ and Π_{in} can be measured, we can find δf_i. This procedure is more complicated than the simpler frequency sweep method and must be considered less well established at present.

There have been many theoretical studies of modal density for both acoustical and structural systems. Generally, the modal density calculations, when tested experimentally, have turned out to be fairly reliable. Modal density is one of the easier parameters to calculate and it seems quite sensible to calculate it if at all possible. In many cases, it will turn out that the appropriate formulas for this calculation are available.

The following is a partial list of system elements for which calculations of modal density exist:

1. Flat plates with various boundary restraints,
2. Flat plates of complex construction including layered plates,
3. Shells and shell segments, including spheres, cones, and cylinders,
4. Acoustical spaces of most shapes, including rectangular, spherical, cylindrical; and volumes representing combinations of these,
5. Various beam and girder shapes including flexural and torsional deformations.

Fortunately, modal count tends to be an extensive property of a system. That is, the total mode count may be estimated by adding the number of modes expected for the various parts of the system. In this way, mode count can be predicted for fairly complex structures.

As an example, consider the estimation of modal count for the equipment shelf shown in Fig. 9.2. Suppose that the two end plates have a diameter of 1 ft and the shelf is 3 ft

long, consisting of four 4 inch webs. This complicated structure is made up of six plates of varying shapes, but it is known that the mode count of a plate of thickness h and area A is given by

$$N = \frac{\sqrt{3}A}{hc_\ell} \Delta f \ . \qquad (9.3.6)$$

Since $h = 3/16$ in. and $c_\ell = 17{,}000$ ft/sec, (the speed of sound in the plate material) are the same for all six plate segments, the total mode count is found by adding that due to the parts, or by using the total area of the structure, which is

$$A_{tot} = (2\ \frac{\pi D^2}{4}) + 4(3)\ (1/3) = 1.6 + 4 = 5.6\ ft^2 \qquad (9.3.7)$$

to give a mode count

$$N = \frac{(1.7)\ (5.6)}{(0.03)\ (17{,}000)} \cdot \Delta f = 1.9 \times 10^{-2} \Delta f \qquad (9.3.8)$$

Thus, in the 1 kHz octave band (Δf=710Hz) we would expect to find about 13 resonant modes. The exact spacing and location of these modes along the frequency axis would depend on details of construction, but the number of modes spread over this 710 Hz interval would not. Thus, stiffening the structure by the addition of gusset brackets and the like will perturb the resonance frequencies, but the modes would still occur at intervals of about 50 Hz along the frequency axis.

9.4 Input Power Prediction

The input power is one of the quantities that is presumed known in the SEA calculation. However, it is only in rare instances that the input power will be known directly. If one is exciting the structure with a shaker and using a

force gauge between the shaker and the structure, it is possible to measure the input power directly. One is more likely to know a mean square force on the structure and some description of the spatial distribution of the load. This is the case of loading by a turbulent flow or acoustical noise pressure field. In this situation, the spatial character of the excitation is defined by a correlation function that will determine how well the spatial shape of the resonant modes will correlate with the excitation.

In a few situations, the excitation may be thought of as highly localized and taken to occur at a point in the system. Eq. (9.3.5) gives an estimate for input power in this instance, assuming the mean square force is known. However, this situation is not as easily realized as it might appear. The difficulty is that the structure has a very low input impedance at a resonance, so that if the shaker has a finite impedance, its force output will drop. This is illustrated in Fig. 9.3. The result is that the effective value of mean square force driving the structure is significantly below the apparent value obtained by multiplying the mean square current times the blocked force-current relation for the exciter.

In the cases of excitation by an acoustical noise field or a turbulent boundary layer, relations have been developed for the input power for a variety of structures that includes flat plates, cylinders, cones and other axisymmetric shapes. The appropriate relations for these cases are presented in Section II. To illustrate how we would use this parameter to calculate input power, we first consider excitation of a flat homogeneous plate by a turbulent boundary layer.

It turns out that the most important determinant of the power injection by a turbulent boundary layer is the ratio of convection speed of the pressure variations (about 80% of the free stream flow speed) to the bending wave speed. For aircraft speeds and aircraft skin panels, the bending speed is usually less than the convection speed. In this case the input power to the structure in the band Δf is known to be [15].

$$\Pi_{in} = \frac{\langle p^2 \rangle_{\Delta f} A_p^2}{R_{in}} \quad \frac{\lambda_p \phi_1}{A_p} \tag{9.4.1}$$

where $\langle p^2 \rangle_{\Delta f}$ is the mean square turbulent pressure measured on the panel in the band Δf, A_p is the area of the panel, $R_{in}=4M\delta f$ is the input point resistance of the panel. The bending wavelength on the plate is λ_p and the displacement thickness of the boundary layer profile is δ_1.

We can also find the power input to a structure from a sound field using the expressions for coupling loss factor already presented. Using

$$\Pi_{in} = \omega \eta_{acoust,\ struct}\, E_{acoust,\ tot}, \tag{9.4.2}$$

the following expression results for the power input from a sound field

$$\Pi_{in} = \frac{\langle p^2 \rangle_{\Delta f} A_p^2}{R_{in}}\ \sigma_{rad}\ \frac{\lambda^2}{2\pi A_p} \tag{9.4.3}$$

where $\langle p^2 \rangle_{\Delta f}$ is the mean square pressure measured on the surface of the panel, λ is the wavelength of sound, and σ_{rad} is the so-called radiation efficiency of the panel defined by

$$\sigma_{rad} = \frac{R_{rad}}{\rho c A_p}\ . \tag{9.4.4}$$

The other parameters are as previously defined. Thus, on the basis of the above, the designer can predict the power injected into a panel by a turbulent boundary layer or an acoustical noise field in terms of the pressure measured on the panel and other panel properties. Such estimates are then to be used in the band by band calculation of energy distribution throughout the system.

9.5 Conclusions

The SEA parameters are naturally occurring quantities in the theory of energy sharing of systems. These parameters may be evaluated by the designer by both analytical and experimental means. In many cases, they are related to more conventional system descriptors. Certainly, this is true for the energy dissipation, expressed by the loss factor. Mode count or modal density are not concepts original with SEA, but they are not widely used parameters in conventional structural dynamics. The coupling loss factor is a parameter that is unique to SEA studies, but even here we find that is often relatable to previously known parameters such as radiation resistance, transmissibility, and junction or point input impedance.

Of course, the particular coupling loss factors and other parameters that we need to find depend fundamentally on the choice of subsystems and their interconnections in the SEA model. This is the topic of the final chapter in this part dealing with the preliminary design process.

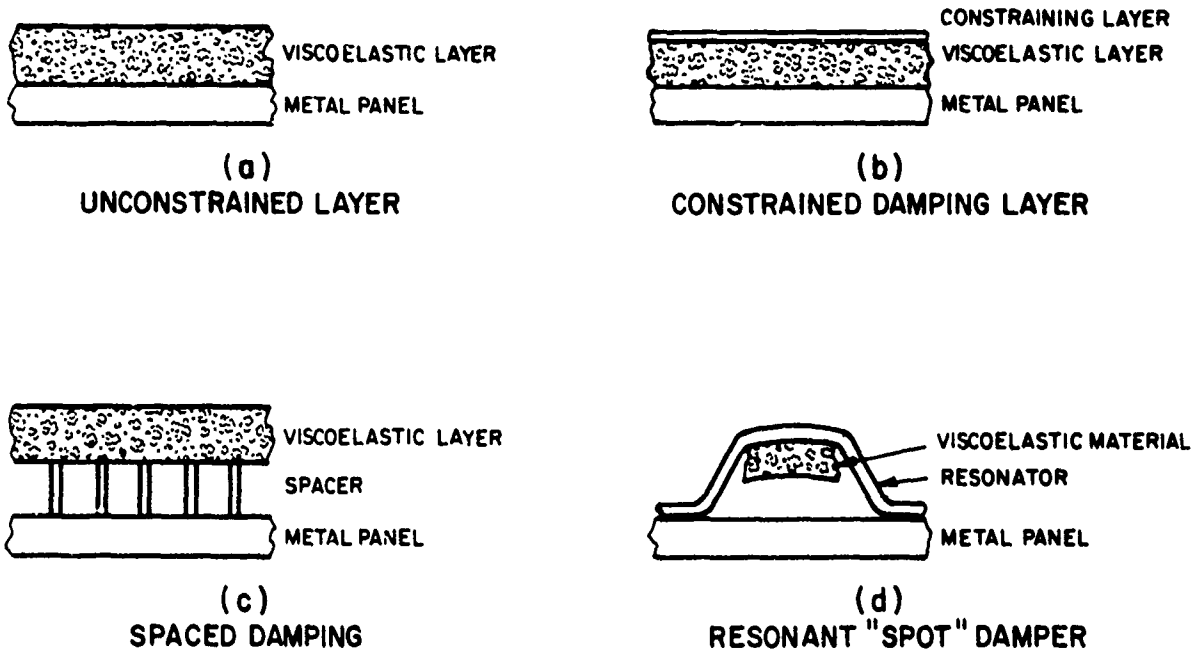

FIG. 9.1

VARIOUS FORMS OF APPLIED DAMPING

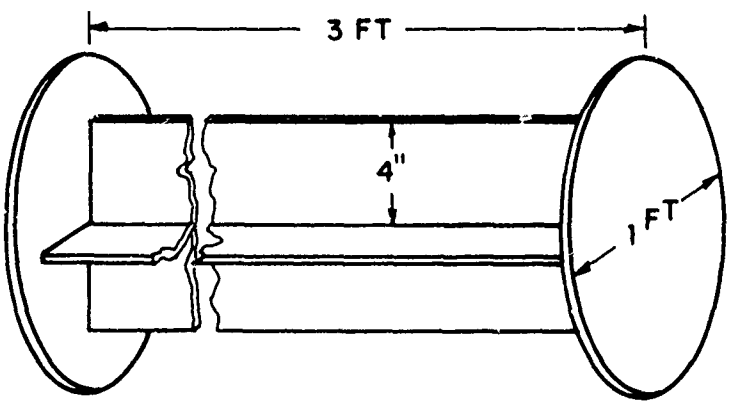

FIG. 9.2

EQUIPMENT SHELF MADE FROM 3/16 IN. ALUMINUM PLATE

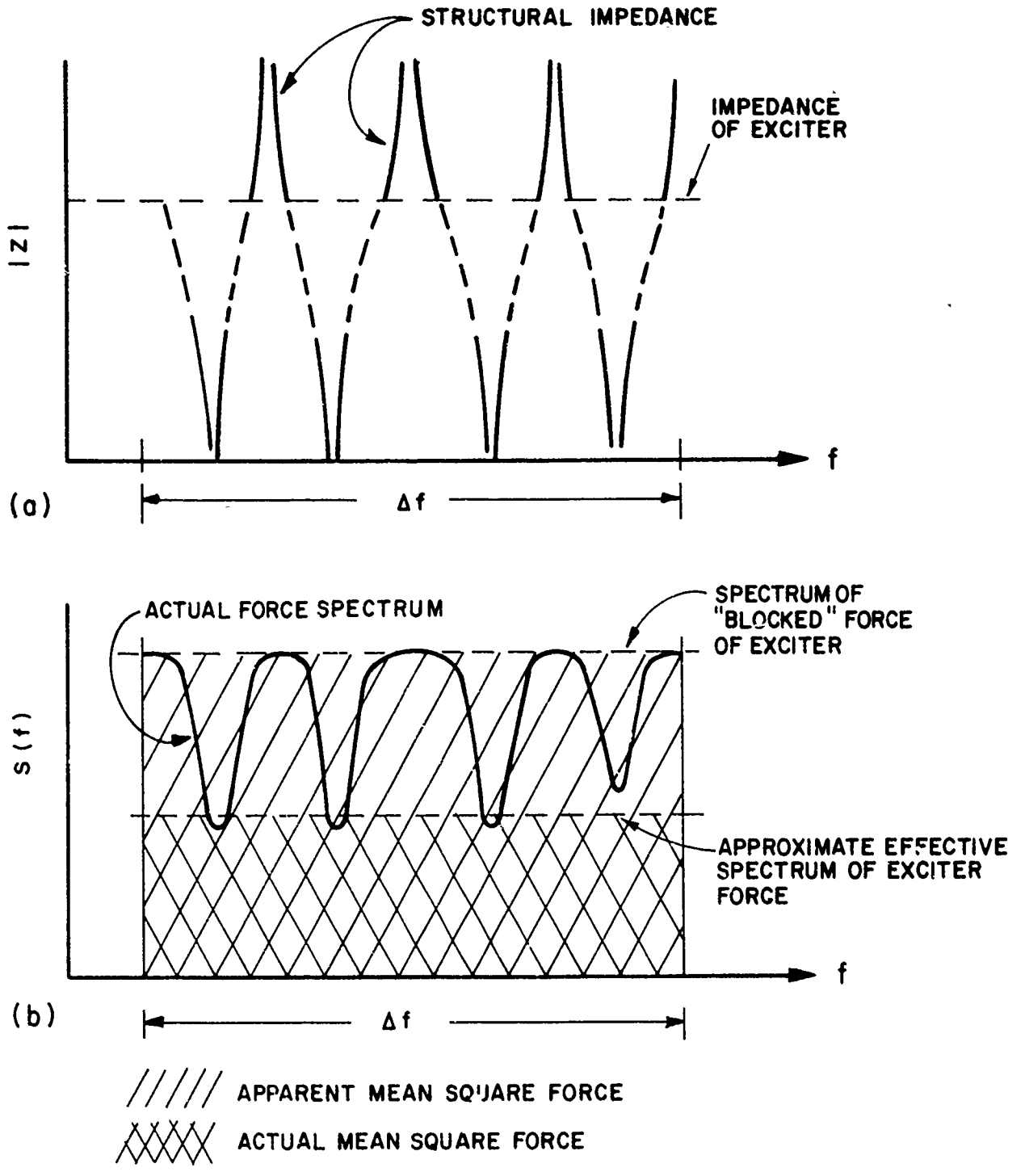

FIG. 9.3

THE IMPEDANCE OF THE STRUCTURE AND THE INTERNAL IMPEDANCE OF THE EXCITER ARE SHOWN IN (a). THE APPARENT FORCE SPECTRUM BASED ON THE INPUT CURRENT AND SHAKER CHARACTERISTICS ARE SHOWN IN (b). ALSO IN (b) ARE SHOWN THE ACTUAL FORCE SPECTRUM AND ITS "FLAT" EQUIVALENT BASED ON THE IMPEDANCE DIAGRAMS IN (a)

CHAPTER 10. MODELING THE SYSTEM

10.0 Introduction

We have now worked our way back from the use of the energy estimate, how that estimate is derived, and what the parameters are that enter the energy estimate to the most basic step of all in SEA -- the definition of the SEA model. This part of the effort is one of the earliest steps in the use of SEA in a design task. Fortunately, unless the basic system changes, this may only have to be done once. As various design modifications are made, perhaps with the goal of reducing response, the coupling and other parameters will change and the energy and associated response estimates will also change.

In a way, however, those aspects of the response estimation task that we have been discussing are deductive, and in that sense, straightforward. In the model definition phase, the designer must extract from the physical system - a fuselage and attached electronics pod, for example - a model consisting of groups of resonant interacting modes that will allow an estimate of response to be made. This is the synthetic part of the designer's task, and it is less straightforward to describe in detail just how this is to be accomplished in any particular case.

In this final chapter of Section I, we examine the procedures for developing SEA models insofar as a largely synthetic and inductive process can be set down as a set of procedures. Since the principal motivation for this report is the application of SEA to high-speed flight vehicles, the discussion uses examples from this area of engineering, but the procedures have much broader application. The real development of synthetic procedures, however, must occur as the experience of the designer with SEA methods is increased and, consequently, the important step is to begin to use SEA to make estimates in the first place.

10.1 Definition of Subsystems

SEA is able to provide estimates of complex system response because of our ability to group modes together and deal with them statistically rather than individually and deterministically. The modes are grouped according to the

following principles:

1. They all resonate in the band Δf_i in the entire SEA model, all parameters are evaluated as averages over the frequency interval Δf also.

2. Modes are grouped by major sections of the system that are to be identified in the final response estimates. Thus, all wing modes, fuselage modes, electronic pod modes, etc., that resonate in the band Δf would be grouped separately.

3. For any section, there may be differing classes of modes that one may wish to identify. For example, a truss or beam may have both torsional and flexural modes that resonate in Δf. These modes may be grouped together if we expect them to be well coupled, or they may be treated as separate subsystems.

A class of modes of a section of a system, resonating in the band Δf, is an SEA subsystem and represented by a "box" in a diagram like that in Fig. 8.1. The expected mode count N_i labels the energy storage capacity of the box. It is important to realize that modes that resonate outside the band Δf (so-called non-resonant modes) are not included in the modal count N_i, which pertains to resonant modes only. These non-resonant modes may play a role in transmitting energy from one sub-system to another, but the energy of vibration that they acquire in doing so is nearly always substantially less than that of the resonant modes. Consequently, we do not count the vibrational energy of non-resonant modes in estimating response.

One of the criteria for modal similarity in defining the subsystem is that the modes have nearly the same damping. Thus, the dissipation of energy by the "box" can be represented by a single loss factor η_i as was done in Chapter 8. A detailed study of the individual modes would show some variation in their damping. Theoretical analyses of permissible variations in damping have not been carried out, but we might assume that the individual modal loss factors could vary over a factor of three or so and the estimates of response based on the average damping would not be too far off. If a mode or group of modes has damping values that differ by a factor of 10 from the mean, than that group should probably be "split off" to form another subsystem.

Another criterion for modal similarity relates to the interaction with the loading environment. Thus, a particular form of excitation, such as acoustical noise, will excite flexural waves on skin panels most directly. In-plane compressional vibration of the skin would be only weakly excited. If the damping and coupling between in-plane and flexural modes were such that equal modal energy between these modes were to be expected, then only a single subsystem representing the skin structure might be necessary. If appreciable difference in modal energy might be expected, or if the distinction between in-plane and flexural or transverse motions is important for some other reason, then the skin structure should be represented by (at least) two subsystems. In this case, the "flexural" subsystem would have an input power Π_{in}, but the in-plane modal subsystem would be excited only by its coupling to the flexural subsystem. There are other considerations as well. The larger that Δf is made, the greater the number of resonant modes for each subsystem and, according to the discussion of Chapter 7, the smaller the variance in the estimate. On the other hand, if the bandwidth is too great, the assumption of uniform loss factor and coupling loss factor for all modes will not be accurate. Also, too broad a bandwidth causes frequency resolution to be lost, which may be important in some applications.

As a final item on the identification and definition of subsystems, it is worthwhile emphasizing that certain elements of a structural and environmental system are not SEA subsystems. For example, a turbulent boundary layer is not an SEA subsystem since it cannot be represented as a set of linear resonators or modes of oscillation. A turbulent flow must be regarded as a source of power, and not a modal subsystem. An acoustical environment may be treated as a power source but in some circumstances (a reverberant test chamber for example) it may be treated as another subsystem.

10.2 Identifying and Evaluating the Coupling Between Subsystems

The identification of the coupling between modal groups that exchange energy can be quite subtle. Certain features of the problem are fairly obvious, and should be dealt with first in the modeling process. For example, consider the system shown in Fig. 10.1, consisting of an exterior shell of an airborne computer that is excited by acoustical noise, and internal frame, and a circuit board mounted into the frame and, of course, an air space within the shell.

According to the procedures indicated in the preceding section, the first task is to divide the system into its major structural and acoustical systems. This division is shown in Fig. 10.2. We note that at least two of the elements have different classes of modes that we may want to treat separately, but for the time being, we shall treat each of the boxes in Fig. 10.2 as an SEA group of "similar" modes.

We now inquire about the energy transfer mechanisms at work in this system. Most obviously, power will be transferred through the mechanical connections between the shell and the frame and the frame and the circuit board. Also, the surface of contact between the enclosed sound field and the shell on one hand and the circuit board on the other. These power flow paths are shown in the diagram in Fig. 10.3.

A "first cut" at finding the circuit board response in this example might be to settle for the system as shown, proceed with evaluation of the parameters (Chapter 9), solve the energy equations for the energy of the circuit boards (Chapter 8) and interpret this energy as strain and acceleration spectra of the component on the boards (Chapter 7). We might then investigate the relative roles of acoustical and vibrational transmission, evaluate stiffening the frame, putting acoustical absorbing material within the shell, or changing the construction of the mountings of the frame into the shell. As each of these changes were made, coupling and damping loss factors would change and the response estimates would likewise change, indicating an increased or decreased vibration of the circuit boards. The basic model configuration would be unchanged, however.

At some point we might want to improve our model by considering effects thus far ignored. One of these is the role of nonresonant modes in the transmission of vibrational energy. The diagram of Fig. 10.3 for example indicates that if the frame were perfectly rigid and there were no resonant modes of the frame in the band Δf, then there would be no energy transferred to the circuit boards by the structural path. This is obviously not so, since a rigid translation of the frame would transfer energy from the shell to the circuit boards. In modal terms, this energy transfer is a result of the nonresonant excitation of modes that have resonance frequencies above the band Δf.

In a similar fashion, acoustical excitation of the shell will result in vibration and nonresonant modes of the shell that may be quite effective in exciting resonant acoustical

modes of the cavity within the shell. Since we are treating the external acoustical fields as a power source in this example, the effect of nonresonant motion of the shell is to add an additional power source directly to the cavity. These two modifications due to nonresonant vibration of subsystems that connect other subsystems are shown in Fig. 10.4. With this change in the model, the additional coupling loss factor η_{13} must be evaluated, as well as the input power $\Pi_{4,in}$. Obviously, we should expect the calculated circuit board vibrations to change as a result of these changes, but the change may not be very great. If the predictions turn out to be quite insensitive to this modification, then one would quite likely revert to the model of Fig. 10.3 for systems of this type.

The preceding discussion illustrates why modeling is a matter of judgement. The model of Fig. 10.4 is more precise than that of Fig. 10.3, but it is also more detailed and more cumbersome. It is only after the revised calculations have been made with the greater detail included that one can tell whether or not the extra effort is justified.

10.3 Subsystems Within a Section of the System

In paragraph 10.1, we noted that a section of a vehicle could contain groups of resonant modes that were sufficiently dissimilar so that separate subsystems might be necessary to model the system. In the following we explore this idea further and illustrate its effects on the model by returning to Fig. 10.2.

If the two types of shell and frame modes are each treated as a separate subsystem, then all the subsystems and their interactions are as shown in Fig. 10.5. Clearly, what began as a fairly simple model of the circuit board excitation in Fig. 10.3 has become a very complex model indeed. Is the complexity necessary? Generally no, but a blanket answer cannot be given. If the process of refining the SEA model in going from that shown in Fig. 10.3 to that shown in Fig. 10.4 were to result in significant changes in the estimate for board vibration, then the further refinement in going to a model like that of Fig. 10.5 might be deemed useful. One should always keep in mind the general results for estimation variance discussed in Chapter 7. If the refinements in the model causes the modal densities of certain subsystems to get to be too low, then the variance may increase so much that the more refined mean value estimate has little significance.

Most of the changes from Fig. 10.4 represented by Fig. 10.5 are fairly evidence, but we should comment on the energy transfer $\Pi_{1a,1b}$ and $\Pi_{2a,2b}$ between the new subsystems. Considering the frame first, we can note that there are two ways of coupling flexural and torsional motion in a beam. Unless the cross section of the beam has a high degree of symmetry (I-beam or box section), there will generally be continuous coupling between these forms of motion. Likewise, end conditions on the beams can cause coupling. If a simple beam is clamped at an angle other than $\pi/2$ to the centerline, flexural waves will reflect from this boundary as a combination of flexural and torsional motions.

It will be clear by now that the number of kinds of structural and acoustical subsystems of interest in SEA is very great. Many of the parameters needed to analyze systems comprised of these subsystems are listed and evaluated in Section II of this report. Even so, it is often necessary to estimate values for parameters of systems that may not be in the tables. In these cases, one can often treat the actual system as "somewhere in between" two limiting cases. For example, a short tab connecting two structures might be bracketed by a long beam connection and a rigid connection between the structures. Also, one can often determine the coupling loss factor experimentally.

10.4 Discussion

We must keep in mind that although the major emphasis in this report is the use of SEA in preliminary design, one of the major advantages of SEA is that the model and the associated estimates of response can be continually sharpened and refined as more detail regarding the system is developed. Thus, at the very early stages, the major structural sections may be modeled as homogeneous cylinders, plates, etc. Also, we would probably use broad frequency bands, octave bands for example, for the frequency resolution. This would keep the number of parameters down to a reasonable limit and more realistically reflect our knowledge of the system. As our knowledge of the details of the system increased, the model could include more modal groups (subsystems) and a finer division along the frequency scale (we could change to third-octave bands, for example).

None of the other estimation schemes has this capability of continual adjustment in the procedure to accommodate the increased knowledge about the system. In a way, we can think

of the SEA model as a communication channel that is able to accommodate a certain amount of input data (system parameters) to predict a response (output). A more complex model represents a channel with greater information handling capacity, and we can adjust the model to handle the available information. Thus, SEA is an estimation tool that can be used throughout a project from preliminary to final design.

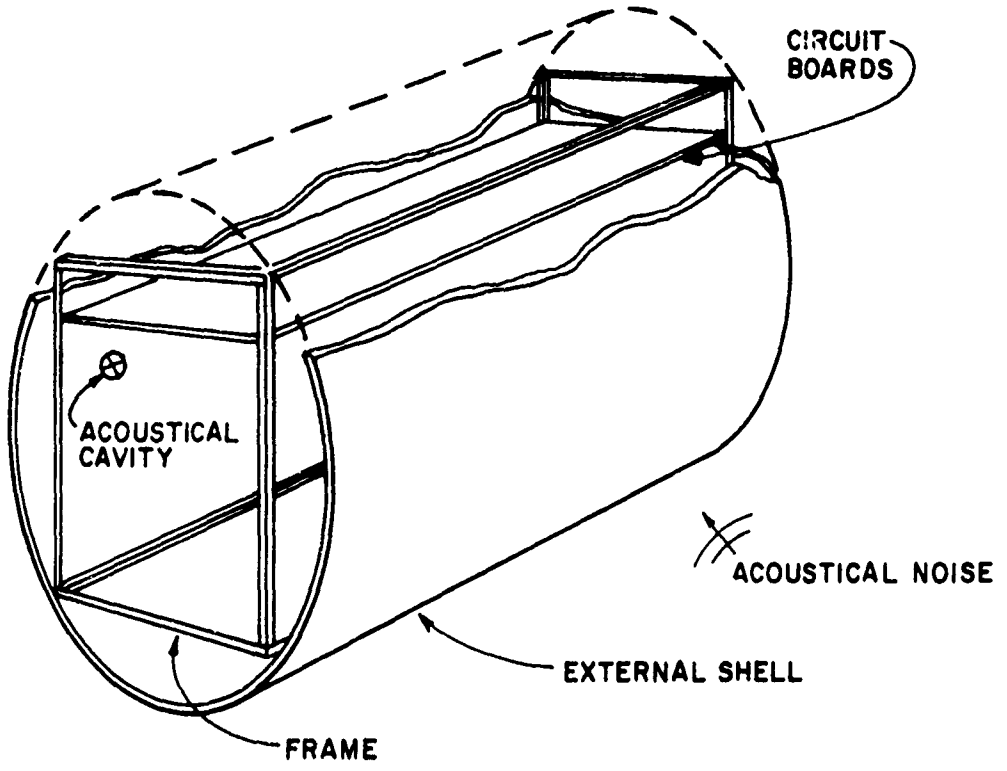

FIG. 10.1

DIAGRAM OF AIRBORNE COMPUTER ASSEMBLY

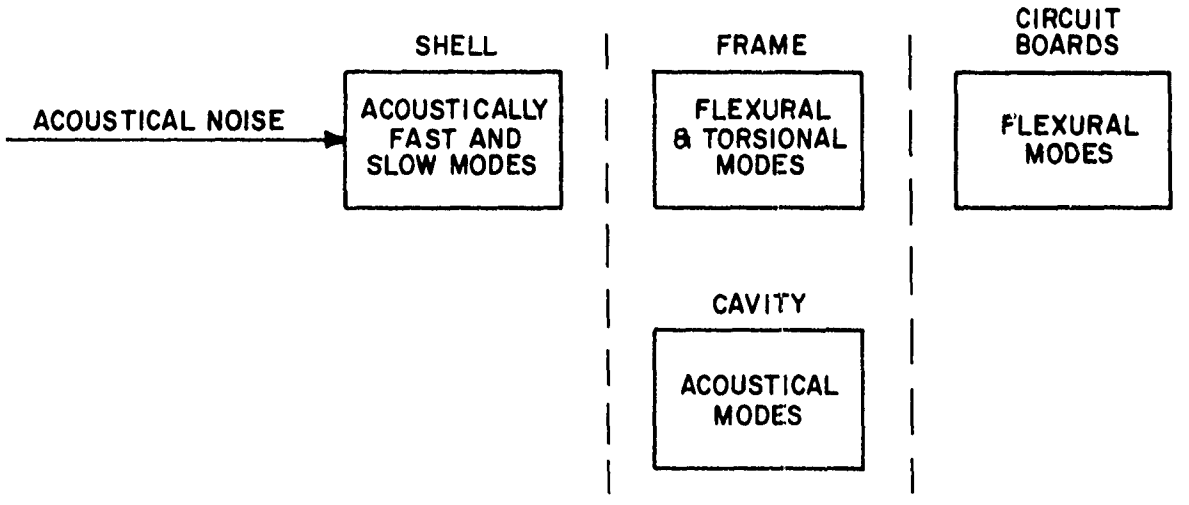

FIG. 10.2

MAJOR SECTIONS OF THE SYSTEM SHOWN IN FIG. 10.1

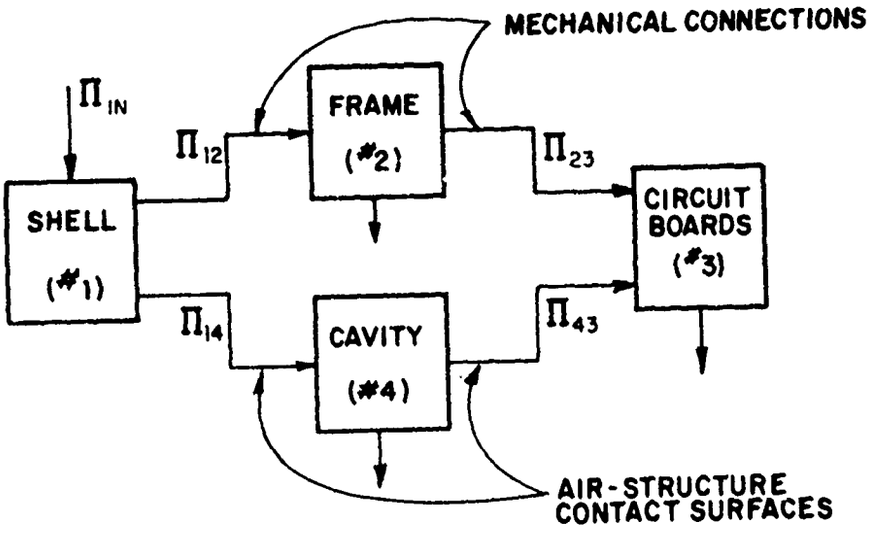

FIG. 10.3

SYSTEM OF FIG. 10.2 WITH POWER
TRANSFER THROUGH INTERFACES SHOWN

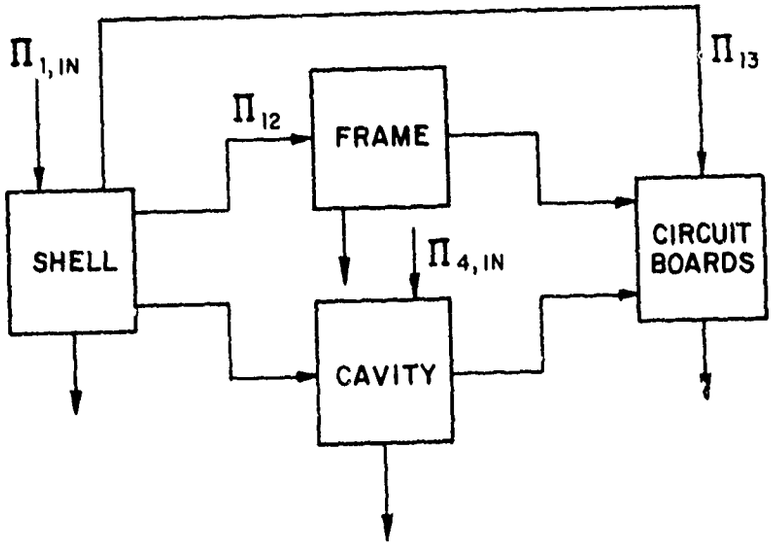

FIG. 10.4

MODIFICATIONS IN DIAGRAM OF FIG. 10.3
DUE TO NONRESONANT MOTIONS OF FRAME AND SHELL

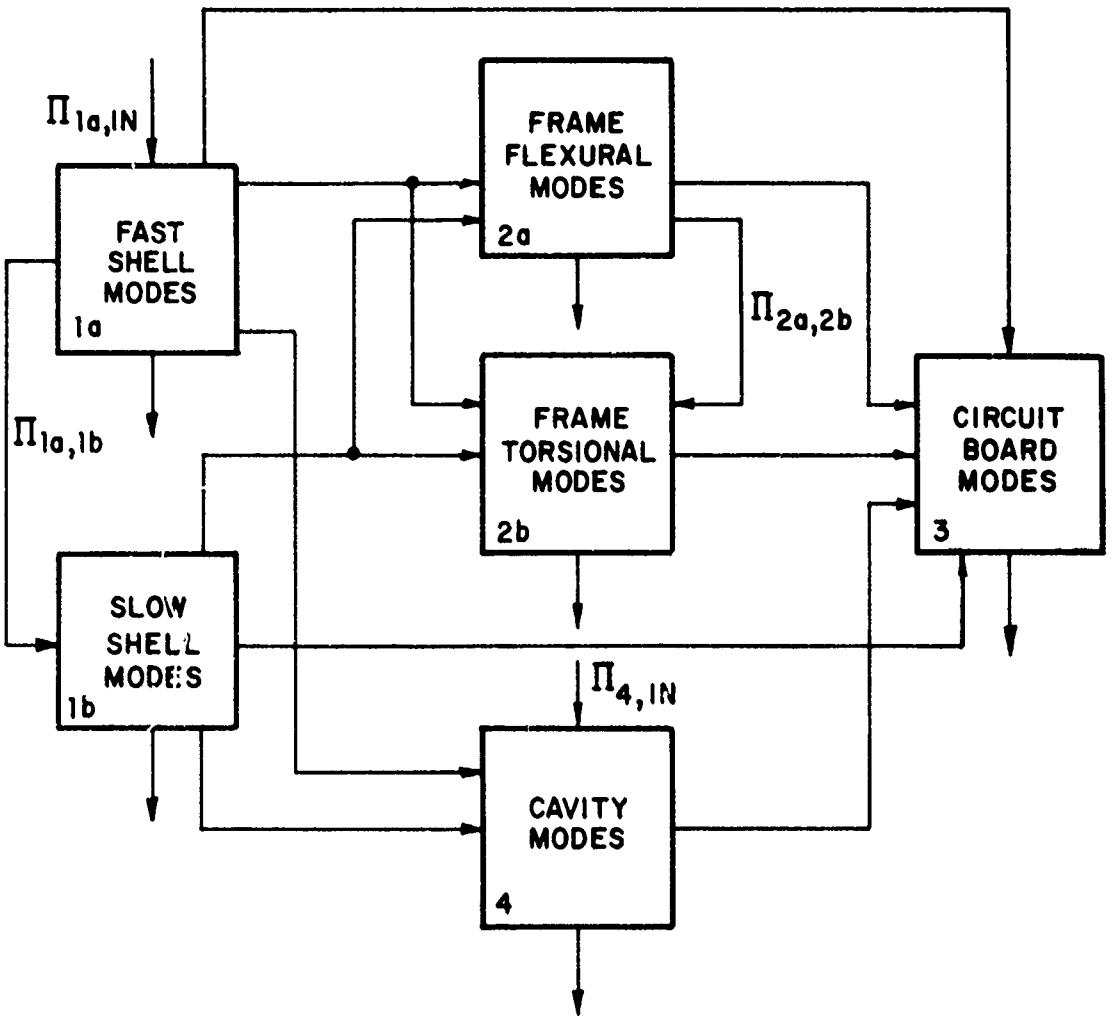

FIG. 10.5

THE SEA MODEL OF THE SYSTEM OF FIG. 10.1 WITH A GREATER NUMBER OF MODAL GROUPS AND INTERACTION REPRESENTED

SECTION II - EVALUATION OF SEA PARAMETERS

CHAPTER 11. PARAMETER EVALUATION - THE ENGINEERING BASE OF SEA

11.0 Introduction

In Part I and Section I of Part II of this report, we have concentrated on the theory for and use of SEA in response prediction. The role of the parameters in the various equations for energy and response of the subsystems - parameters such as damping loss factor, mode count and coupling loss factor - has been adequately pointed out. These we term SEA parameters because they enter in all SEA predictions and to a degree, they are used in a way that is unique in the SEA application.

This section is concerned with providing information on the evaluation of SEA parameters. This evaluation may be experimental, theoretical, or a "guesstimate" based on similarity with other situations for which the parameters have been found previously. Indeed, for many practical situations we may expect the guesstimate to be the primary "method" for finding SEA parameters.

Experimental procedures may be "direct" as when, in the case of mode count, one proceeds by counting resonant peaks. The procedure may be "indirect" as when one infers a coupling loss factor from the result of a vibrational response experiment. We present both direct and indirect methods here for all the parameters . The best method in any situation will depend on the range of parameter values involved, as discussed in the paragraphs that follow.

Theoretically derived parameter values are very often used for modal densities or mode count and the coupling loss factor. A few results are available from the literature -- several are quoted here. Situations not covered in the text may be treated from the references which should serve as adequate back-up for new calculations or a quoted result on a similar system that may serve as a useful estimate.

11.1 What are the SEA Parameters?

The SEA parameters are measures of the dissipation of vibratory energy the number of resonant modes in a frequency band available to store vibratory energy, and the coupling between the energy containing subsystems.

Chapter 12 describes how damping is measured or estimated analytically. The mechanisms of damping or dissipation vary significantly from one system to another. The losses in mechanical energy may result from molecular effects in polymers, air pumping at joints of built-up structures, or the motions of dislocations in metals. If the losses are not too great, however, a single parameter may be used to describe the dissipation effect in any of them. This parameter is called the "loss factor", and is the damping descriptor most often used in SEA.

In Chapter 13 we discuss how one evaluates the mode count; i.e., the number of resonant modes of a subsystem that are available for the storage of energy in a frequency band. The *mode count*, which is the fundamental quantity, may sometimes be estimated as a product of a *modal density* and the frequency bandwidth for that experiment, Δf. The mode count will not deviate very much from this estimate if the density of modes is great enough or the bandwidth for the experiment is wide enough so that the mode count estimate is at least 10 modes or so.

An important point to remember regarding the modes that we deal with in SEA is that they should be "similar". This means that they are of the same mechanical type, that they are excited in the same way, and that they are coupled to adjacent systems in similar ways. Suppose that a subsystem has two types of modes -- say, flexural and torsional, and that this subsystem is joined into other subsystems in such a way that we suspect that the energies of the flexural and torsional modes are not equal. Then the mode count of flexural and torsional modes should not be added to give the modal count of the subsystem in that frequency band, but in fact, two subsystems should be defined, each with its own mode count.

The coupling loss factor (CLF) is the parameter that governs the power flow from one subsystem to another. Not surprisingly, it depends upon the general mechanical parameters of both subsystems to which it refers. Chapter 14 gives a discussion of experimental procedures which may be

used to determine the CLF. The results of calculations of CLF for a variety of system types -- both acoustical and structural -- are also presented.

The chances are, however, that the designer who is attempting to use SEA to obtain response estimates, may not find his particular subsystem "connection" in the group represented in Chapter 14, simply because the odds are not in his favor. Relatively few cases have been worked out in sufficient detail to allow direct application, and the number of possible connections between subsystems is very large. Often, the cases that are known may be an acceptable approximation for the purposes of estimation. The designer will usually have to set up experiments to evaluate the CLF for his situation, or use the references as a way of learning the analytical techniques for a new theoretical derivation.

11.2 How Accurately Can (Must) We Know SEA Parameters?

The requirement for accuracy of the SEA parameters depends upon the requirement for accuracy in response estimates. The accuracy required in response estimates depends in turn upon the use to be made of the estimate. Typical uses include acoustical noise radiation, malfunction of electronic or control components and structural fatigue.

The estimation of sound radiation usually involves accuracy of the order of a few decibels (dB). This is sufficient to determine the annoyance, reduction in personal performance, or speech interference effects of noise. The prediction of troublesome sound levels for any of these criteria is the least demanding of all estimates of response, since the form of response estimate is usually the product of a ratio of loss factors and a ratio of modal counts. Thus, a 10 percent uncertainty in the parameters could amount to a 40 percent (or 1.5 dB) uncertainty in the estimate, even if the response level of the "source" subsystem is known exactly. Since there may be at least an uncertainty of a couple of decibels in the "known" level, the uncertainty in the radiated sound may be at least 3 dB or more.

The prediction of electronic malfunction or structural fatigue requires much more accurate estimation of response. For steady state vibration, a 1 dB change in vibration level can amount to a 100 percent change in expected life. Thus, the expected uncertainty in the estimate with only a 10 percent uncertainty in the parameters is greater than desirable.

On the other hand, current estimates -- even those based on test data from similar systems such as the Mahaffey-Smith procedure [2] have uncertainties that are at least as large as 3 dB. In order to predict the life of a structure or component reliably, the SEA parameters must be known within a few percent and the response of the "source" subsystem should be known to an accuracy of less than 0.5 dB. It is unlikely that such estimation accuracy is achievable, particularly with the mix of missions characteristic of current aircraft.

Typically, we may expect an accuracy of our estimates of modal count and loss factors to be about 10 percent, whether theoretically or experimentally determined. Thus, a purely theoretical prediction of structural fatigue or equipment malfunction cannot be achieved by the use of SEA. On the other hand, the SEA estimates are at least as accurate as other procedures, and in addition, the estimates retain functional dependence on the acoustical and structural parameters. Consequently, one can get an indication of how the system might be changed to reduce the vibration or noise, and increase component life.

11.3 How to Use This Section of the Report

Part I and Section I of Part II have discussed the basic theory of SEA and the use of SEA to predict response for engineering purposes. This section does not attempt to explain SEA or its computational procedures. Its purpose is to present methods for finding values of the SEA parameters -- both theoretically and experimentally -- and to give some values and formulas that have been found from earlier work.

Even though the report is a collection of formulas, graphs and diagrams in typical fashion, it will be found advisable to read through each chapter, even though only part of the chapter may be totally relevant to the problem at hand. The reason is that there is overlap in nomenclature and descriptions of experimental techniques between the various procedures and explanations. Rather than make the text too wordy with a great deal of repetition, the discussions have been kept as brief as possible. The result, however, is that a reading of only the material of direct interest may be somewhat confusing unless the rest of the chapter up to that point is read also.

CHAPTER 12 THE DAMPING PARAMETER

12.0 Introduction

In this chapter, we provide methods, formulae and data for the damping or dissipation parameter in SEA. This is commonly measured by the "loss factor" η, but may be known or expressed in a variety of other parameters. The loss factor η is defined as the ratio of energy dissipated per second to the average energy stored in the system.

$$\eta = \frac{1}{2\pi f} \frac{\Pi_{diss}}{E_{tot}} = \frac{T\ \Pi_{diss}}{2\pi\ E_{tot}} \qquad (12.0.1)$$

where $T\ \Pi_{diss}$ is the energy dissipated per cycle of vibration having period $T = 1/f$.

The loss factor can be related to a number of other dissipation parameters that occur in vibration and wave analysis. These factors and their relation to η are shown in Table 12.1. This variety exists because of the importance of dissipation mechanisms in many fields and the natural ways of experimentally determining damping in each field. We shall use the loss factor η for damping almost exclusively in this chapter.

The information on damping is presented in four paragraphs in this chapter. Paragraph 2.1 deals with experimental techniques, which may be applied to the various configurations discussed the later paragraphs. Paragraph 2.2 is concerned with the damping that is naturally available in the material from which the system is constructed. In paragraph 2.3, we discuss damping in built-up structures, which are the kind that interest us in the estimation of response in aerospace applications. Finally, in Paragraph 2.4, we discuss the construction and damping properties of various special add-on treatments that are commercially available.

12.1 Measurement of Damping

Although there is a good deal of tabular and theoretical information available regarding the damping of various structures, the most commonly used method of determining damping is simply to measure it. Fortunately, the accuracy to which the damping is required to be known is not too great, and simple experimental methods can readily achieve them.

There are two basic experimental strategies involved in these measurements: steady-state and decay methods. The steady-state methods are as follows:

a. Frequency response bandwidth for a single mode of oscillation.

b. Frequency response irregularity of a multi-degree-of-freedom system.

c. Measurement of input power.

Technique(a) is the well known "half-power bandwidth" technique. If an experimental arrangement such as that shown in Fig. 12.1 is employed, then a single resonant response like that shown in Fig. 12.2 can usually be found. The loss factor is found from this plot as

$$\eta = \Delta f/f_o \qquad (12.1.1)$$

In order for the result (12.1.1) to be useful, we must be able to single out a single resonance, which requires that $\Delta f/\delta f << 1$, where δf is the average separation between resonant modes of the structure. The ratio $\Delta f/\delta f$ is called the "modal overlap" parameter. When it is large (greater than 2 or 3 for instance), the frequency response curve shown in Fig. 12.2 will not be realized because of the interference between individual resonance curves. In this instance, the response will have the appearance of the curve shown in Fig. 12.3.

If δf_{max} is the measured difference in frequency

between two adjacent maxima in the response curve, then one can demonstrate that the damping loss factor of the system is given by [16]

$$\eta \simeq 0.4 \langle \delta f_{max} \rangle / f \qquad (12.1.2)$$

where $\langle \delta f_{max} \rangle$ is the average value of the separation for a number of adjacent maxima and f is the center frequency of this group of maxima. Parenthetically, we should note that when $\eta f/\delta f > 3$, (conditions of high modal overlap) an individual response maximum does not occur at a modal resonance frequency but is the result of the in phase response of a number of modes at the observation point.

Finally, damping can sometimes be inferred from a measurement of input power to a system. Such an experimental arrangement is shown in Fig. 12.4. A measurement of force and acceleration (or velocity) at the driving point allows one to determine Π_{in}. Measuring the rms acceleration of the structure allows the determination of $\langle v^2 \rangle = \langle a^2 \rangle / 4\pi^2 f^2$. The loss factor is then given by

$$\eta = \Pi_{in} / M \langle v^2 \rangle \omega \qquad (12.1.3)$$

where M is the mass of the structure.

In addition to the steady state methods, there are transient methods for measurement of damping. These depend on relations between the loss factor and various measures of the rate of decay of a system as detailed in Table 12-1. If one wishes to observe the decay of a single mode of the system, then an arrangement like that shown in Fig. 12.5 may be used. If a single mode is to be studied, then the excitation may be a pure tone. The gate is used to cut-off the excitation, and may also be used to drive the position of the shaker armature out of contact with the structure. Such a provision is useful if the shaker itself provides enough structural damping to affect the measured decay rate.

If the modes are closely spaced so that δf is not much greater than ηf, the abrupt termination of the excitation will cause additional modes to be excited, and a decay curve like

that shown in Fig. 12.6 will result. Such a result can be avoided by using broader bandwidths of noise excitation that encompass several modes of vibration, or by using a gating function that is not so abrupt, but still fast enough not to interfere with the decay process.

In the case of high modal overlap, the strategy for damping measurement must change, and this is the case for steady state measurement also. In this case, even a pure tone excites several modes, so that one may use several shakers to simulate the proper generalized force for a given mode. Such an approach is used for the lower modes of aircraft, but is not very suitable for higher frequency panel type modes of substructures. In the latter situation, one simply uses a band of noise to ensure that many modes of vibration are excited and decay together. In this case, an average loss factor for the modal group is obtained.

The sensing of response is made with a microphone or accelerometer, as appropriate for sound fields or structures. A short time rms of the signal is taken (averaging time a few milliseconds or less, depending on the frequency) and the logarithm taken and the signal displayed. The decay rate DR in dB/sec is found and the loss factor is found from

$$DR = 27.3 f\eta \ . \qquad (12.1.4)$$

A storage oscilloscope is useful for this measurement because a graphic level recorder, widely used in sound measurements, is too slow for many structural decay experiments.

12.2 Damping Values for Materials [17]

Most aerospace structures are constructed from aluminum alloys which have loss factors in the range from 0.002 to 0.005. Such damping values are generally smaller than the measured damping of built-up structures by a sizable factor. Thus, it is generally presumed that the damping of real structures due to the metal itself is of little consequence in comparison to the damping due to joints, rivet contacts, and other similar features.

In Fig. 12.7, we show a graph of values of loss factors for various materials. Metals have an internal loss factor ranging from 10^{-3} to 2×10^{-1}. The larger values are not encountered in aluminum alloys, but may be found in cast iron and special alloys of manganese and copper. Polymer materials have a similar range of loss factors, but are "softer" than metals by a factor of 10 or more. Elastomeric materials are a factor of 10^4 softer then metals, but have higher loss factors than do either metals or polymers, ranging from 0.1 to about 5. Polymers and elastomers have great significance in their role as components of add-on damping treatments, which will be dealt with later on.

The damping provided by the material from which an aerospace vehicle is constructed is so low compared to the values measured for built-up structures that we normally do not consider this form of damping to be significant. However, add-on damping treatments do have a high degree of material damping in their polymeric or elastomeric elements, and consequently, we are interested in the damping of such materials. In particular, the damping provided by these materials is frequency and temperature sensitive, and aerospace structures are excited over broad frequency ranges and are exposed to large changes in ambient temperature. This subject is well covered by many sources, but it is worthwhile to give a brief review of it here.

Polymeric materials undergo a transition in behavior in terms of their static stiffness from a soft, rubbery (or elastomeric) behavior to a harder, or glassy phase as a certain temperature Θ is passed. The transition is not sharp, but occurs gradually and is therefore, not a "normal" phase transition like that which occurs for example in water between its liquid and solid phases.

In addition, the dynamics of the material undergo a transition in frequency at any temperature about the transition temperature of the material. That is, if the material is in its "rubbery" state at room temperature (and zero-frequency) then if the specimen is cycled quickly enough, the material does not have sufficient time to accommodate, and it acts dynamically as though it were in its more rigid, glassy form.

The time required for the polymer to "slip its bonds" and behave in a rubbery fashion is called the relaxation time for the material, denoted a_Θ. As a result of experimental

studies on a variety of materials, the relaxation time for polymers has been found to follow the relation

$$\log a_\Theta = - \frac{8.86(\Theta-\Theta_0)}{120+(\Theta-\Theta_0)} \qquad (12.2.1)$$

where $\Theta_0 = \Theta_t + 50K$ (expressed in degrees centigrade) and Θ_t is the transition temperature mentioned above. Thus, polymeric materials have a dynamic stiffness characterized by a single transition effect that is temperature dependent. The relaxation time gets smaller as the temperature increases, and the frequency of transition increases.

A diagram of the behavior of loss factor and modulus for a rubber material is shown in Figure 12.8 [17]. The tendency for the transition frequency f_c to rise as the temperatures is increased is clearly evident from the behavior of the maximum in the loss factor function and the line of inflection in the stiffness modulus. A great deal of data has been collected for various polymer materials and is available in standard reference works [17].

From the above discussion, it might be inferred that polymers in the glassy state are not good damping compounds. Generally, this is true although such materials may be used occasionally where some damping is desirable. Nevertheless, high modulus damping materials are desirable, particularly, in their application is unconstrained layers. To achieve such behavior an elastomer, such as polyvinyl chloride (PVC) is loaded with a stiff filler material. This filler has two important effects - it increases the overall rigidity of the material and it amplifies the strain in regions near the filler particles. Thus, the stiffness and damping of the combination are both increased [18].

The mechanisms of damping in metals include thermal conduction, grain boundary motion, molecular site transition, and dislocation oscillations. At larger amplitudes, non-linear effects such as plastic flow also occur. Because of the complexity of mechanisms, but more importantly, because of the wide range of activation energies for these processes, there is little possibility of developing such simple functions as that shown in Fig. 12.8 to illustrate the internal damping of metals. Accordingly, the best we can do in this instance is to refer to reference material in which values of material damping of various metals are tabulated [17].

12.3 Damping of Built-Up Structures

We note above that aerospace structures that are made up of aluminum alloy sheets, ribs, stringers and rivets will under test display a loss factor of the order of 0.02, whereas the loss factor of the metal itself is likely to be of the order of 0.002. Although the vehicle designer has very little control over the damping obtained this way, it is nevertheless useful to review what is known regarding the damping of built-up structures.

It is reasonably well established that the increased damping is due to the riveted joints of the structure. There are at least two theories regarding the source of this increased damping. One of these [19] assumes that the damping is due to surface slip and plastic deformation of the contacting asperities of the overlapping surfaces. The resulting damping is nonlinear. The damping in this case should increase as the level of vibration increases.

The second theory assumes that the dissipation is due to viscous flow in the region between the metal surfaces along the riveted joints. If a liquid is present, such as oil, this mechanism is fairly obvious - as the metal surfaces vibrate, the gap changes its depth in a cyclic fashion. To stay in contact, therefore, the liquid must flow in and out of the narrow gap, and viscous dissipation is substantial. But it turns out that even if no liquid is present, the flow of air in and out of the gap is capable of dissipating sufficient energy to account for the observed damping [20]. The obvious implication of this mechanism is that the damping will be reduced as the air pressure is reduced and so, we might expect less damping as altitude is increased.

The theory of damping by gas-pumping is rather complicated, but we can summarize the results here. The formal expression for the loss factor has only been found for high frequencies (when the flexural wavelength on the plate is of the order of a rivet spacing or less), but we may presume that the general parameter dependence will likely apply to lower frequencies also. The loss factor for the case in which the plate vibrates and the attached beam is assumed stationary is [20]

$$\eta = \frac{A_b c^2 \gamma P}{16\pi^3 f^3 A_p m_p \kappa_p h c_\ell} \, H(\Theta) \qquad (12.3.1)$$

where

A_b = area of overlap

A_p = area of structural panel

m_p = surface density of panel

κ_p = radius of gyration of plate cross section

γ = ratio of specific heats of gas

c_ℓ = longitudinal wave speed in plate material

h = gap thickness

p = gas pressure

c = speed of sound in gas

The function $H(\Theta)$ is a measure of the ease of flow of the gas within the gap and $\Theta = h/\delta$ is the ratio of the gap depth to the length parameter

$$\delta = 2\ (\nu/\omega)^{\frac{1}{2}}$$

where ν is the kinematic viscosity of the gas. A graph of this function is presented in Fig. 12.9.

A comparison of the prediction according to Eq. (12.3.1) and laboratory studies of the damping of a single beam riveted to a plate is shown in Fig. 12.10. In this the plate is 1/64 inch thick and the attached beam is 1/4 x 1 x 17 inches. The correspondence between the theoretical and measured values of damping is impressive. In particular, the known tendency for the observed value of damping to have a broad range of values near 0.01 for built-up structures is supported by this data and the calculations.

The results on air pumping are presented here because this is practically the only theory that gives reasonable predictions of damping in riveted, aerospace type structures. We do not wish to infer that this is a closed matter, however.

Certainly there are many cases in other areas of acoustical and vibration engineering in which the damping in built-up structures is not due principally to this mechanism.

12.4 The Damping of Add-On Systems

Since the energy of vibration tends to be inversely proportional to damping an increase of damping is frequently desired to reduce vibration amplitudes. Since the "natural" loss factor will be of the order of 0.01, we must increase the damping so that the loss factor of the structure becomes of the order of 0.1 in. order to have an appreciable effect on the response. To achieve such a high level of damping, however, one must usually resort to some kind of "add-on" damping treatment. The performance of such treatments is the subject of this section.

The most widely used add-on damping systems are

(1) a free or unconstrained layer of damping material, applied either by troweling, spraying, or in the form of tiles;

(2) a constrained layer of damping material, in the form of a tape with foil and elastomeric adhesive, or with the elastomer and constraining sheet applied separately;

(3) spaced damping consisting of a spacing structure and either a free or constrained layer of damping.

(4) A resonant damper designed to produce high damping for a particular mode of vibration.

Diagrams of these various damping systems are shown in Chapter 9 and in the present chapter also.

Free (Unconstrained) Layer [21]. It is convenient to examine results for the unconstrained and constrained treatments separately, both with and without a spacing layer. Some typical free layer configurations are shown in Fig. 12.11. The base panel is "1", the elastomer layer is "3" and, when present, the spacer layer is "2". The loss factor of this composite is (assuming stiffness of the damping layer is small compared to the structural stiffness) [21]

$$\eta = \eta_3 \frac{E_3}{E_1} \frac{h_3 w_3 H_{31}^2}{I_1} \qquad (12.4.1)$$

where

η_3 = loss factor of layer 3, discussed in paragraph 12.2

E_3 = Young's modulus of layer 3

E_1 = Young's modulus of layer 1

h_3 = thickness of layer 3

w_3 = width of layer (take as unity when treatment covers material)

H_{31} = distance between neutral axes of layers 1 and 3

I_1 = moment of inertia of layer 1.

The interpretation of Eq. (12.4.1) is straightforward and revealing. The first factor is a ratio of material parameters only, and we note that $\eta_3 E_3/\eta E_1$ is the relative dissipation in the damping layer to the apparent dissipation in the base structure for equal strains. The desirability of combining "high" stiffness and loss factor in the damping material is obvious from this expression. The second factor is geometric - it is a ratio of the moment of inertia of the damping layer to that of the base structures. It represents the square of a strain amplification factor produced by the geometry of the configuration. Thus, the purpose of the spacing layer "2" is to increase the strain in the damping layer and consequently obtain more damping.

As a practial matter, it is possible to increase the damping by a factor of 10 or so by spacing the material away from the structure. At higher frequencies this "gain" will be less, because the spacing layer will tend to shear and not stretch the damping layer as shown in Fig. 12.11. A typical curve of loss factor achieved with a spacing structure is shown in Fig. 12.12. The frequency and temperature dependence of η will be that of η_3, as discussed in paragraph 2.2.

Constrained Layers. The use of a constraining layer above the damping layer is another device to amplify strain in the damping layer. In this instance, the constraining layer augments shear in the damping material rather than elongation as in spaced free layer damping. A comparison of constrained layer and free layer distortions is shown in Fig. 12.13. In aerospace applications, the damping is thin and also soft compared to the base structure and the constraining layer. In this circumstances a fairly complicated formula results for the loss factor of the composite structure, which is best presented graphically.

Fig. 12.14 shows the dependence of the composite loss factor on the "shear parameter" χ, a parameter that is essentially inversely proportional to frequency. The general formula for χ is

$$\chi = \frac{G_3 w_3}{h_3} \left(\frac{\lambda_b}{2}\right)^2 \left(\frac{K_1+K_2}{K_1 K_2}\right) \qquad (12.4.2)$$

where $K_i = E_i h_i$ is the extensional stiffness of the layer, λ_b is the bending wavelength, G_3 is shear modulus of the damping layer (damping is due to shear in this configuration, not to extension as in Eq. (12.4.1) and Fig. 12.11) w_3 is the width of the damping layer (coverage is not necessarily complete) and h_3 is the thickness of the damping layer. Subscripts correspond to the diagram in Fig. 12.15. Since

$$\lambda_b \sim 1/f^{\frac{1}{2}} ,$$

one has $\chi \sim f^{-1}$.

The optimal value of the shear parameter χ is given by

$$\chi_{opt} = (1+Y)^{-\frac{1}{2}} (1+\beta^2)^{-\frac{1}{2}} \qquad (12.4.3)$$

where Y is the "structural parameter". The value of Y for various configurations of interest is shown in Fig. 12.16. The parameter β is the loss factor for shear in the damping material and is usually very close in the value to η_3. The maximum composite loss factor η_{max} is given by

$$\eta_{max} = \beta Y \left[2+Y + 2/\chi_{opt}\right]^{-1}. \qquad (12.4.4)$$

This expression is graphed in Fig. 12.17 as a function of damping layer loss factor for various configurations (structural parameters).

By combining the information in Figs. 12.14, 12.16, and 12.17, along with material damping information from paragraph 12.2, the damping of any constrained layer system may be estimated. Constrained layers are preferred for aerospace application because they tend to have less weight for a given damping. This is demonstrated in Fig. 12.18, which shows a comparison of damping versus added weight for free and constrained layers. It is evident that as long as the acceptable weight increase is less than 10 per cent, one would achieve much more damping from the constrained layer. The penalty that one pays for this performance is the narrow frequency range of performance. That is, the constrained layer treatment must be more closely "tuned" to the desired frequency range.

TABLE 12.1

COMPARISON OF COMMONLY USED DAMPING MEASURES

Dissipation Descriptor	Symbol	Units	Relation to η
Loss Factor	η	-	η
Quality Factor	Q	-	$1/\eta$
Critical Damping Ratio	ξ	-	$1/2\ \eta$
Reverberation Time	T_R	seconds	$2.2/f\eta$
Decay Rate	DR	dB/sec	$27.3f\eta$
Logarithmic Decrement	δ	nepers/sec^{-1}	$\pi f\eta$
Wave Attenuation*	m	nepers/m	$\pi f\eta/c_g$
Mechanical Resistance**	R	newt-sec/m	$2\pi f\eta M$
Damping Bandwidth (Half-Power)	BW	hertz	$f\eta$
Imaginary Part of Modulus $E_r + iE_i$	E_i	newt/m^2	E_i/E_r
Acoustical Absorption Coefficient***	α	-	$8\pi fV/cA$

*c_g is group velocity for system in meters/sec.

**M is the system mass

***A is area of walls, V is room volume, c is speed of sound.

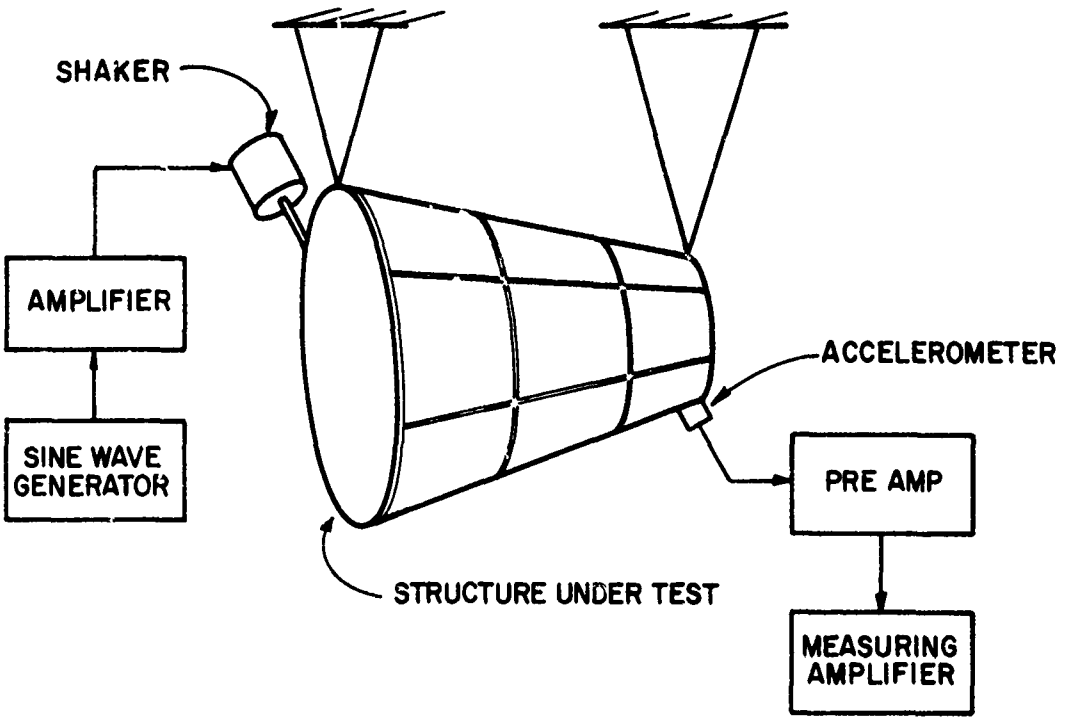

FIG. 12.1

EXPERIMENTAL ARRANGEMENT FOR MEASURING FREQUENCY RESPONSE OF A STRUCTURE

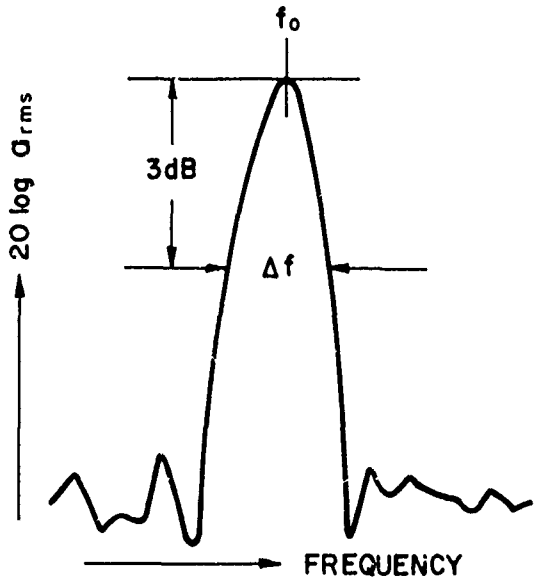

FIG. 12.2

RESPONSE CURVE FOR A SINGLE MODE

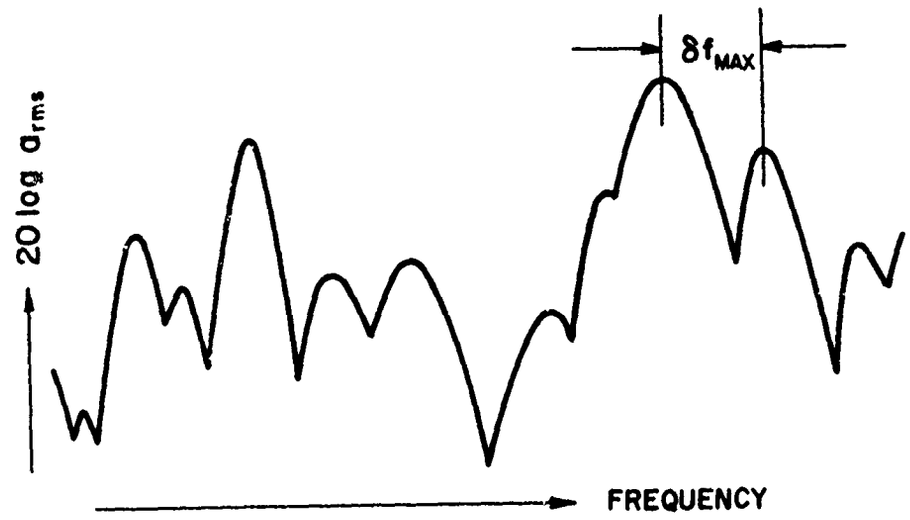

FIG. 12.3

RESPONSE CURVE FOR A SYSTEM WITH HIGH MODAL OVERLAP

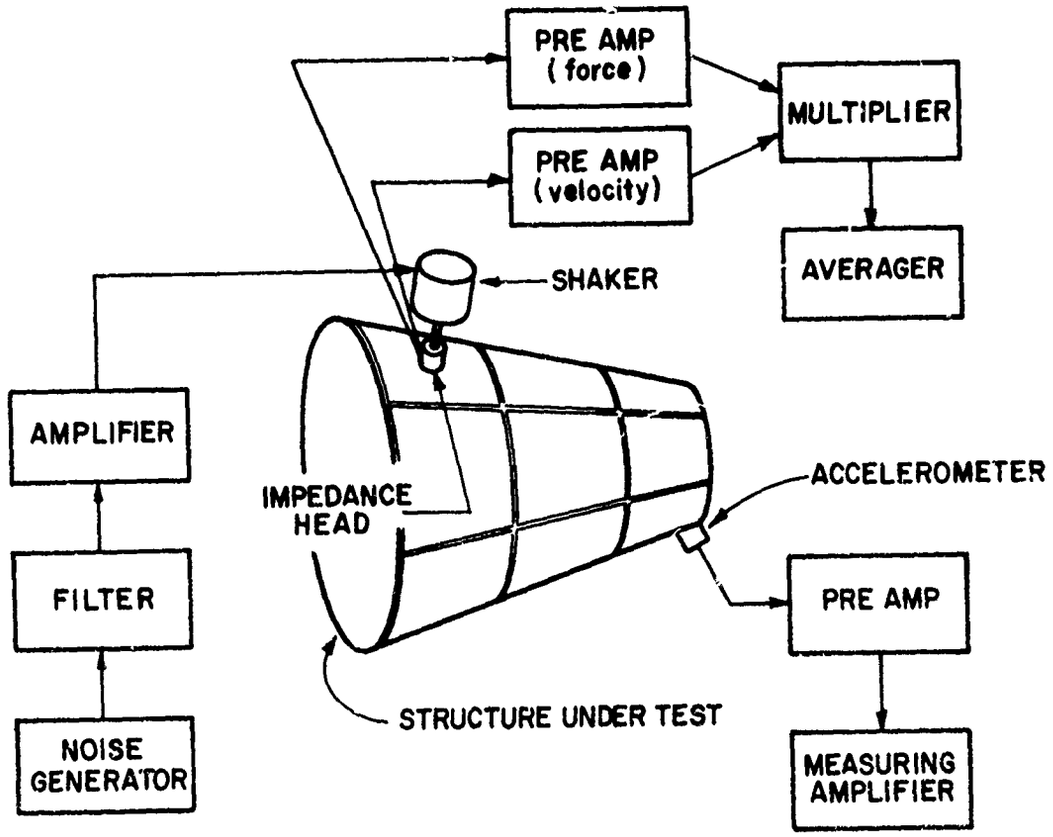

FIG. 12.4

ARRANGEMENT FOR DETERMINING DAMPING FROM INPUT POWER AND AVERAGE RESPONSE

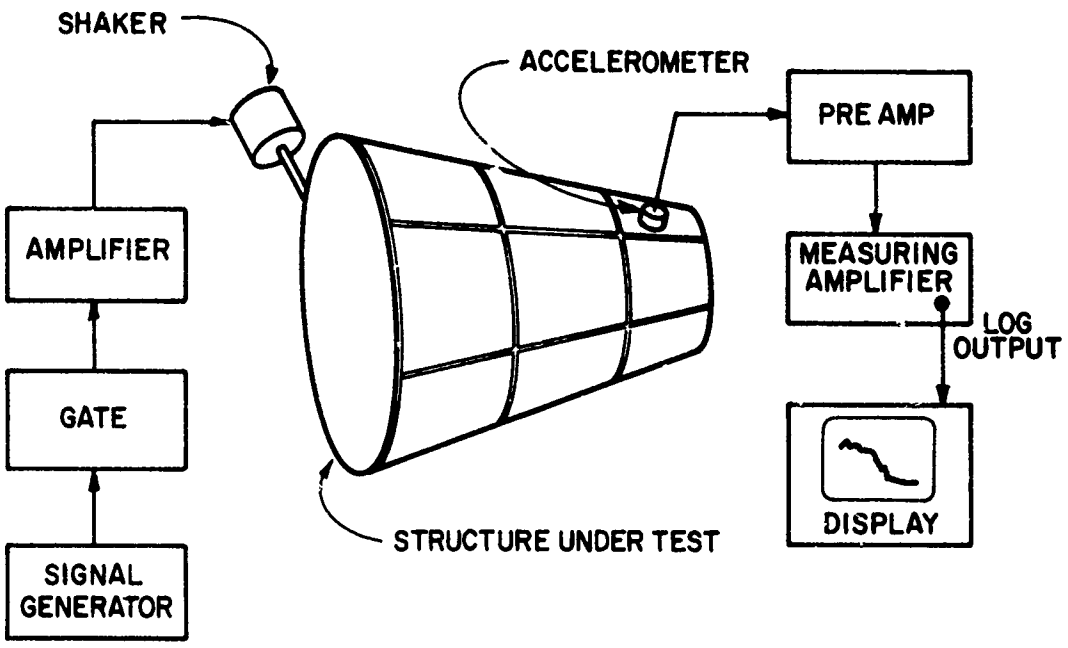

FIG. 12.5

ARRANGEMENT FOR MEASURING DECAY RATE OF STRUCTURAL VIBRATIONS

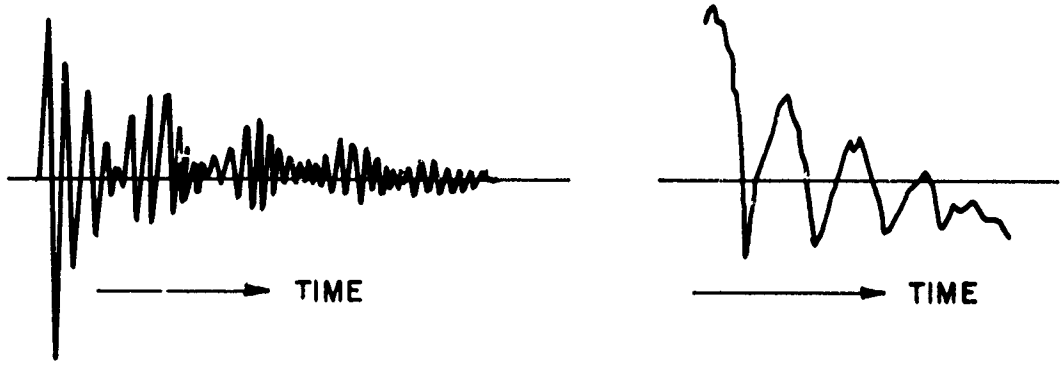

(a) LINEAR PRESENTATION

(b) LOG RMS PRESENTATION

FIG. 12.6

SIMULTANEOUS DECAY OF TWO MODES HAVING SLIGHTLY DIFFERENT NATURAL FREQUENCIES

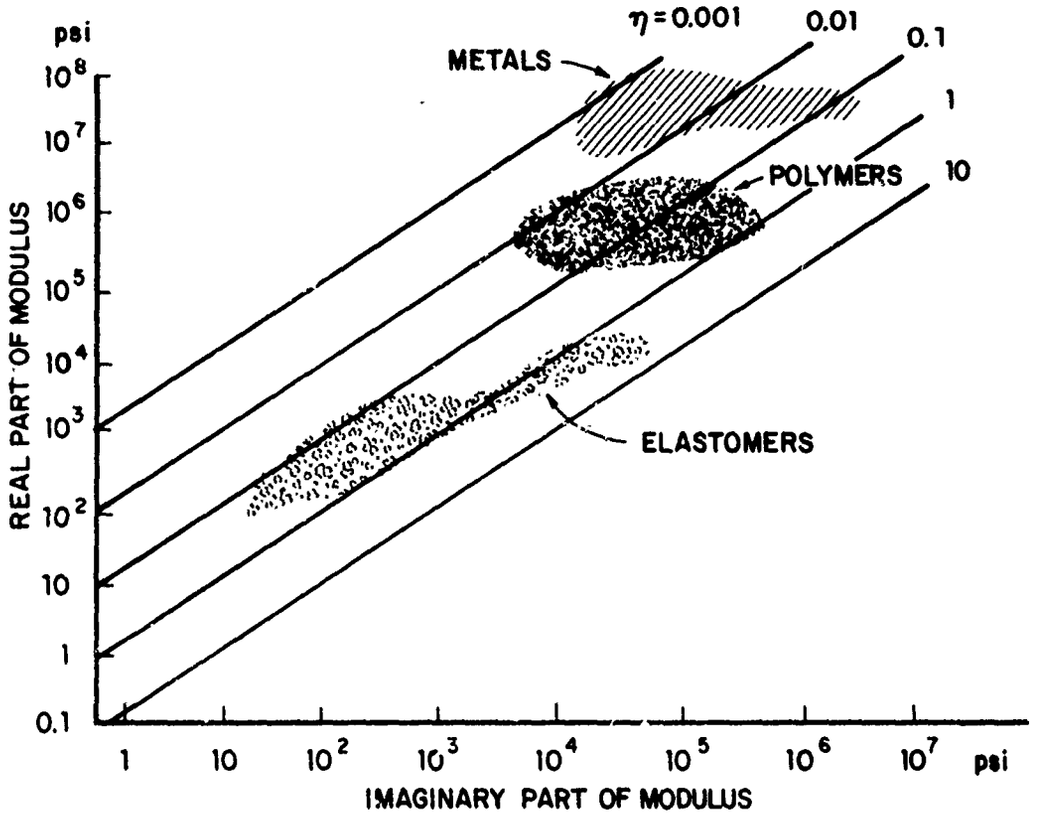

FIG. 12.7

LOSS FACTORS AND ELASTIC MODULI FOR VARIOUS CLASSES OF MATERIALS (ADAPTED FROM REF 3)

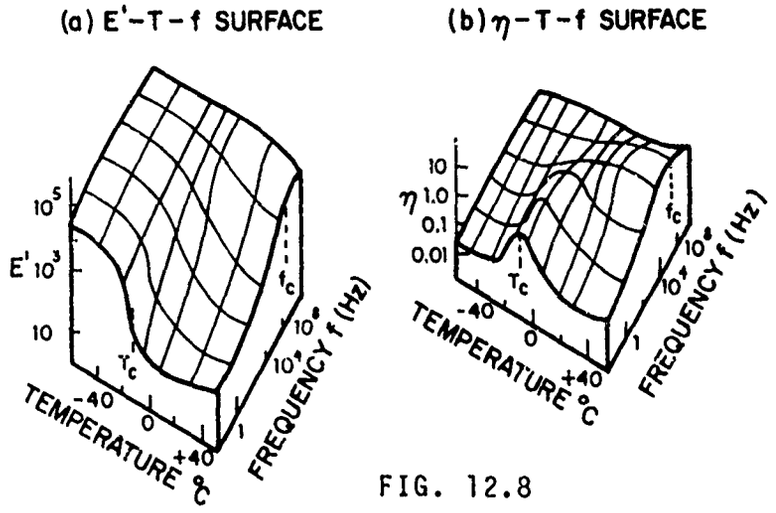

FIG. 12.8

EFFECTS OF TEMPERATURE AND FREQUENCY IN THE TRANSITION REGION ON THE STORAGE MODULUS AND LOSS COEFFICIENT OF BUNA N RUBBER

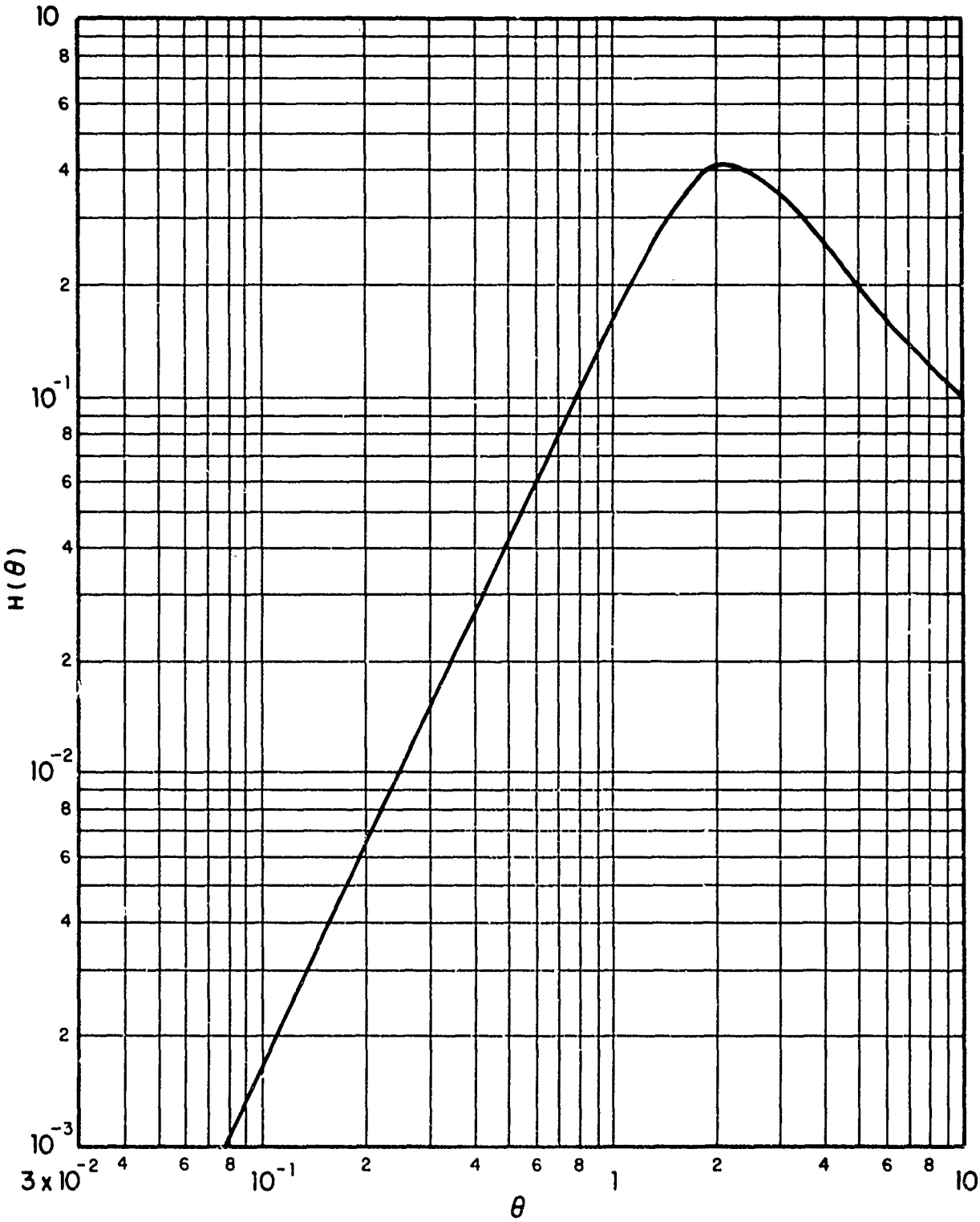

FIG. 12.9

DEPENDENCE OF LOSS FACTOR ON RATIO OF GAP BETWEEN PLATE AND BEAM TO VISCOUS BOUNDARY LAYER THICKNESS

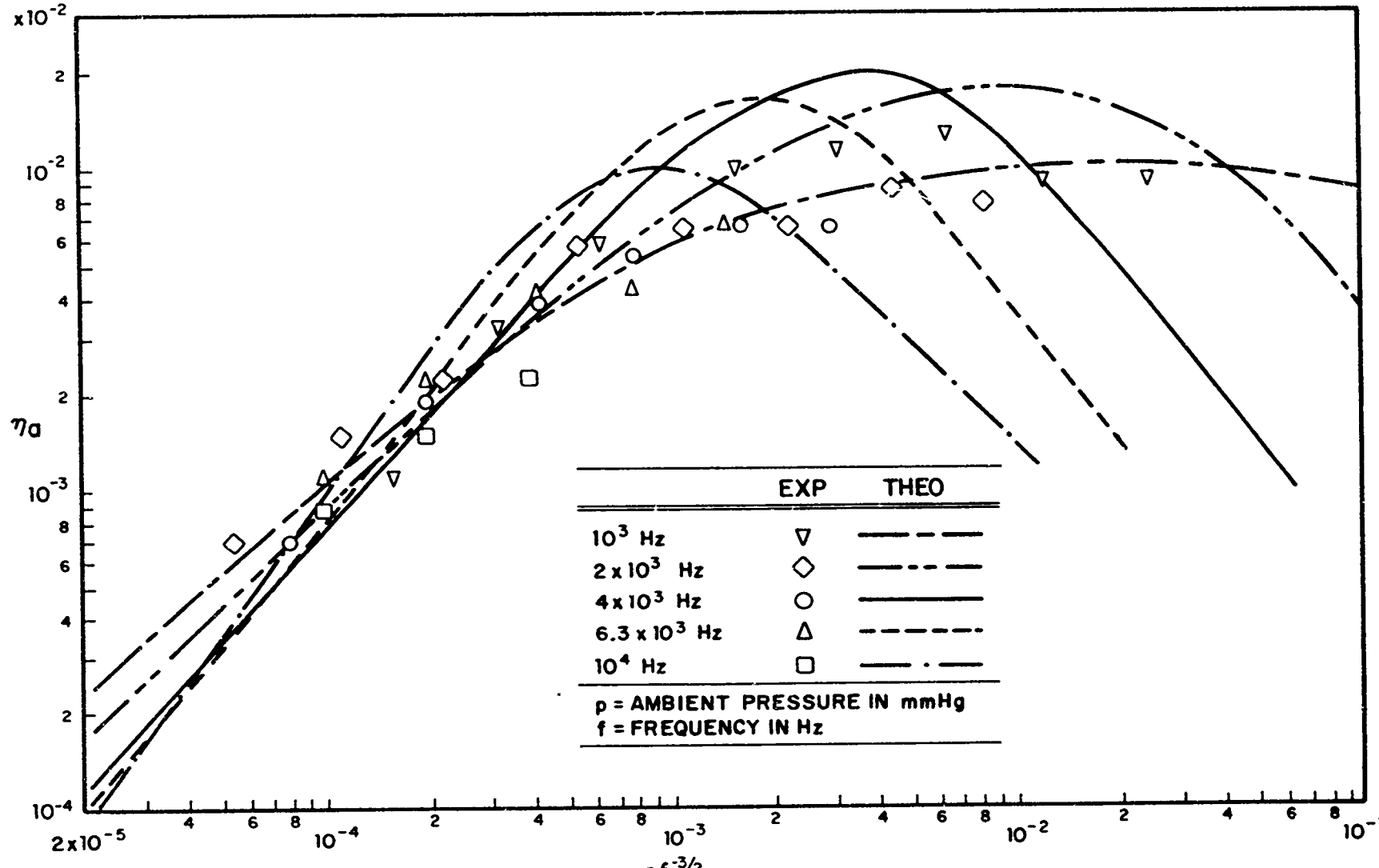

FIG. 12.10

DEPENDENCE OF AIR PUMPING LOSS FACTOR ON AIR PRESSURE AND FREQUENCY: GAP THICKNESS 5×10^{-3} CM

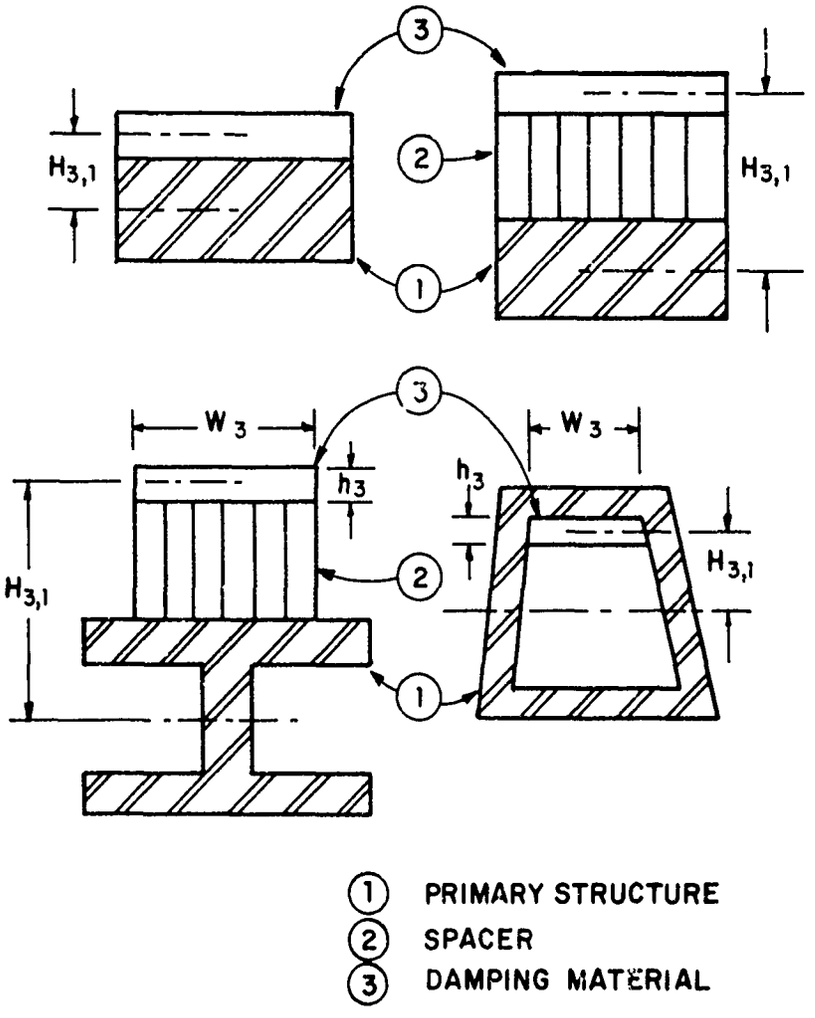

FIG. 12.11

TYPICAL FREE-LAYER CONFIGURATIONS

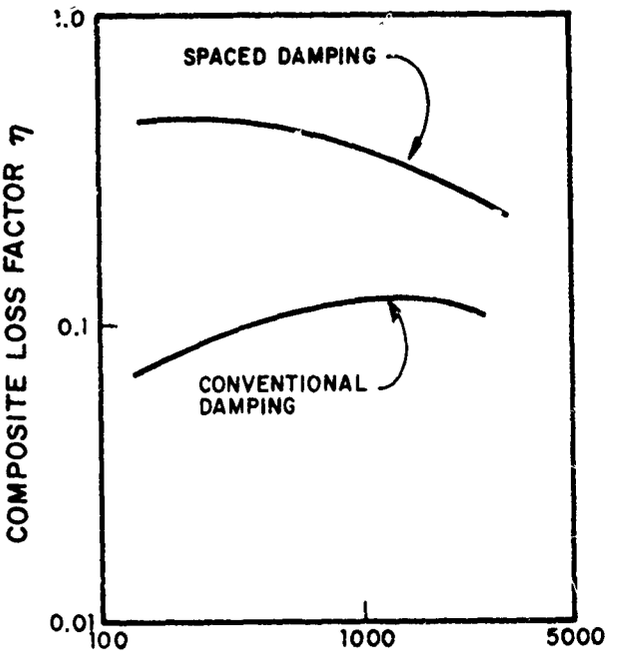

(a) COMPOSITE LOSS FACTOR VS. FREQUENCY FOR SPACED DAMPING AND CONVENTIONAL DAMPING APPLIED TO A 12"x2"x0.25" SOLID STEEL BEAM. DAMPING MATERIALS AND COVERAGE THE SAME IN BOTH CASES.

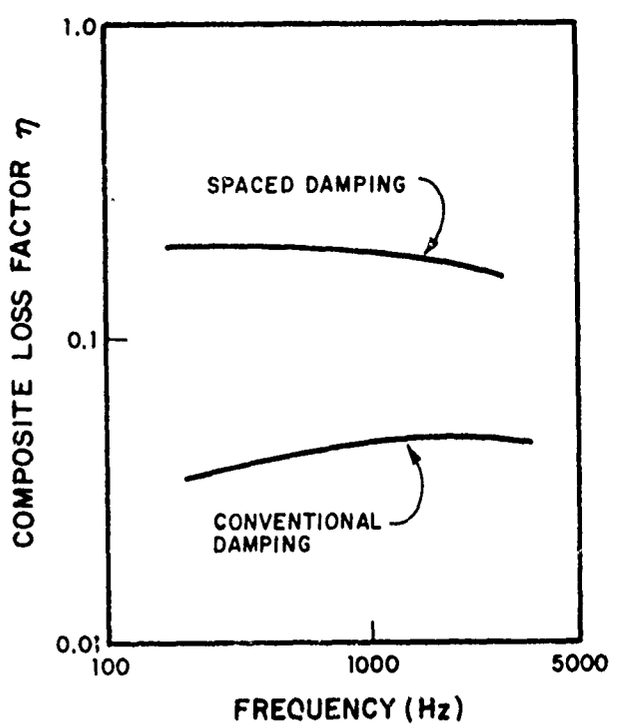

(b) COMPOSITE LOSS FACTOR VS. FREQUENCY FOR SPACED DAMPING AND CONVENTIONAL DAMPING APPLIED TO A 0"x1/8" SQUARE TUBULAR BEAM. DAMPING MATERIALS AND COVERAGE THE SAME IN BOTH CASES

FIG. 12.12

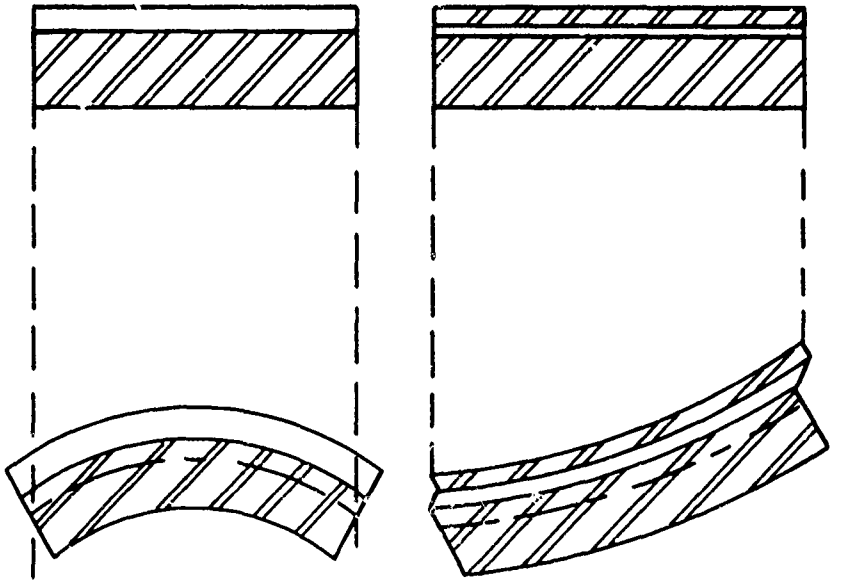

FIG. 12.13

SYSTEMS WITH VISCOELASTIC LAYERS

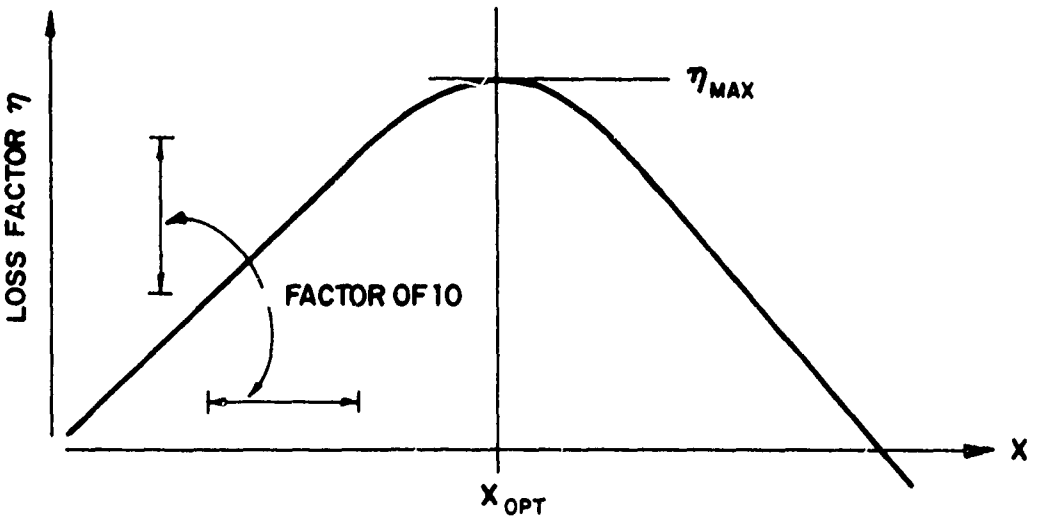

FIG. 12.14

COMPOSITE LOSS FACTOR OF CONSTRAINED DAMPING LAYER ON BASE STRUCTURE

FIG. 12.15

CONFIGURATION OF CONSTRAINED LAYER COMPOSITE

STRUCTURE		STRUCTURAL PARAMETER γ	STRUCTURE		STRUCTURAL PARAMETER γ
PLATES WITH THIN TAPE	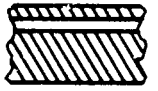	0.1	PLATES WITH THICKNESS RATIO OF 2 TO 1		2.0
HIGHLY ASYMMETRIC COMPOSITES	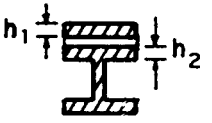	$\gamma = \frac{h_1}{2h_2}$	IDENTICAL PLATES OR THIN-CORE SANDWICH	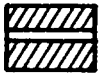	3.0
I-BEAMS WITH EQUAL FLANGES AND DEPTH RATIO OF 2 TO 1		0.75	SYMMETRIC FINNED COMPOSITES	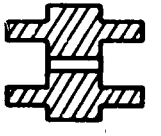	> 3
IDENTICAL I-BEAMS		1.0	THICK-CORE SANDWICH	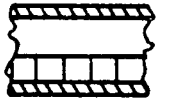	> 3

FIG. 12.16

TYPICAL VALUES OF STRUCTURAL PARAMETER

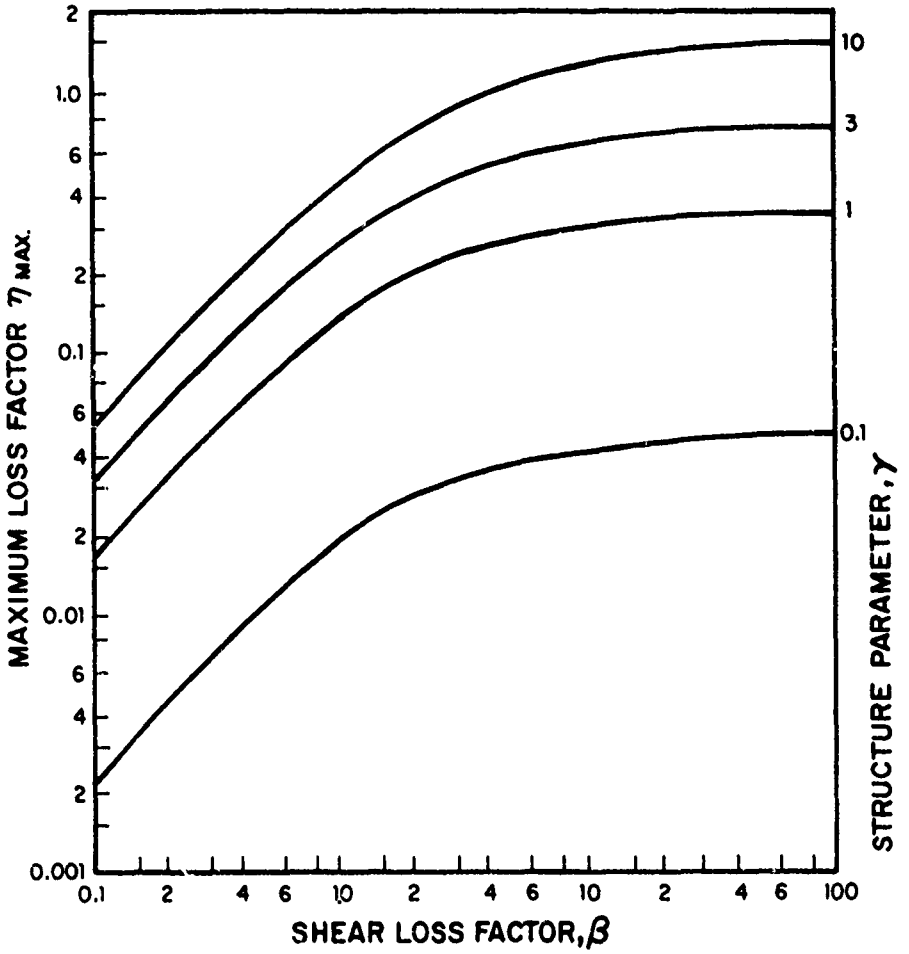

FIG. 12.17

MAXIMUM DAMPING OF
CONSTRAINED LAYERS VS. MATERIAL LOSS FACTOR

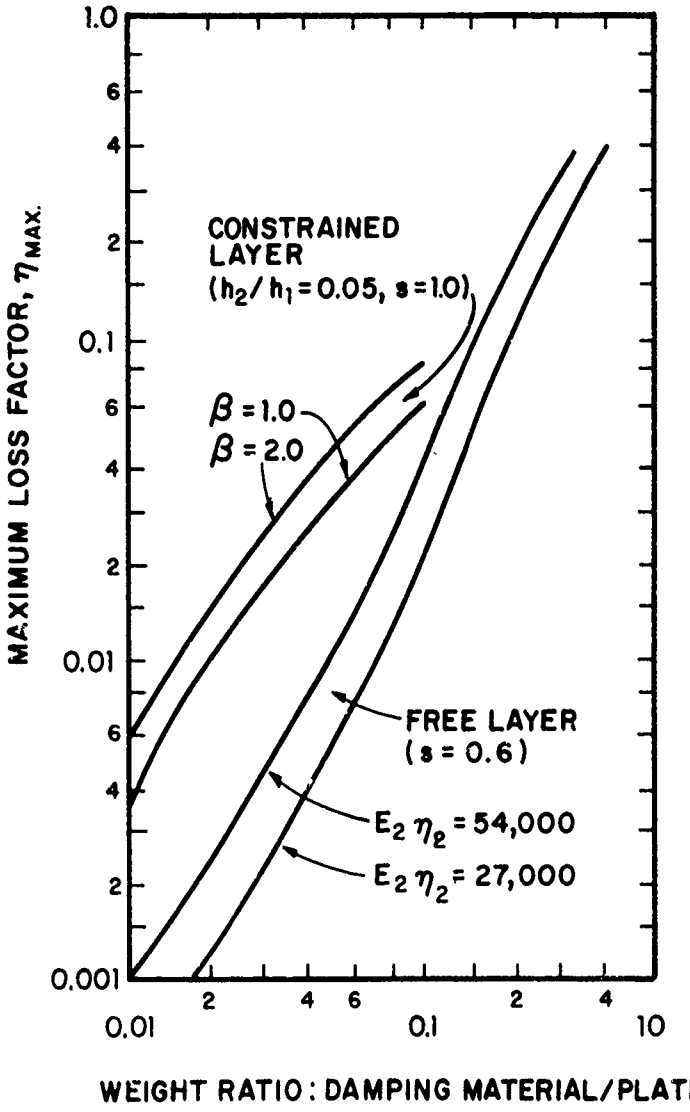

FIG. 12.18

COMPARISON OF FREE AND CONSTRAINED – LAYER TREATMENTS ON STEEL PLATES. SUBSCRIPTS 1 AND 2 REFER TO PLATE AND DAMPING MATERIALS RESPECTIVELY

CHAPTER 13. EVALUATING THE MODE COUNT

13.0 Introduction

The mode count is important in response prediction because it tells us how many resonant modes are available to store energy in the subsystem being studied. In Part I and Section I of Part II, we have seen that this parameter enters most of the equations for response, if not directly, then indirectly through the consistency relation for the coupling loss factors. Mode count also enters relations between modal response and subsystem response in a frequency band containing many modes.

When the mode count is experimentally determined, it can enter the predictions directly, but when we determine it theoretically, we are more likely to calculate the modal density, the number of modes per unit frequency interval. Indeed, we more often find the modal density appearing in the theoretical expressions rather than the mode count. Although the modal density is a simpler quantity to calculate, we should not lose sight of the fact that it is the expected mode count that is fundamental, and that systems that have small mode count may still be modeled as SEA systems even though the concept of modal density is inappropriate.

The mode count (or modal density) is the SEA parameter that is generally the easiest to determine. In frequency regions in which there are few modes and the modal density may be difficult to calculate, a simple measurement on the system (or a model of it) can often be made. In frequency regions in which the modes are very dense, and it is difficult to resolve them experimentally, one can usually make an adequate theoretical estimate. Thus, by a combination of experimental and calculational procedures, one can usually determine the mode count to acceptable accuracy.

Division of the problem into regimes of sparse and dense modal distribution is reminiscent of the situation with regard to damping. In fact, it turns out to be true for all the parameters, including coupling loss factors as well, that different functional forms or different experimental methods for their evaluation are required, depending on the density of modes.

In this chapter, we first discuss the measurement of mode count and subsequently, the theoretical formulae for important cases of acoustical spaces and structural subsystems.

13.1 Experimental Procedures for Determining Mode Count

The simplest and most common set-up for finding mode count is that shown in Fig. 13.1. The idea is simply to excite the system with a pure tone, usually at a point, and observe the response at a second point as the excitation frequency is slowly swept over the band of interest. For the mechanical structure in Fig. 13.1, the excitation is with a shaker and response is measured by an accelerometer. If the system is an acoustical system, excitation would be with a small loudspeaker or horn driver and response would be measured with a microphone.

Even though simple, this procedure can given erroneous or incomplete results unless certain precautions are taken. To make certain that as many modes as possible are excited; the excitation should be near a free boundary for a structure or a rigid wall for a sound field, since all the modes have antinodes along such boundaries. To further enhance the likelihood of all modes being excited and sensed, several source and receiver locations should be chosen. If the graphs are overlaid, modes that barely respond on one sweep will respond more on another. Even if some of the modes are missed, the estimates are only sensitive to the relative error in mode count. Thus, if two out of twenty modes are missed, only a 1 dB error in the mode count will result. This error would normally result in a 1 dB error in a response prediction also.

Some other features of the experimental set up should be mentioned. For example, the use of a logarithmic presentation on the chart is preferable to a linear presentation. With logarithmic output, modes that respond with small amplitude are much more likely to be seen. Also, the sweep must be slow enough so that two modes are not simultaneously excited and beat against each other, or so that a mode that is decaying does not beat with the non-resonant response at the shaker frequency. Such beats will cause additional peaks on the chart which might be mistaken for modal resonances.

The procedure just described works as long as the separation between modes δf is at least three times the bandwidth of a mode, $\pi/2 \ \eta f$ or

$$\pi\eta f/2\delta f \leq 0.3. \qquad (13.1.1)$$

If the average modal separate δf is too small, then too many modes will be missed by the sine-sweep test. In this event, an alternate, but less proven technique may be useful.

The alternate procedure relies upon the result that, as shown in Part I, the average input power due to a force $L(t)$ in a band Δf is [see Eq. (2.2.24)]

$$\Pi_{in} = \langle L^2 \rangle_t / 4M\delta f \qquad (13.1.2)$$

and the mean square response is, therefore,

$$\langle v^2 \rangle = \Pi_{in}/2\pi f\eta M = \langle L^2 \rangle_t / 8\pi f\eta M^2 \delta f \qquad (13.1.3)$$

Thus, if $\langle v^2 \rangle$ is measured for a known $\langle L^2 \rangle$ and η, one can infer δf. In this procedure, the difficulty is to control the mean square force, as discussed in Chapter 12. Even if one cannot precisely determine $\langle L^2 \rangle$, the relative response of the system in different bands can determine relative values of δf. Then if the exact value of δf is known in a few bands, it can be determined in all the bands.

13.2 Mode Counts of Acoustical Subsystems

The average frequency separation between modes in a one-dimensional acoustical system of length ℓ and sound speed c is

$$\delta f = c/2\ell \qquad (13.2.1)$$

This formula applies to any cylindrical space in which one-

dimension is significantly greater than the other two and the wavelength of sound is greater than the greatest cross-dimension ℓ_c:

$$\lambda > 2\ell_c \text{ or } f_c < c/2\ell_c \cdot \qquad (13.2.2)$$

The modal separation for a thin, flat acoustical space of area A and perimeter P is given by

$$\delta f = 2\pi fA/c^2 + P/c \qquad (13.2.3)$$

This formula is valid as long as the wavelength of sound is greater than twice the depth ℓ_D of the space

$$\lambda > 2\ell_D \text{ or } f < c/2\ell_D \qquad (13.2.4)$$

The modal separation for a three-dimensional space of volume V, surface area A and total edge length ℓ is given by

$$1/\delta f = 4\pi f^2 V/c^3 + \pi fA/2c^2 + \ell/8c \qquad (13.2.5)$$

These formulas and the cases they relate to are shown in Figs. 13.2, 13.3 and 13.4. Generally these results are adequate to supply good estimates of mode count for subsystems or elements that have standing sound waves as the energy storage mechanism.

13.3 Flat Structures

The simplest structure that we can write the modal density for is the homogeneous flat panel of area A

$$\delta f = hc_\ell/\sqrt{3}\ A \qquad (13.3.1)$$

where h is the thickness of the panel cross section and c_ℓ is the longitudinal wavespeed in the panel material. If the material is steel, aluminum or glass, then

$$c_\ell = 17{,}000 \text{ ft/sec}$$

and if h is expressed in ft, one has

$$\delta f = h(\text{ft}) \times 10^4/A(\text{ft}^2) \qquad (13.3.2)$$

If the panel is not homogeneous, but is of a sandwich or other layered construction, a similar but more complicated relation can be given. The wave velocity c_ϕ must be known as a function of frequency $\omega=2\pi f$. It is then substituted into

$$\delta f = \frac{c_\phi^2}{\omega A}\left[1 - \frac{\omega}{c_\phi}\ \frac{dc_\phi}{d\omega}\right]^{-1} \qquad (13.3.3)$$

For example, it often happens for such structures that the wave speed increases as a power of the frequency

$$c_\phi = B\ \omega^n \qquad (13.3.4)$$

in which case

$$\delta f = \frac{B^2\omega^{2n-1}}{A}\ (1-n)^{-1} \qquad (13.3.5)$$

When n = 0 (acoustical case, Figure 13.3), $\delta f \sim 1/f$ as found in Equation (13.2.3). When n = 1/2 (homogeneous plate), then δf = const., as found in Eq. (13.3.1). For other constructions, a dynamical analysis of the panel construction must be carried out to determine c_ϕ.

In some cases, a plate will be orthotropic, i.e., stiffer along one direction than the other, as shown in Fig. 13.5. If these two directions are labelled "1" and "2", the modal density $n(f) = 1/\delta f$ is in effect an average value between isotropic plates of the two stiffnesses

$$1/\delta f = \frac{1}{2}\,\omega A\,\{\frac{1}{c_1^{\,2}}\,(1 - \frac{\omega}{c_1}\,\frac{dc_1}{d\omega}) + \frac{1}{c_2^{\,2}}\,(1 - \frac{\omega}{c_2}\,\frac{dc_2}{d\omega})\} \tag{13.3.6}$$

or, if the construction is such that $c_1, c_2 \sim \omega^n$, we have

$$1/\delta f = \frac{1}{2}\,\omega A(1-n)\,\{\frac{1}{c_1^{\,2}} + \frac{1}{c_2^{\,2}}\} \tag{13.3.7}$$

where c_1 and c_2 are the wavespeeds in the two principal directions. Obviously if $c_1 = c_2$, we revert to Eq. (13.3.5).

13.4 Mode Count of Curved Structures

Since most aerospace structures consist of complete or segments of curved shells, the effect of curvature on mode count of structures is of great significance. Although a fair amount of work has been done on such structures, we are not able to write simple formulas for the mode count in all instances. In this paragraph we provide some of the available results that are of greatest interest in the present context.

Circular Cylinders. The modal density of a circular cylinder may be considered a variation of the modal density of

a flat structure of the same area and construction (homogeneous, layered, etc.) but modified to the account of the effects of curvature. The form of the modal density is shown in Fig. 13.6. The characteristic frequency that separates the high frequency flat plate behavior from low frequency cylinder behavior is the so-called ring frequency f_{ring}, defined by

$$f_{ring} = c_\ell / 2\pi a \qquad (13.4.1)$$

where c_ℓ is the longitudinal wavespeed introduced in paragraphs 3.3 and a is the radius of curvature of the cylinder.

Using results from Szechenyi [22] we can present simple curve-fitting formulas for the modal density, which are as follows:

$$\frac{\delta f(\text{flat plate})}{\delta f(\text{cylinder})} = \left(\frac{f}{f_{ring}}\right)^{1/2}; \quad \frac{f}{f_{ring}} \leq 0.5$$

$$= 1.4 \frac{f}{f_{ring}}; \quad 0.5 < \frac{f}{f_{ring}} < 0.8$$

$$= 0.8 \frac{0.1}{F - 1/F} \left\{ F \cos\left[\frac{1.75}{F^2}\left(\frac{f_{ring}}{f}\right)^2\right] - \frac{1}{F} \cos\left[1.75 F^2 \left(\frac{f_{ring}}{f}\right)^2\right] \right\};$$

$$\frac{f}{f_{ring}} > 0.8 \qquad (13.4.2)$$

where the quantity F represents the band limits over which the average is taken from

$$F \frac{f}{f_{ring}}$$

to

$$\frac{1}{F} \frac{f}{f_{ring}} \quad .$$

Thus, F = 1.222 for a 1/3 octave band and 1.414 for an octave band.

Doubly Curved Shells. Occasionally a shell or a segment of a shell will be in the form of a doubly curved surface, as shown in Fig. 13.7. A torus is an example of such a shell. Torodial sections are frequently used to join a cylinder with a spherical cap, for example. Suppose the shell has area A, longitudinal wavespeed c_ℓ, and cross-sectional radius of gyration κ. Then if R_1 and R_2 are the two principal radii of curvature, we can define two ring frequencies

$$f_{r1} = \frac{c_\ell}{2\pi R_1} \; ; \quad f_{r2} = \frac{c_\ell}{2\pi R_2} \tag{13.4.3}$$

and we arbitrarily assume $R_2 > R_1$ so that $f_{r2} < f_{r1}$.

With this hypothesis, Wilkinson [23] has computed the modal densities for a doubly curved shallow shell.

$$f < f_{r2} < f_{r1}; \quad n(f) = 1/\delta = 0. \tag{13.4.4}$$

There are no resonant modes in this frequency regime. In the frequency range "between" the two ring frequencies, $f_{r2} < f < f_{r1}$

$$\frac{\delta f(\text{flat plate})}{\delta f(\text{shell})} = \frac{\sqrt{2}}{\pi} \frac{f^{\frac{3}{2}}}{(f^2-f_{r1}^2)^{\frac{1}{2}}(f_{r1}-f_{r2})^{\frac{1}{2}}} F(\pi/2,\kappa) \tag{13.4.5}$$

and in the frequency range above the two ring frequencies $f_{r2} < f_{r1} < f$

$$\frac{\delta f(\text{flat plate})}{\delta f(\text{shell})} = \frac{2}{\pi} \frac{f^2 F(\pi/2,\ 1/\kappa)}{(f^2-f_{r1}^2)^{\frac{1}{2}}(f+f_{r1})^{\frac{1}{2}}(f-f_{r2})^{\frac{1}{2}}} \tag{13.4.6}$$

where $\kappa = (f+f_{r1})^{\frac{1}{2}}\ (f-f_{r2})^{\frac{1}{2}}/\{2f(f_{r1}-f_{r2})\}^{\frac{1}{2}}$,and $F(\pi/2,\xi)$ is the elliptic integral of the first kind, defined by [24]

$$F(\pi/2,\xi) = \frac{\pi}{2}\int_0^{\pi/2} (1-\xi^2\sin^2 t)^{-\frac{1}{2}}\, dt. \tag{13.4.7}$$

When $|\xi| < 1$ this can be expressed in the series [24]

$$F\left(\frac{\pi}{2}\ ,\xi\right) = \frac{\pi}{2}\sum_{n=0}^{\infty} \frac{\Gamma(n+\frac{1}{2}(2n)!}{\Gamma(\frac{1}{2})(n!)^{\ 3}}\ 2^{-2n}\xi^{2n} \tag{13.4.8}$$

When $f >> f_{r1}$, then $|\xi| >> 1$ and Eq. (13.4.6) becomes

$$\frac{\delta f(\text{flat plate})}{\delta f(\text{shell})} = 1 \tag{13.4.9}$$

Thus, the modal density again becomes equal to that of a flat plate of equal area at high frequencies and short wavelengths.

Two interesting special cases can be derived from the relations (13.4.4, 5, 6). If $R_2 \to \infty$ and $f_{r2} \to 0$, the shell modal density becomes for $f < f_r$.

$$\frac{\delta f(\text{flat plate})}{\delta f(\text{cylinder})} = \frac{\sqrt{2}}{\pi} \frac{f^{\frac{3}{2}} F[\pi/2, \sqrt{(f+f_r)/2f_r}]}{(f^2-f_r^2)^{\frac{1}{2}} f_r^{\frac{1}{2}}} \quad (13.4.2')$$

and for $f > f_r$.

$$\frac{\delta f(\text{flat plate})}{\delta f(\text{cylinder})} = \frac{2}{\pi} \frac{f^2 F[\pi/2, \sqrt{2f_r/(f+f_r)}]}{(f^2-f_r^2)^{\frac{1}{2}}(f+f_r)^{\frac{1}{2}} f_r^{\frac{1}{2}}} \quad (13.4.2")$$

On the other hand, $R_1=R_2$ for a spherical cap, and the middle range vanishes to give, for $f < f_r$

$$\frac{\delta f(\text{flat plate})}{\delta f(\text{sphere})} = 0 \quad (13.4.10)$$

and for $f > f_r$

$$\frac{\delta f(\text{flat plate})}{\delta f(\text{sphere})} = \frac{2f^2}{\pi(f^2-f_r^2)} F(\tfrac{\pi}{2}, 0) = \frac{f^2}{f^2-f_r^2} . \quad (13.4.11)$$

For a sphere, therefore, the modal density approaches its asymptotic flat plate value very quickly above the ring frequency and there is a total depletion of modes below the ring frequency.

Conical Shells and Shells of Varying Radius of Curvature. A large number of structural shells of aerospace interest are sections of surfaces of revolution in which the curvature varies along a coordinate. It is possible to develop a general theory

for the mode shapes and resonant frequencies for such shells as recently reported by Pierce [25] and Germogenova [26].

When the radius of curvature increases linearly along the axial coordinate, the shell is a cone. It is not possible to find a general expression for the modal density for these structures, but as shown in Chapter 15, it is possible to find the mode count for particular situations.

Although general formulas for mode count are not available for shells of revolution, many situations can be worked out to a satisfactory degree of accuracy by following the procedures in the references.

13.5 One-Dimensional Structure

A commonly encountered aerospace structure is the one-dimensional beam, stringer, or frame member. Although the one-dimensional geometry tends to simplify the mode count prediction, the dynamics of such structures can be rather complex. A simple beam of rectangular or circular cross section has separate propagation modes for flexural, torsional, and longitudinal wave propagation. However, channel or hat-section stringer or frame has coupling between these motions so that the actual vibrational modes combine the "pure" wave types.

Fortunately, the additive properties of mode count simplifies the process of prediction. We may calculate mode counts on the hypothesis that the coupling does not occur and then add the mode counts for the pure modes to obtain our estimate for the mixed motions when the geometry of the beam cross-section or end conditions are such that we expect such coupling to be important.

The average modal separation δf of a one-dimensional system of length ℓ and phase speed $c_\phi(\omega)$ is given by

$$n(f) = 1/\delta f = \frac{2\ell}{c_\phi}\left[1 - \frac{\omega}{c_\phi}\frac{dc_\phi}{d\omega}\right] . \qquad (13.5.1)$$

In the case of longitudinal, the phase speed c_ϕ is independent of frequency:

$$1/\delta f(\text{long'l}) = 2\ell/c_\ell; \quad c_\ell = \sqrt{E/\rho} \tag{13.5.2}$$

Where E is the Young's modulus and ρ is the lineal density of the beam. In the case of torsional waves

$$1/\delta f(\text{torsional}) = 2\ell/c_t; \quad c_t = c_s\sqrt{J/\kappa_\phi^2 A} \tag{13.5.3}$$

where J is the moment of rigidity for the cross-section in question, κ_ϕ is the radius of gyration about the c.g. of the cross-section, A is the area of the cross-section of the beam, and c_s is the speed of shear waves in the material. The quantity J for various cross-sections of interest may be found in references on the strength of materials.

The bending wave speed is generally dispersive, as it is in plates. Again, if $c_\phi \sim \omega^n$, then

$$1/\delta f(\text{flexural}) = \frac{2\ell}{c_\phi}(1-n) \tag{13.5.4}$$

which is ℓ/c_ϕ for $n = 1/2$. For more complex cross-sectional shapes, the more general formula (13.5.1) must be used.

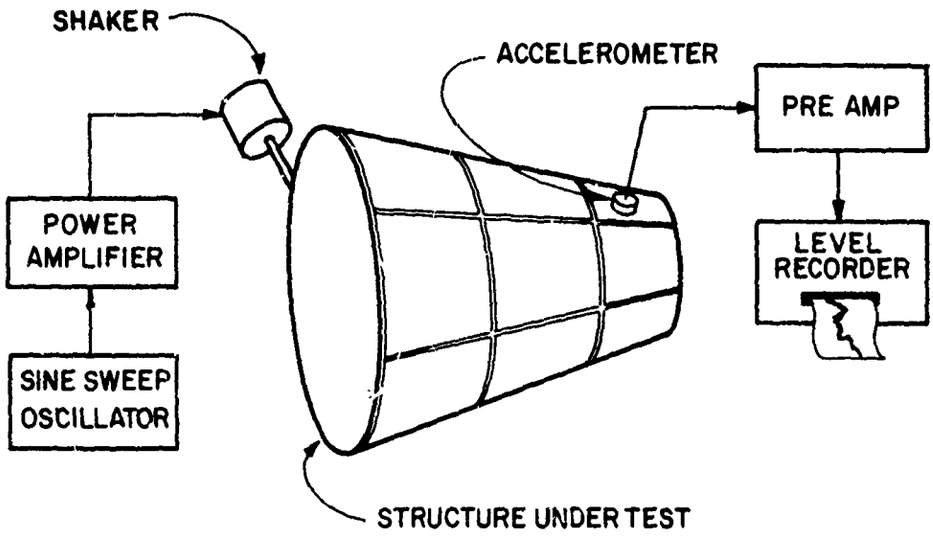

FIG. 13.1

ARRANGEMENT FOR FINDING MODE COUNT
BY SINE SWEEP TECHNIQUE

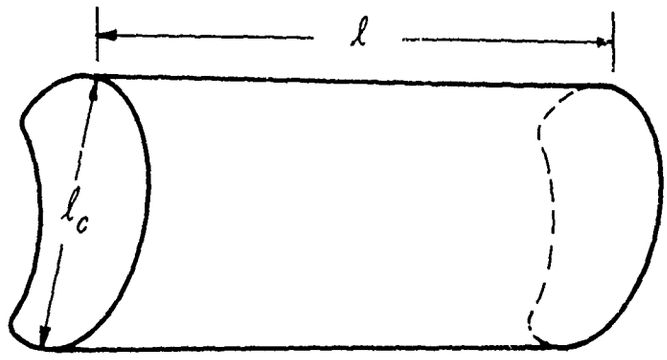

FIG. 13.2

ACOUSTICAL SUBSYSTEM ; 1-DIMENSIONAL CYLINDER

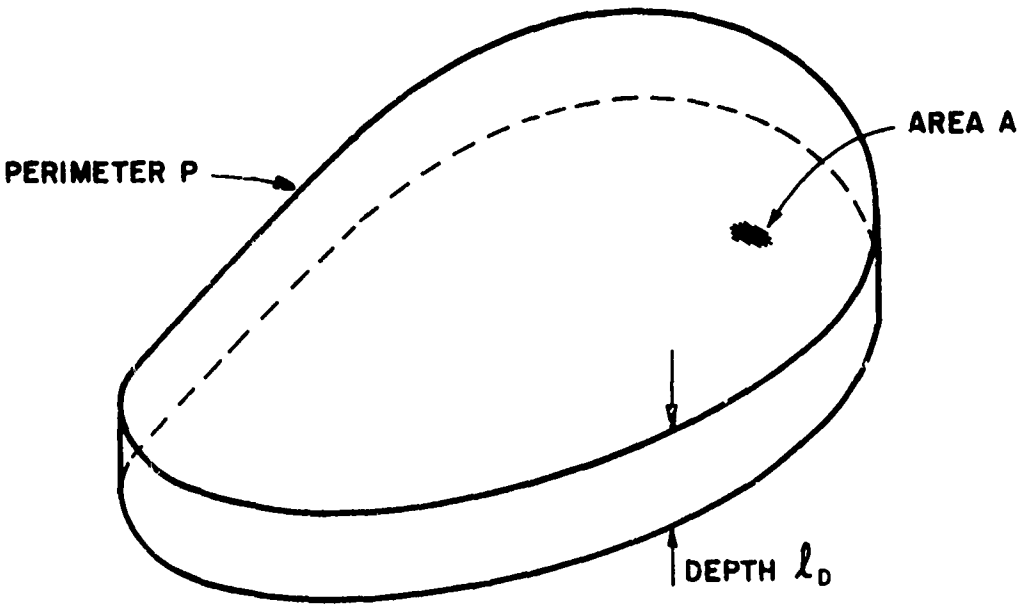

FIG. 13.3

ACOUSTICAL SUBSYSTEM; 2-DIMENSIONAL CAVITY

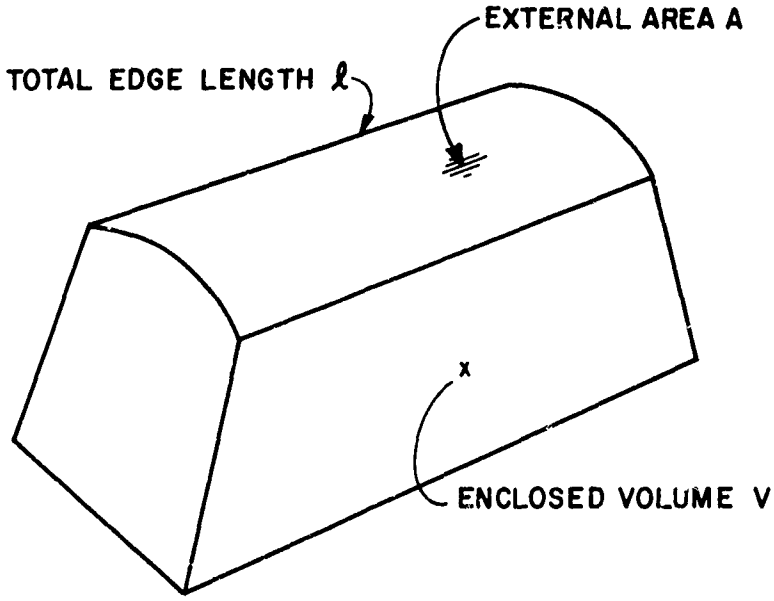

FIG. 13.4

ACOUSTICAL SUBSYSTEM : 3-DIMENSIONAL

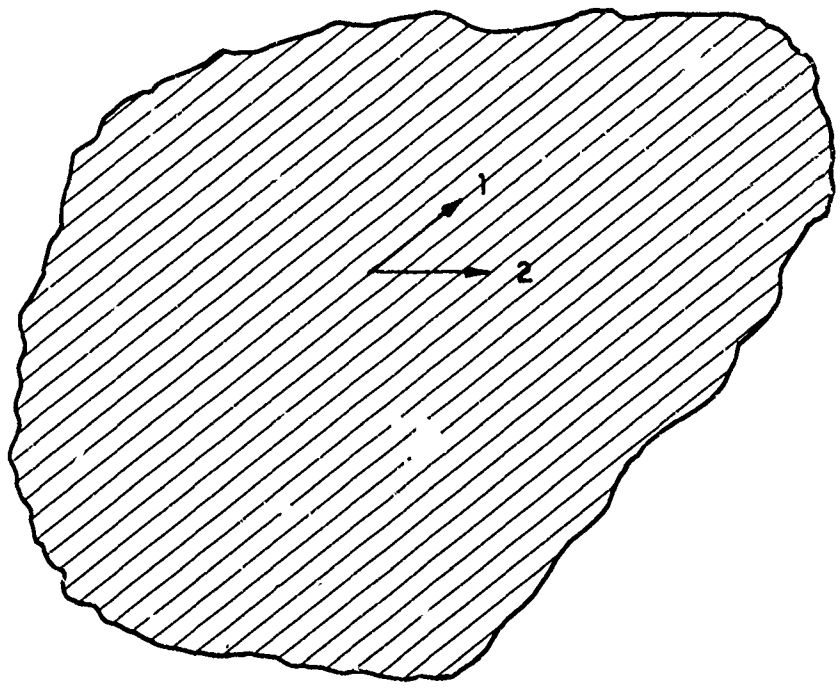

FIG. 13.5

ANISOTROPIC PLATE : PHASE SPEED c_1 IN 1-DIRECTION, c_2 IN 2-DIRECTION

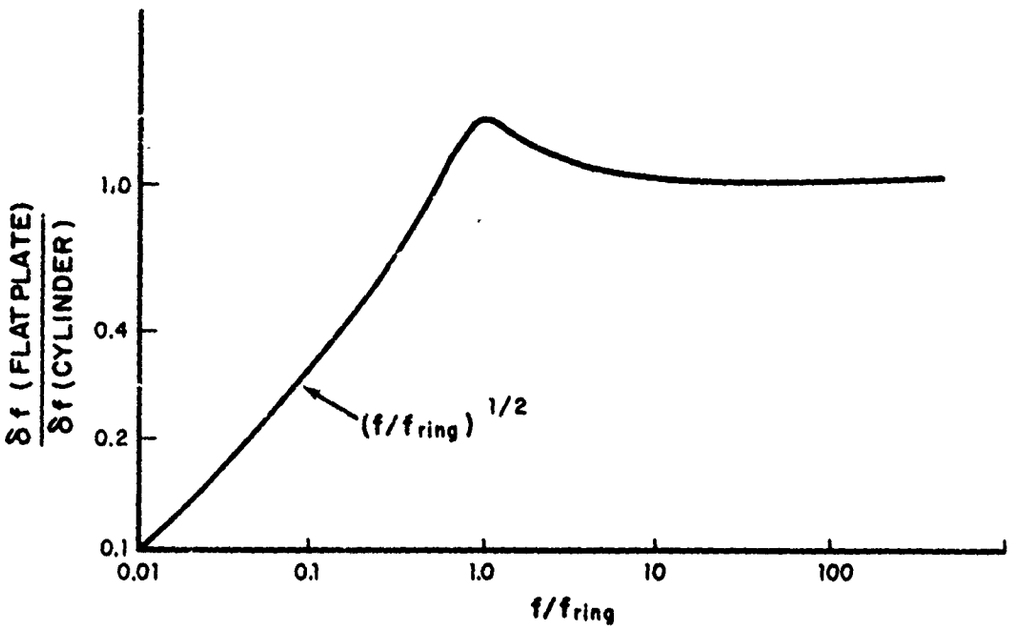

FIG. 13.6

MODAL DENSITY OF CYLINDER

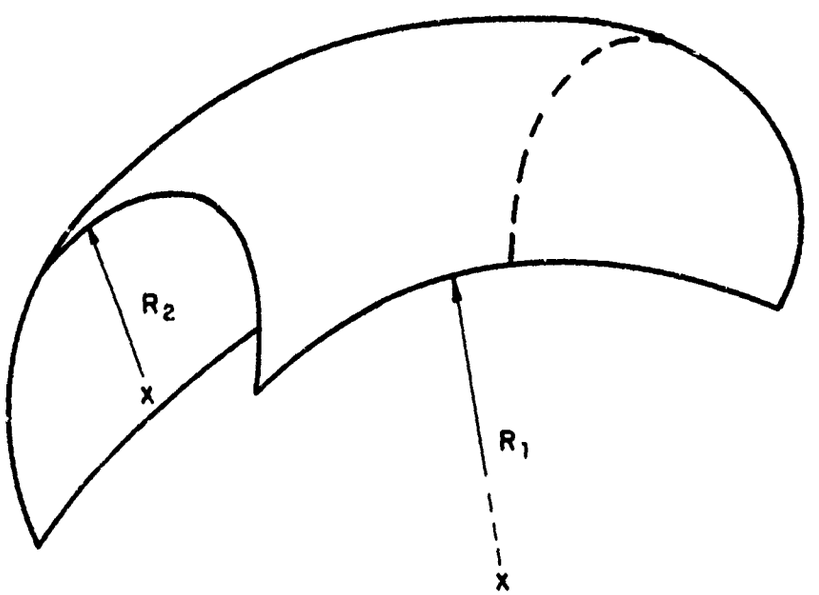

FIG. 13.7

SECTION OF A TORUS, A SHELL WITH TWO CONSTANT RADII OF CURVATURE

CHAPTER 14 EVALUATING COUPLING LOSS FACTORS

14.0 Introduction

This chapter is concerned with presenting known values of the coupling loss factor (CLF) and methods for obtaining the CLF. In contrast to modal densities and damping, parameters that are well known outside the context of SEA, the coupling loss factor is uniquely associated with SEA. As we have seen in Part I and Part II, Section I, however, it is sometimes possible to relate the CLF to parameters (such as structural input impedances) that may have been evaluated for other purposes.

There are a variety of ways that the CLF may enter a calculation - as a "radiation resistance", as a ratio of power flow to stored energy, or as a frequency average over junction impedance functions. In addition, there is a variety of acoustical and mechanical systems that are of interest in aerospace applications that may be joined together. This richness of possibilities makes it very difficult to give an exhaustive listing of CLF values that will cover all potential cases of interest. Nevertheless, we present here known CLF data on some systems of interest and indicate wherever possible how information on other systems may be generated either by experiment or calculation.

The chapter is organized by the kinds of subsystems that are in contact with each other. Thus, we begin with coupling between two acoustical spaces. In this case, it happens that there is a great deal of experimental and theoretical data available on the CLF, or more precisely, a related parameter, the transmission loss. The second category of coupled systems is that in which one is structural and the other is a sound field. In this case, the coupling loss factor is related to the radiation resistance of the structure, for which there is a fair amount of information in the literature, some of which is experimental, but most is theoretical.

The final paragraph of the chapter is concerned with structure-structure interactions. These interactions are the most difficult for several reasons. First, experiments on such interaction are difficult to carry out and the number of reported results is fairly small. Second, the

kinds of motion may be quite complex for some structures and the "impedances" may be matrix quantities. Third, the formal derivation of CLF values for these cases can be extremely complicated, so that theoretical results, while conceivable, may require such extensive analyses that we are reluctant to do the work, particularly in a preliminary design situation.

14.1 Coupling Between Acoustical Spaces

In acoustical spaces, the response is measured by the m.s. pressure in a band, $\langle p^2 \rangle$. If the dimensions of the space (call it subsystem 1) are greater than an acoustical wavelength, then the power incident upon a wall of A_w is

$$\Pi_{inc} = \langle p_1^2 \rangle \quad A_w/4\rho c \tag{14.1.1}$$

where ρ is the density of air and c is the speed of sound. The transmissibility of the wall is defined as

$$\tau = \Pi_{trans}/\Pi_{inc} = 4\rho c \; \Pi_{trans} \; \langle p_1^2 \rangle \; A_w \tag{14.1.2}$$

where Π_{trans} is the power transmitted through the wall into the receiving acoustical space.

The transmitted power can be related to the CLF since, in the absence of flow back from the receiving system (subsystem 2) to the "source" cavity (subsystem 1), an assumption that is made in most acoustical transmission studies, one may also write

$$\Pi_{trans} = \omega \eta_{12} E_1 = 2\pi f \eta_{12} \langle p_1^2 \rangle V_1/\rho c^2 \tag{14.1.3}$$

and, consequently, comparing (14.1.2) and (14.1.3), we can make the association:

$$\eta_{12} = \tau\ c\ A_w/8\pi f V_1 \qquad (14.1.4)$$

All of the voluminous data on transmission loss (TL),

$$TL \equiv -10 \log \tau \qquad (14.1.5)$$

becomes, therefore, a source of information on the coupling loss factor between acoustical spaces [27].

Unfortunately, as large as this data base is, it is primarily oriented to building constructions (gypsum board, brick, plaster, etc.) and relatively little data by comparison is available for aerospace constructions. Also, building constructions tend to be formed from flat panels so that the curved geometries characteristic of aerospace construction are not well represented. For these reasons, it will often be necessary to determine η_{12} experimentally for systems representative of aerospace configurations.

Experimental Determination of CLF for Acoustical Spaces. The experimental procedure for finding η_{12} is to excite one of the cavities with a source of sound as shown in Fig. 14.1 (usually the loudspeaker is driven by a band of noise) and to infer τ from the m.s. pressure in the two spaces. Since the transmitted sound power into cavity 2 must be dissipated there, one has

$$\Pi_{trans} = \frac{\langle p_2^2 \rangle V_2}{\rho c^2}\ 2\pi f \eta_2 \qquad (14.1.5)$$

where η_2 is the loss factor and V_2 is the volume of cavity 2. This parameter is usually measured by a decay rate experiment of the kind discussed in Chapter 12, using the relation

$$DR\ (dB/sec) = 27.3\ f\eta_2\ , \qquad (14.1.6)$$

Using (14.1.5), (14.1.2) and (14.1.4), we then obtain

$$\tau = \frac{\langle p_2^2 \rangle}{\langle p_1^2 \rangle} \quad \frac{8\pi f V_2}{c A_w} \eta_2 = \eta_{12} \quad \frac{8\pi f V_1}{c A_w} \tag{14.1.7}$$

or,

$$10 \log \eta_{12} = L_{p_2} - L_{p_1} + 10 \log \eta_2 + 10 \log V_2/V_1 \tag{14.1.8}$$

where, of course, L_p is the sound pressure level. Thus, a simple measurement of sound pressure levels in the cavities and of decay rate of the receiving space is sufficient to determine the CLF. One should be careful, however, that the difference in sound pressure level $L_{p_1} - L_{p_2}$ should be at least 10 dB to ensure that the assumption that all the transmitted power is dissipated in the receiving space is satisfied.

Data on CLF for Aerospace Structures. The transmission loss of a thin flat steel panel has been measured and calculated by Crocker [28] whose data is shown in Fig. 14.2. A flat aluminum structure has a TL minimum at the critical frequency

$$f_c = 12{,}500/h \text{ (mm)} \tag{14.1.9}$$

where h is the thickness of the panel in millimeters. For frequencies an octave or more below f_c, the TL is well approximated by the so-called "mass law" formula [29]

$$TL_M = 20 \log f + 20 \log W - 33 \tag{14.1.10}$$

where f is the frequency in hertz and W is the mass density

of the panel in lb/ft^2. Since aerospace structures are fairly thin, we are usually interested in the frequency range well below f_c and this mass law formula will give an acceptable approximation for TL.

Eq. (14.1.10) is derived from the non-resonant transmissibility of the panel, but one must sometimes include a resonant transmissibility, particularly if the structure has many reinforcing ribs or frames. The resonant transmissibility is given by

$$\tau_{res} = \frac{2}{\pi} \frac{\rho^2 c}{m_s^2} \frac{V_l}{A_w} \frac{\sigma_{rad}^2}{\eta_w} \qquad (14.1.11)$$

where σ_{rad} is the radiation efficiency of the structure, m_s is the mass per unit area of the structure (wall) and η_w is its loss factor. The parameter $\sigma_{rad} = R_{rad}/\rho c A_w$, and R_{rad} is evaluated from data presented in paragraph 14.2.

For frequencies above the critical frequency, the transmission loss (or coupling loss factor) depends on the damping of the wall η_w in the form [30]

$$TL(f>f_c) = TL_M + 10 \log \eta_w + 10 \log \left(\frac{f}{f_c} - 1\right) + 3 \qquad (14.1.12)$$

where TL_M is given by Eq. (14.1.10) and η_w is to be determined by the methods of Chapter 12. Since most aerospace panels have a fairly high critical frequency, we are not ordinarily interested in the condition $f > f_c$. On the other hand, lightweight sandwich constructions used in fatigue resistant designs may have a much lower critical frequency. For such constructions

$$f_c \approx 7000/t \text{ (mm)} \qquad (14.1.13)$$

where t is the total thickness of the aluminum sandwich in mm. Thus, an 8 mm thick sandwich will have a critical frequency of 900 Hz. We may well be concerned with finding the CLF in frequency bands up to 4 or 5 kHz, in which case we would have to use Eq. (14.1.12).

The relations (14.1.10) and (14.1.12) apply an octave or so away from $f = f_c$. To "fill in" the range $f \approx f_c$, a transition curve like that appearing in the data shown in Fig. 14.2 can be used. The resulting curve will usually provide an estimate of TL that is accurate enough for estimation purposes.

Cylindrical Structures. Sound transmission through cylindrical structures is complicated by an additional frequency parameter, the ring frequency

$$f_r = c_\ell / 2\pi a \qquad (14.1.14)$$

where a is the radius of the cylinder. As noted in Chapter 13, above this frequency the cylinder acts as a flat plate, so that the flat plate CLF formulas apply. At and below f_r, membrane stiffness effects cause changes in the transmission loss, as may be seen in the experimental data shown in Fig. 14.3. Deviations from the prediction according to Eq. (14.1.10) and the data at and below f_r may be taken as representative of the effect of the ring frequency on TL. [22]. Near f_r, the TL is reduced 2 to 3 dB and below f_r the TL is increased by 3 to 4 dB as compared to flat plate values.

14.2 Coupling Between Structures and Acoustical Spaces

The CLF between a structure and a sound field is most simply expressed by the average radiation resistance of the structure interacting with an infinite space. This is an acceptable approximation when the wavelength of sound is a third or less a typical dimension of the cavity. At lower frequencies, a mode-to-mode CLF may have to be developed.

When the radiation resistance of the structure is a suitable measure, the CLF between the structure and the acoustical cavity, η_{sa}, is given by

$$\eta_{sa} = R_{rad}/\omega M_s \tag{14.2.1}$$

where M_s is the mass of the structure. This radiation resistance R_{rad} has been calculated for several structural systems of interest in aerospace applications. The coupling from the acoustical space to the structure can be found from the consistency relation,

$$\eta_{as} = \eta_{sa} N_s/N_a \tag{14.2.2}$$

where N_s and N_a are mode counts for the structure and the acoustical space respectively, as determined in Chapter 13.

Radiation from Finite Flat Panels. The radiation resistance of one side of a flat panel of area A_p and perimeter P is given by [31]

$$R_{rad} = \rho c A_p \left\{ \frac{\lambda_c P}{\pi A_p} \frac{2}{\pi} \sin^{-1} \left(\frac{f}{f_c} \right)^{\frac{1}{2}} \right\} \beta \quad (f < f_c)$$

$$= \rho c A_p \{1 - f_c/f)\}^{-\frac{1}{2}} \quad (f > f_c) \tag{14.2.3}$$

where f_c is the critical frequency given in Eqs. (14.1.9) and (14.1.13) and λ_c is the wavelength of sound at the critical frequency. The parameter β is related to edge fixation. If the edges are simple supports, $\beta = 1$; if they are clamped $\beta = 2$. Usually these values will bracket more realistic mounting conditions, for which one may use $\beta = \sqrt{2}$. This formula applies at frequencies on octave or more above the fundamental panel resonance frequency.

Radiation from a Support on the Panel. When a supporting member such as a stringer or frame is attached to the panel, the radiation at frequencies below the critical frequency is increased. The amount of increase depends on the stiffness of the stiffener and its lineal mass. The increment in radiation resistance is given by

$$\Delta R_{rad} = \rho c A_p \left\{ \frac{4\lambda_c L}{\pi^2 A_p} \left(\frac{f}{f_c}\right)^{\frac{1}{2}} D\left(\frac{f}{f_c}\right) \right\} \qquad (14.2.4)$$

where L is the length of the stiffener and D is a function that depends on the lineal mass m of the stiffener and the mass per unit area of the panel m_s according to the parameter

$$M_o = 2\, m/\lambda_c m_s \quad . \qquad (14.2.5)$$

We have graphed 10 log $D(f/f_c)$ in Fig. 14.4. The plot in this Figure assumes that the critical frequency of the beam is $0.01 f_c$, the critical frequency of the panel. For aerospace structures, this would mean a beam critical frequency of 100 Hz or so, a reasonable value for most constructions.

Radiation Resistance of Cylinders. The radiation resistance of a cylinder of area A_c above the critical frequency f_c is the same as for a flat structure above f_c, and is given by Eq. (14.2.3)

$$R_{rad} = \rho c A_c (1 - f_c/f)^{-\frac{1}{2}}; \quad f > f_c \qquad (14.2.6)$$

As noted earlier, the critical frequency of aerospace structural panels is usually well above the ring frequency. In this event, the structure behaves as a flat plate in the frequency range $f_R < f < f_c$ and the following radiation resistance formula applies:

$$R_{rad} = \rho c A_c \left\{ \frac{4\lambda_c}{\pi^2 A_c} \left(2\pi R + L\right) \sin^{-1}\left(\frac{f}{f_c}\right)^{\frac{1}{2}} \right\} \beta;$$

$$f_R < f < f_c \qquad (14.2.7)$$

where R is the radius of the cylinder and L is the length of any stiffeners on the cylinder. The parameter β relates to fixation of the supports in the same way that it did in Eq. (14.2.3). [Note that if the critical frequency is less than the ring frequency (a situation that can occur for equipment pods) than this range corresponds to $f_c < f < f_R$ and Eq. (14.2.6) applies.]

When $f_r < f_c$ and $f < f_r$, we can write the following expression for the radiation resistance of a cylinder [22]

$$R_{rad} = \frac{\sqrt{3}\rho c A_c}{2\beta} \left(\frac{f}{f_R}\right)^{\frac{3}{2}} \frac{f_R}{f_c} \qquad (14.2.8)$$

where

$$\beta = 2.5 \sqrt{\frac{f}{f_R}} \quad \text{for} \quad f < 0.5 \quad f_R$$

$$\beta = 3.6 \quad \frac{f}{f_R} \quad \text{for } 0.5 \ f_R < f < 0.8 \ f_R.$$

Using Eqs. (14.2.6, 7, 8), one can estimate the coupling of the curved surface of a cylinder with either an internal or external sound field. The radiation resistance of the flat ends of the cylinder may be estimated from Eqs. (14.2, 3, 4).

Departure from Simplified Results at Low Frequencies. As noted in Chapter 12, the mode count in frequency bands is reduced as one lowers the frequency of interest, particularly if proportional bandwidth filters are used. The result is that modes have less of a chance of "overlapping" each other and the coupling between systems shows substantial variations. Under these circumstances, one may have to calculate mode-to-mode values of CLF. There are not many instances for which this has been done, but there is work by Fahy [32, 33] on such coupling between the vibration of structures and the acoustical modes of the contained fluid.

The frequency below which the simplified values of radiation resistance presented above may be in error has been estimated for the cases of the coupling between a wall of a box-like enclosure and the enclosed fluid. If the panel has thickness h and dimensions a x b and the box has dimensions a x b x c, then the limiting frequency f_ℓ is found from [32]

$$f_\ell = f_c [c^4/2\pi^2(\eta_s+\eta_a)(a+b)(abc)\ f_c^4(\Delta f/f)]^{2/7} \qquad (14.2.9)$$

where f_c is given by Eq. (14.1.9) and (14.1.10), η_a and η_s are the loss factors of the acoustical space and the structure respectively, and Δf is the bandwidth in which the data is taken. Normally such data is taken in constant percentage bands so that $\Delta f/f$ is a known constant.

The limiting frequency for cylindrical structures differs from that of flat structures because of the increased importance of membrane stresses. The expression for f_ℓ in this instance is given by [21]

$$f_\ell \approx f_r [c^2/\pi^2 \ell a^2 (\eta_a+\eta_s) f_r^3 (\Delta f/f)]^{\frac{1}{2}} \qquad (14.2.10)$$

where ℓ is the length of the cylinder, a is its radius, and f_r is the ring frequency given in Eq. (14.1.14). The formulas in (14.2.9) and (14.2.10) are designed to be conservative, and the actual departures from predictions based on the CLF formulas of paragraph 14.2 may well occur at an octave or so lower than f_ℓ as predicted by these formulas.

In the range $f < f_\ell$, the calculation of CLF between the sound field and the structure becomes very complex and highly specialized to the geometry and structural details. The references should be consulted for details on the computational procedures to be followed in such cases.

14.3 Coupling Between Structural Subsystems

The most common interface between subsystems in flight

vehicles is in the form of a mechanical connection between the structural elements. The number of possible subsystems to be connected together (cylinders, plates, cones, beams, etc.) and the variety of kinds of connectors (rivet lines, brackets, welds, etc.) results in quite a large array of structural connections of possible interest to the designer. In this section, we quote results from various theoretical and experimental studies of the coupling loss factor for structures. We also indicate how some of the existing results might be extended to cover other cases of interest.

The first system to be discussed is a structural beam (stringer or frame) that separates two panels. Since the beam will reflect some of the flexural wave energy incident on it and transmit the rest, one can define a transmissibility τ for the wave energy in the same way that such a parameter was introduced for the transmission between two acoustical spaces. If the mechanical power incident on one side of a beam or length L is Π_{inc} and the power transmitted to the second side of the beam is Π_{trans} the transmissibility

$$\tau \equiv \Pi_{trans}/\Pi_{inc} \tag{14.3.1}$$

is related to the coupling loss factor η_{12} (where the source side is "1" and the receiving side is "2") by the relation

$$\eta_{12} = \frac{c_g L}{2\eta^2 f A_1} \tau \ . \tag{14.3.2}$$

Most measurements and calculations of transmission of vibrational energy are designed to evaluate τ, from which η_{12} may be inferred.

Experimental Methods for Finding η_{12}. There are three principles that may be applied in the measurement of the coupling loss factor for structural connections.

(1) The receiving system may be damped sufficiently so that very little of the energy received by it will "return" to junction. Alternately, one may say that $\eta_2 >> \eta_1 + \eta_{12}$. In this event, the

apparent damping of subsystem "1" will be $\eta_1+\eta_{12}$. If η_1 can be found separately (estimated, measured by "clamping" subsystem "2", etc.) then η_{12} can also be determined.

(2) The receiving system is very heavily damped at its boundaries and a steady state excitation is applied to system 1. The mean squared velocity of system "2" is a measure of the transmitted power and the mean squared velocity of system 1 measures the power incident on the boundary. The experiment determines τ, from which η_{12} may be found in accordance with Eq. (14.3.2)

(3) The receiving system is sufficiently damped so that its modal energy E_2/N_2 is appreciably less than the modal energy of the source structure, E_1/N_1, but the damping is not so great as in cases (1) and (2). In this circumstance, the vibration of subsystem "2" is almost directly proportional to the value of η_{12}.

As an example of case (1) above, consider the experimental set-up shown in Fig. 14.5 [34]. In this experiment, the damping of plate 1 is measured by a decay rate experiment before attachment to plate number 2. The results are plotted as η_1. The damping of plate 2 is increased as much as possible and plate 1 is connected to it in the desired way. The new loss factor η is also plotted and for this situation is equal to

$$\eta = \eta_{12} + \eta_1 . \qquad (14.3.3)$$

Thus by taking the difference between η and η_1, the CLF is found. The CLF has also been interpreted as a transmissibility in Fig. 14.5 according to Eq. (14.3.2). A comparison with the theoretical value of τ_{th} is shown in this figure.

The transmissibility as measured in case (2) above has been found experimentally for beam structures by Heckl [35]. A typical set-up is shown in Fig. 14.6. The source section has no applied damping, the receiving section is heavily damped by a "wedge" of material. The excitation is with a shaker (shown as F in the drawing). The change in velocity level across the beam

$$\Delta L = 10 \log \langle v_1^2 \rangle / \langle v_2^2 \rangle \qquad (14.3.4)$$

is related to the transmissibility

$$\tau = 2 \langle v_2^2 \rangle / \langle v_i^2 \rangle \qquad (14.3.5)$$

where again plate 1 is the source and plate 2 is the receiver.

Finally, one can determine η_{12} from steady state response measurements when the receiving system is not so heavily damped as in cases (1) and (2). The damping must be high enough so that the modal energy of the receiving system is appreciably below that of the directly excited system. The steady state response of the indirectly excited structure $\langle v_2^2 \rangle$ is found in terms of the response $\langle v_1^2 \rangle$ of the directly excited system, as follows

$$\frac{M_2 \langle v_2^2 \rangle}{N_2} = \frac{M_1 \langle v_1^2 \rangle}{N_1} \frac{\eta_{21}}{\eta_2 + \eta_{21}} \qquad (14.3.6)$$

The errors using this method of determining η_{21} tend to be rather high, so that the equation is a better estimator of response from a knowledge of the parameters than it is for estimating parameters when the response levels are known.

Transmission Through Plate Junctions. Theoretical formulas and data are available for panels joined along lines, either by a beam, a framing member, or by a simple bend. Theoretical deviations for line connections between plates are fairly complicated, particularly when the bending and torsional rigidity of the beam must be included. Some of the results are presented here, the background information necessary to make calculations for other systems may be found in the references.

Two plates joined at right angles were studied by Lyon and Eichler [34]. The configuration is shown in Fig. 14.7. The coupling has simple theoretical values for plates of equal thickness and also when one plate is much stiffer than

the other. The expressions for the transmissibility from the semi-infinite plate no. 1 to the infinite plate no. 2 are

$$\tau = 8/27 \text{ (plates of equal stiffness)}$$

$$\tau = D_1/D_2 \text{ (plate 2 much stiffer than plate 1)} \qquad (14.3.7)$$

where $D = m_p \kappa^2 c_\ell^2$ is the bending rigidity of each plate. For homogeneous plates, $D \sim h^3$, so that the second relation above is satisfied if $h_1 \leq h_2/2$. A comparison between theoretical and experimental results for such a junction may be seen in Fig. 14.5.

The transmission from one panel to another through a reinforcing beam has been studied by Heckl [35]. If the panels are of equal thickness, then the transmissibility may be well approximated by

$$\tau = 2 \frac{\kappa_p c_p m_p}{c_{fB} m_B} \left(1+64 \frac{m_p c_{fp}}{\omega m_B}\right) \qquad (14.3.8)$$

where κ_p is the radius of gyration of the plate cross-section, c_p is the longitudinal wave speed in the plate material, m_p is the mass per unit area of the plate, m_B is the mass per unit length of the beam, c_{fp} and c_{fB} are flexural wave speeds for the plate and the beam respectively. A comparison between theoretical and experimental results for a simple plate-beam combination is shown in Fig. 14.6.

In addition to these theoretical results, a number of more complicated systems have been studied experimentally by Ungar, et al. [36].

Junctions of Panels and Beams. Coupling loss factors have been found in a few cases for beams which connect to plates, and these results are presented below. In general, however, such results are sparse and one will likely be

forced to calculate the coupling loss factor. Procedures for such calculations using junction impedances are discussed later in this section.

If a beam is cantilevered to a plate as shown in Fig. 14.8, the CLF may be expressed in terms of junction moment impedances [34]

$$\eta_{bp} = (2\rho_b c_b \kappa_b S_b)^2 \ (\omega M_b)^{-1} \mathrm{Re}(Z_p^{-1}) \ |Z_p/(Z_p+Z_b)|^2 \tag{14.3.9}$$

where Z_p and Z_b are moment impedances of an infinite plate and a semi-infinite beam respectively, given by

$$Z_b = \rho_b c_b^2 S_b \kappa_b^2 \kappa_{fb} (1+i)/\omega \tag{14.3.10}$$

$$Z_p = \omega(1-i\Gamma)/16\rho_s \kappa_p^2 c_p^2 \ . \tag{14.3.11}$$

When the plate and beam are of equal thickness and unconstructed of the same material, this simplifies considerably to become

$$\eta_{bp} = w/4\ell \tag{14.3.12}$$

where w is the beam width and ℓ is its length.

Another imporant situation is for a beam that joins the edge of a plate, as shown in Fig. (14.9). In this case, the CLF can again be found from junction impedances but the impedance functions are matrices since both moment and transverse force cause energy transfer at the boundary. The formulas are not presented here because of their complexity, but a comparison of theoretical and experimental results for 1 x 1/16 in. beam connected to a 1/16 in. thick plate is shown

in Fig. 14.10. When the axis of the beam is perpendicular to the line of the plate edge, then there is theoretically no coupling between flexural and torsional motions of the beam. For such a situation, torsional and flexural motions are decoupled. The total coupling loss factor is a weighted average of the coupling loss factors for flexural and torsional wave types,

$$\eta_{bp} = \delta f_b (\eta_{bp}^{flex}/\delta f_{flex} + \eta_{bp}^{tors}/\delta f_{tors}) \qquad (14.3.13)$$

where δf_{flex} and δ_{tors} are the average frequency spacings between flexural and torsional modes respectively and

$$\delta f_b = (1/\delta f_{flex} + 1/\delta f_{tors})^{-1} \qquad (14.3.14)$$

is the average frequency spacing for all mode types.

Junction Impedances and Coupling Loss Factor. As we have seen, junction impedances play an important part in the evaluation of the coupling loss factor, particularly when the coupling is concentrated over a small area of the plate. Several authors have published tables of these junction impedances. The reader should refer to the publications for junction impedance formulas and data [37].

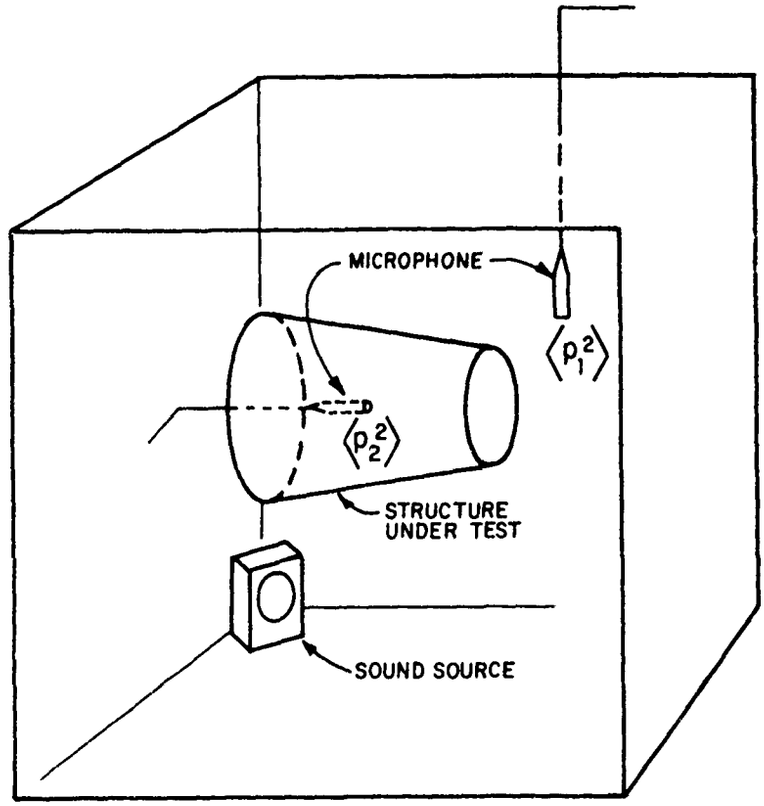

FIG. 14.1

SET UP FOR MEASURING ACOUSTICAL TRANSMISSIBILITY
OF AN AEROSPACE STRUCTURE

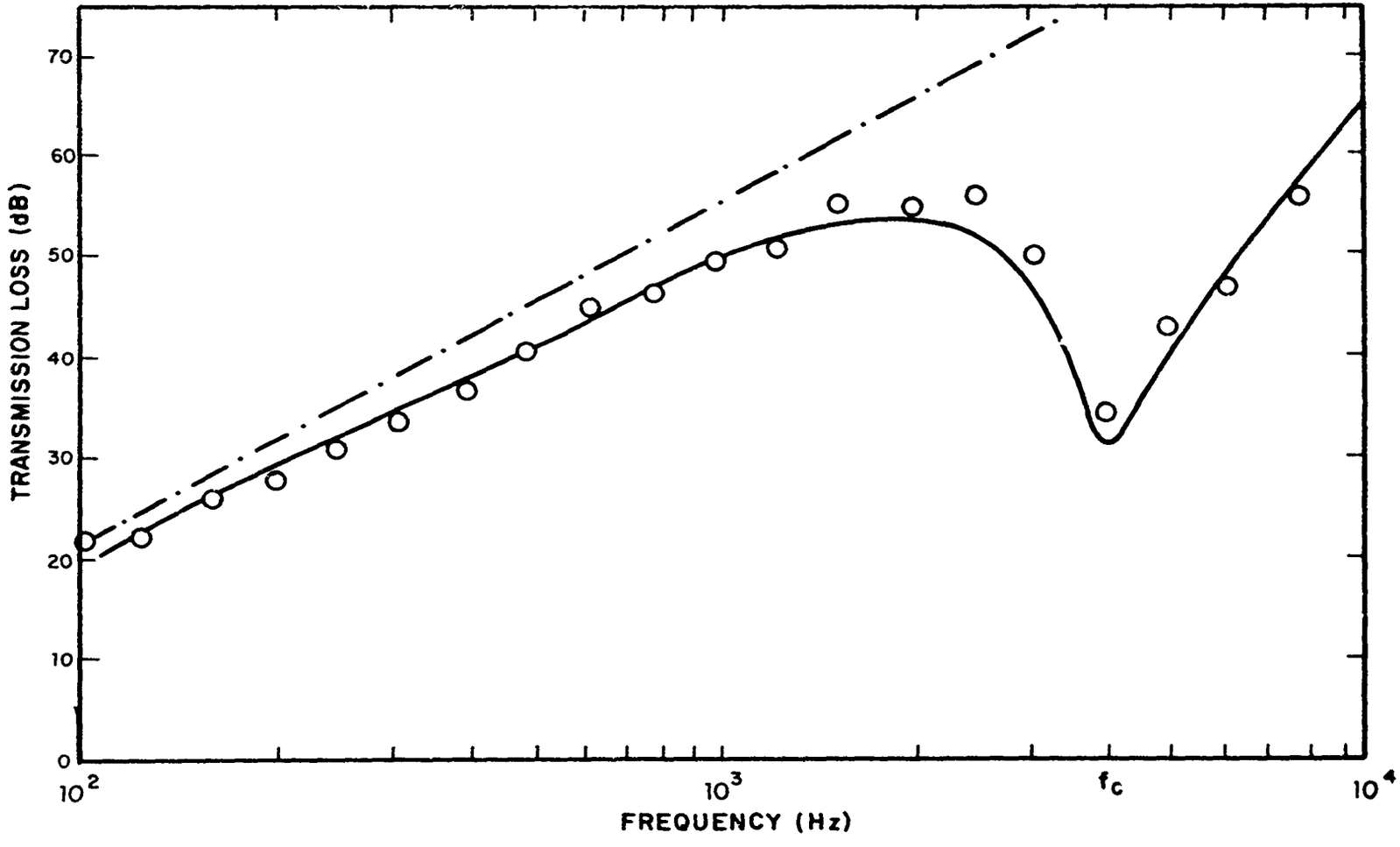

FIG. 14.2
TRANSMISSION LOSS OF STEEL SHEET

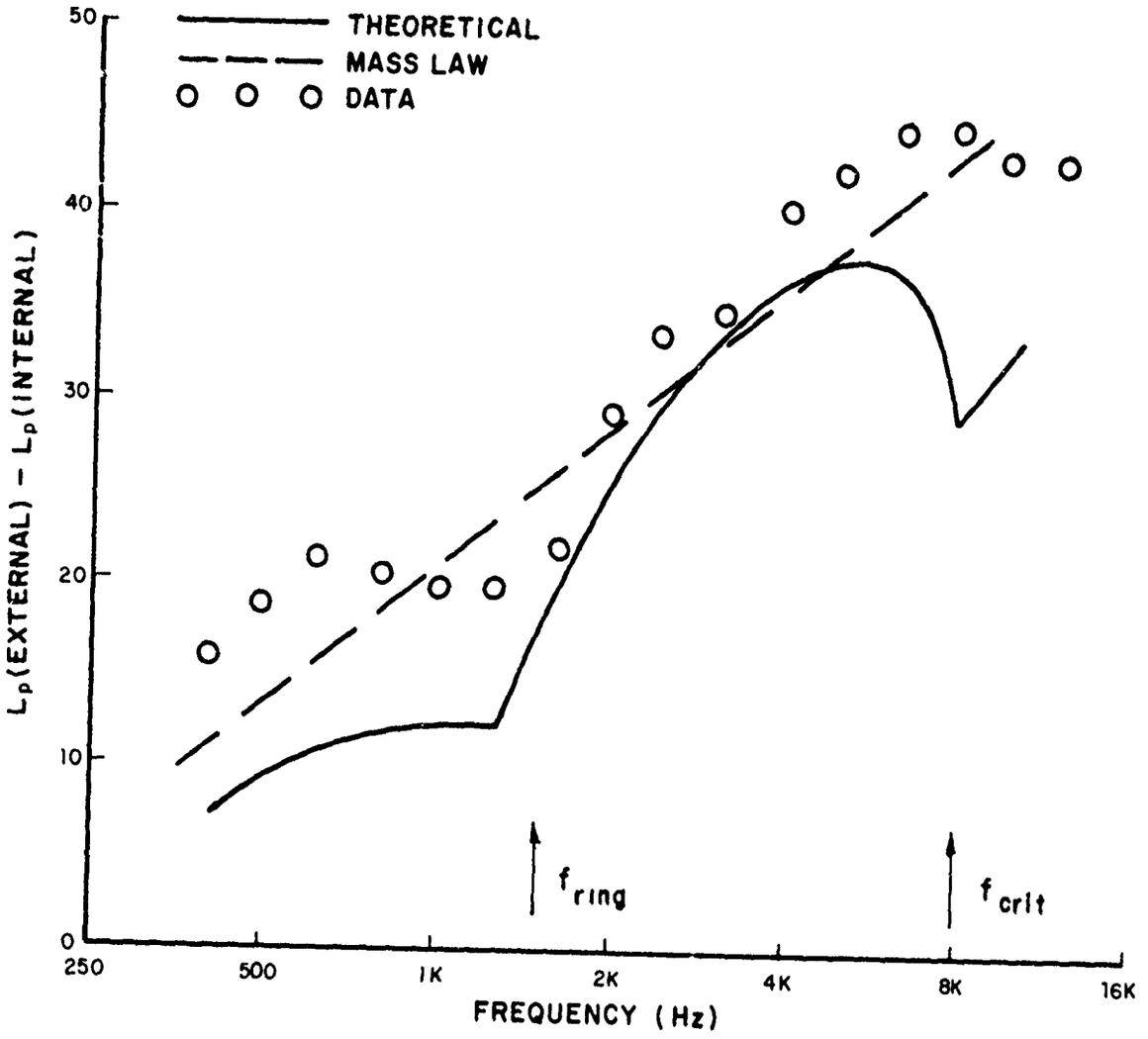

FIG. 14.3

NOISE REDUCTION OF CYLINDER STRUCTURE ;
THEORY AND EXPERIMENT

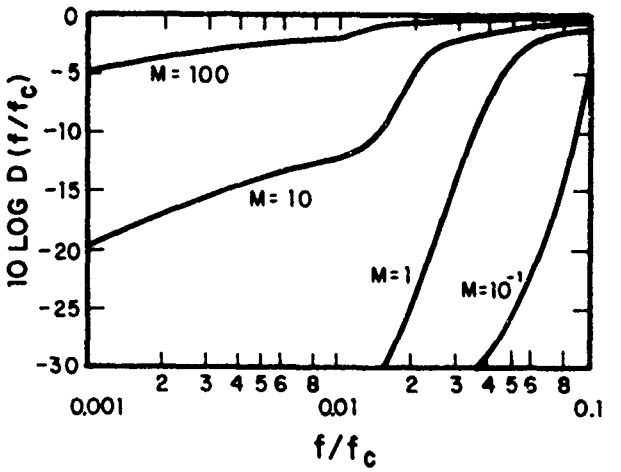

FIG. 14.4

EFFECT ON RADIATION RESISTANCE OF FINITE MASS OF BEAM ON A PANEL

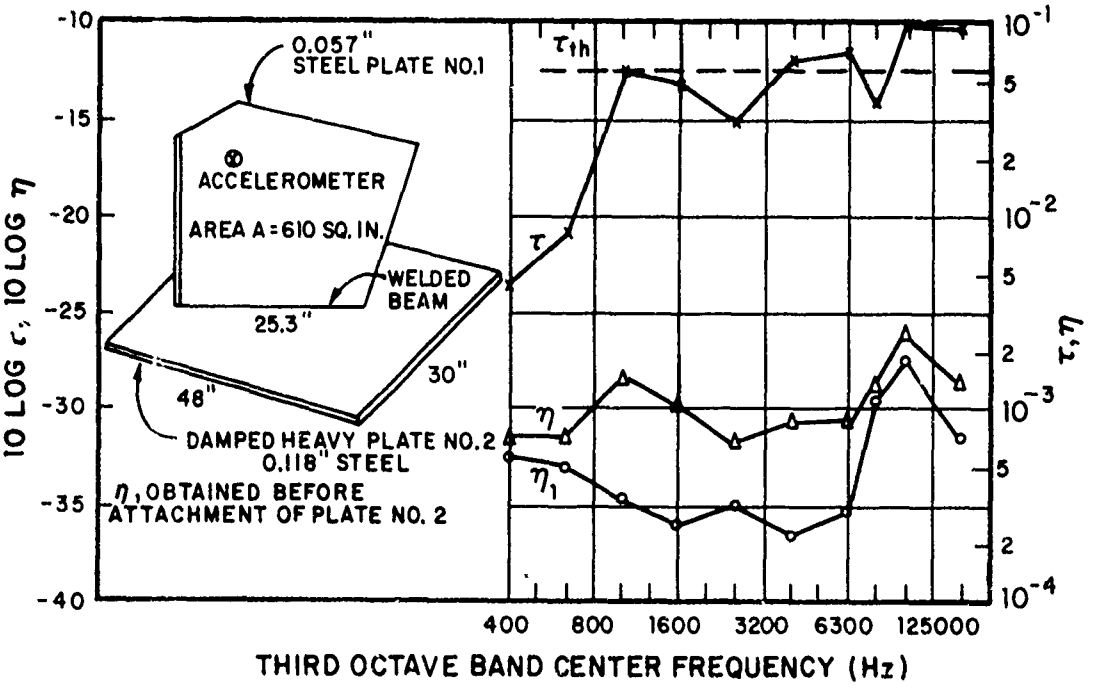

FIG. 14.5

EXPERIMENTAL DETERMINATION OF η_{12} (AND τ) FOR TWO CONNECTED PLATES

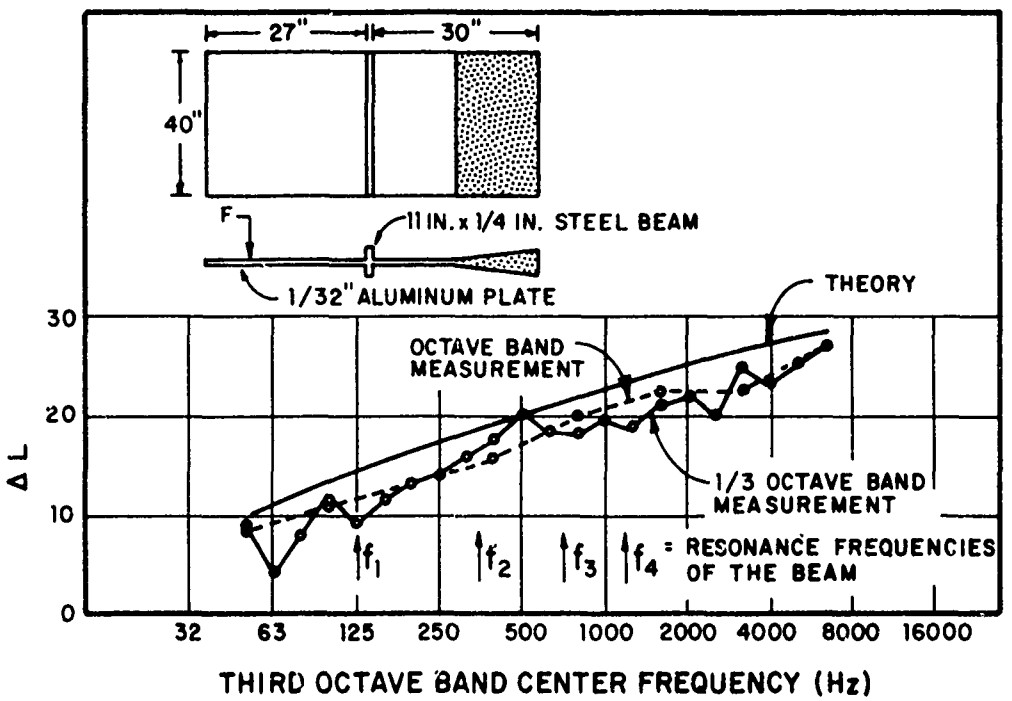

FIG. 14.6

EXPERIMENTAL DETERMINATION OF TRANSMISSIBILITY OF A BEAM ON A PLATE

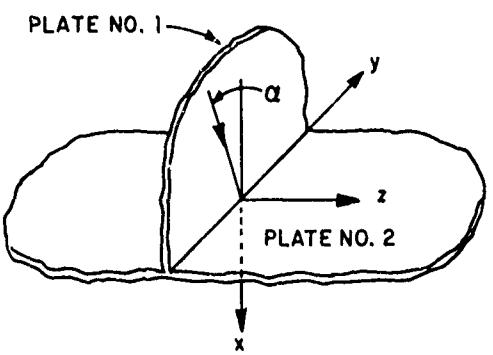

FIG. 14.7

TWO PLATES, RIGIDLY CONNECTED ALONG A LINEAR JUNCTION

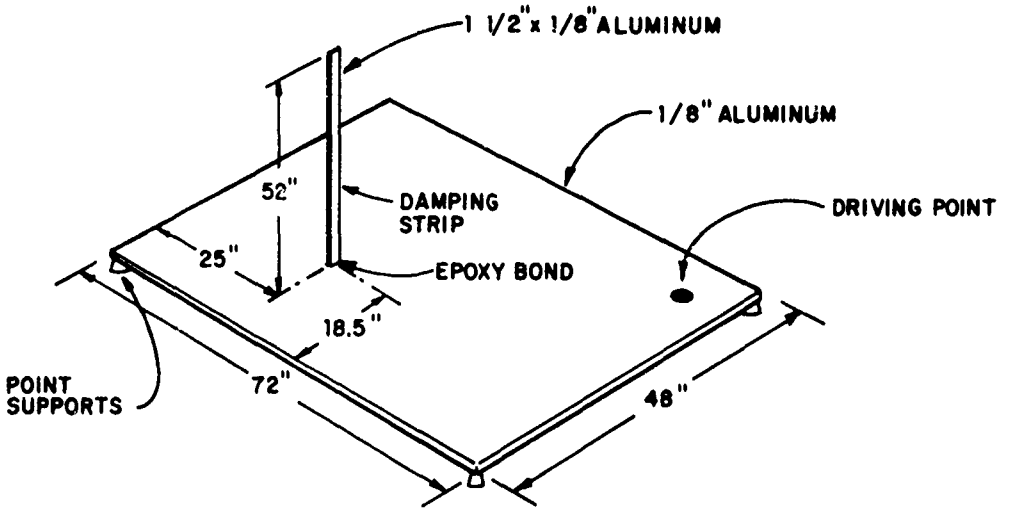

FIG. 14.8

BEAM CANTILEVERED TO A PLATE

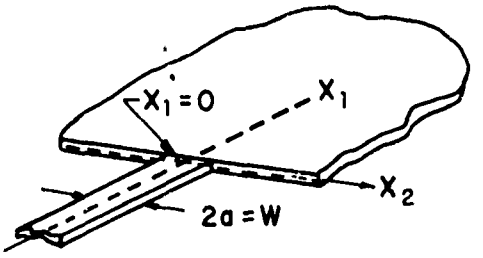

FIG. 14.9

BEAM CONNECTED TO EDGE OF A PLATE

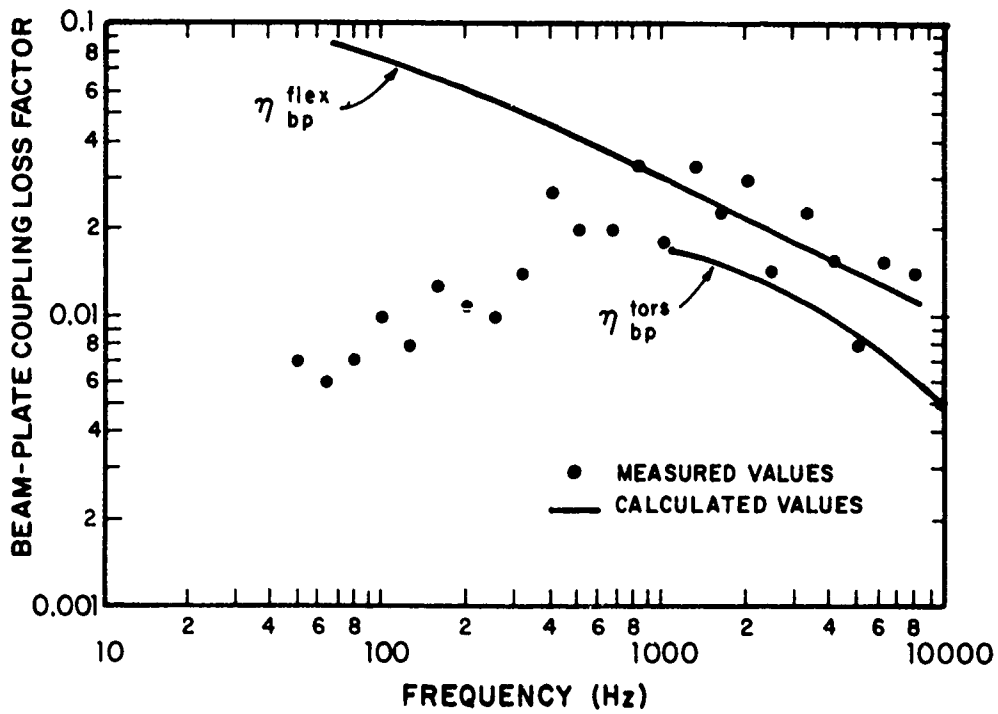

FIG. 14.10

COUPLING LOSS FACTORS FOR A BEAM CONNECTED TO THE EDGE OF A PLATE : THEORY AND EXPERIMENT

SECTION III - EXAMPLE OF RESPONSE ESTIMATION

by Huw G. Davies

CHAPTER 15 VIBRATION OF A REENTRY VEHICLE

15.0 Introduction

This chapter is intended to demonstrate the application of SEA to a specific problem in response estimation. We shall discuss the problem in some detail, and from a variety of aspects. Much of the work in this part is taken from work by J. Manning and others on a reentry vehicle.

The reentry vehicle used in this example is sketched in Fig. 15.1. We shall be concerned here with the vibration of the shell of the vehicle caused by high-speed turbulent-boundary-layer flow, and with the transmission of vibration from the shell to equipment mounted on the upper instrument shelf.

15.1 Modeling the Vehicle

15.1.1 Low Frequency Model of the Vehicle

For very low frequencies (less than 50 Hz in the present case) the vibration of the vehicle is dominated by large scale flexural modes of the whole vehicle. The vehicle thus behaves as a free-free beam of rather complicated cross-section. The numbers of such flexural modes in any third octave band below 50 Hz is small. The modal density of the skin panel flexural modes is also small. Thus the usual techniques of vibration analysis at low frequencies may be used and no advantage is gained from the SEA approach at these frequencies. The analysis techniques required have been described in Appendix VIII of Ref. 38, for example, and we shall not review those techniques here.

The vibration prediction techniques just mentioned become cumbersome when many modes contribute to the vibration level. The transition region in this instance is about 100 Hz, third-octave bands above this frequency have more than two resonant flexural skin modes. (The modal densities involved are discussed later.) The techniques of SEA are thus

applicable above this frequency. In the remainder of this Part we shall consider only vibration at frequencies above 100 Hz.

15.1.2 High Frequency Model

High speed turbulent flow over the surface of the re-entry vehicle generates high frequency vibration of the skin. This vibration is in turn transmitted to the various components carried within the vehicle. Our prediction of the density of resonant skin modes of the vehicle shows that there are many such resonant modes in all the third octave bands above, say, 100 Hz. The techniques of SEA are thus useful in predicting vibration levels of the skin and of the interior components in this frequency range. In what follows we shall be concerned solely with this frequency range. (The term 'low frequencies' will refer to the lower part of this range, that is to say, from 100 to 1000 Hz, in the remainder of this chapter).

As indicated above, we shall restrict attention here to the transmission of vibration from the vehicle skin to the upper instrument shelf shown in Fig. 15.1, and to the subsequent estimation of vibration levels on this shelf. The configuration is clearly similar to that in the example discussed in Chapter 10, and the modeling techniques are thus similar also. We could treat the skin, the stiffness, the ring connector, the instrument shelf, and the interior acoustic space as separate systems, each described by one or more groups of similar modes. This is clearly a very complicated model requiring a large amount of computation. Experience suggests that a simpler model may be adequate to describe the main features of the vibration.

We may note here the work of Manning [7] on the transmission of vibration to a shroud-enclosed spacecraft. Some features of the SEA model used by Manning could be applied to the present system. For example, his theoretical predictions of the coupling loss factors from cylindrical shells to ring stiffeners could be used. However, although features of the geometry are similar, the scale of the fixture studied by Manning is considerably larger than the present fixture. Modal densities of components thus are considerably reduced in the present system, so that the use of multimodal subsystems in our SEA model for these components may not be justified. Clearly then, a reasonable SEA model

can be formed for any case only after some preliminary estimation of such parameters as the modal densities of some of the components of the fixture being studied.

We begin with a two subsystem model. Since the random pressure on the vehicle skin generates mainly transverse motion, the group of transverse modes of the skin itself should describe the skin vibration. The second group of modes that we choose represents the vibration of the instrument shelf. Coupling between the two groups of modes is provided by the ring connector. This two component system requires the evaluation of a minimum number of SEA parameters. Even so, the evaluation of these parameters in this example turns out to be quite involved.

A more complicated model may be used if it appears to be necessary. We note, however, that an advantage of the SEA approach is that groups of modes we may treat separately in a more complicated model will often show up, for example, as an additional dissipative mechanism in the simple model. This added dissipation would be included implicitly in an experimentally obtained value of the loss factor used in the simpler model.

Our model has been chosen deliberately to be simpler than the model used by Manning [7]. This is so for a variety of reasons. As pointed out above we expect that the main features of the vibration can be explained on the basis of a simple model. To a degree we are limited to this simple model by the restricted amount of data available for the prediction of coupling loss factors. We have already noted that there are very few modes of vibration of the ring connector between the shell and the shelf in the frequency range of interest; we would not be justified in treating this ring as a separate subsystem in our SEA model. Finally, since the ring connector provides a fairly strong structural link with the skin, we are justified in neglecting the transmission of vibration from skin to shelf via an airborne path.

15.2 Modal Density

15.2.1 Modal Density of Vehicle Skin

The vehicle skin is treated as a truncated conical-shell of uniform thickness h, semi-vertex angle ϕ, and slant

length L as shown in Fig. 15.2. The shell has a maximum radius a_1 and a minimum radius a_2. The coordinates x and θ describe the surface of the cone.

We follow an approximate description of the cone vibration. We assume that a small section S of the cone with mean radius a has the same vibration properties as a section c on a cylinder of the same material, the same thickness h, and the same radius a(x). In particular, we assume that for resonant vibration at frequency ω, the local wavenumbers (k_x, k_θ) on section S of the cone are the same as the corresponding wavenumbers on the cylinder section C. (This is in the spirit of the treatments of Refs. 25, 26).

For a given mode, the wavenumbers are given by

$$k_\theta = n/a(x), \quad k_x = \frac{m\pi}{L}.$$

We note that these wavenumbers must be functions of the coordinate x. Also, if we write

$$k_p = \left(\frac{\omega}{kc_\ell}\right)^{\frac{1}{2}},$$

as the wavenumber for resonant vibration at frequency ω on a flat plate of the same material and the same thickness as the cone, resonant motion corresponding to the local values of the wavenumbers can only occur if

$$k_\theta(x) = \frac{n}{a(x)} < k_p.$$

The corresponding local k_x wavenumber is subsequently obtained in this case from the frequency equation of a cylinder [3].

$$\frac{\omega a^2}{c_\ell} = (ka)^2 \ (k_x^2 + k_\theta^2)^2 + \frac{k_x^2}{k_x^2+k_\theta^2} \qquad (15.1)$$

where $a(x)$ represents the local radius of the cone. Examination of this equation shows that for a given (m,n) mode resonant at frequency ω three types of solutions are possible. The three cases are sketched in Fig. 15.2 (b).

Case I:

$k_\theta(x) < k_p$ everywhere on the cone. That is, for the given number n, numbers m can be found such that $k_x = m\pi/L$ satisfies Eq. (15.1). The corresponding mode shape at resonance extends over the entire length of the cone.

Case II:

$k_\theta(x) < k_p$ for $x_o < x < x_\ell$, and $k_\theta(x) > k_p$ for $x_\ell > x > x_b$. In this case there are no solutions of Eq. (15.1) for values of $x < x_\ell$. Clearly x_ℓ is given by $n/a(x_\ell) = k_p$. The resonant motion of the corresponding mode is restricted to values of $x > x_\ell$, that is, to the larger end of the cone.

Case III:

$k_\theta(x) > k_p$ everywhere on the cone. No resonant motion is possible for this case.

No simple analytic results exist for the modal density of a cylindrical shell. Hence no simple analytic result can be obtained for the modal density of the cone by our technique of matching cone sections to equivalent cylinder sections. Empirical curves for a cylinder are given in Fig. 15.3 (from Ref. 22). For the cone, the modal density for resonant modes at a given position can be found approximately by using the appropriate value of the radius $a(x)$ in the non-dimensional parameter

$$\nu_o = 2\pi \ f_o a(x)/c_\ell$$

in Fig. 15.3. The parameter f_o here is the center frequency

of the band being considered. In keeping with the three cases discussed above, we note that for a given frequency the local modal density tends to increase towards the larger end of the cone. Of course, at frequencies well above the ring frequency associated with the radius of the smaller end of the cone all the equivalent cylinders have the same modal density as a flat plate of equal area. The modal density of the cone is then the same as that of a flat plate of equal area and the modal density becomes independent of frequency.

15.2.2 Modal Density of Instrument Shelf

The instrument shelf is a fairly stiff assembly. It has been determined experimentally that there are nine resonant modes below 2000 Hz. The modes are not uniformly spaced, and their precise location in frequency is not known. We shall discuss later some ways of overcoming this lack of data.

One approximate theoretical estimate may be obtained by treating the instrument shelf as an equivalent flat plate. This is the same as adding the modal densities of each flange of the shelf structure. Suitable values would be a area $A = 4$ ft^2 and $\kappa c_\ell = 200$ ft^2/sec. This leads to a model density $n_2(\omega) = A/4\pi\kappa c_\ell = 1/200\pi$, giving, for example, 2.3 modes in the third octave band at 1000 Hz. Although it uses reasonable parameter values, this estimate is somewhat high when compared to the experimental values found at lower frequencies. We shall, however, use this estimate in one of the vibration prediction schemes discussed below. We expect that the estimate will be more accurate at high frequencies.

The experimental estimate of the numbers of modes at low frequencies (100 to 1000 Hz) suggests that some third octave bands will contain resonant modes of the shelf, others will not. A reasonable model of the shelf at low frequencies would thus be a one degree of freedom system attached by massless moment arms to the vehicle skin. This model should give reasonable predictions on the shelf vibration at least in the vehicle axial direction, assuming that the ring connector acts as a rigid body. Clearly, this model is most applicable at low frequencies. We shall discuss the parameter values involved here in the next section.

15.3 Coupling Loss Factor

The coupling loss factor required in the present SEA model is that which describes energy transmission between the two groups of modes describing the vehicle skin and the instrument shelf subsystems.

Since the coupling loss factor is often the most difficult SEA parameter to predict accurately we shall discuss its evaluation in some detail. Two highly simplified models of the instrument shelf lead to two theoretical predictions. In addition, some of the data taken by Manning and others may be interpreted in terms of these two models, thus giving two experimental predictions. Finally, in later parts of our discussion we shall show how the data may be used to predict vibration levels on the shelf without explicitly evaluating the coupling loss factor.

15.3.1 Approximate Theoretical Prediction #1 (high frequencies)

The instrument shelf is a fairly complicated assembly; a detailed analysis does not seem feasible. However, as far as the coupling loss factor is concerned, the essential features of the vibration of the shelf may be obtained by treating the shelf as an equivalent flat plate. A further simplification is to treat the skin-shelf transmission as a simple plate-plate transmission. This is certainly justifiable at higher frequencies when wave motion on the cylinder is controlled solely by the material bending stiffness.

The coupling loss factor may then be taken from Chapter 14 (see also Ref. 10):

$$\eta_{21} = \frac{2}{\pi} \frac{L}{k_2 A_2} \gamma,$$

where η_{21} represents the coupling loss factor from shelf to skin, $L = 2\pi a$ is the joint length, k_2 is the wavenumber on the equivalent plate of area A_2 and γ is a geometric factor. Since the material and thickness of the skin and of the equivalent plate are, at least, similar, we taken $\gamma = 8/27$. By substituting in suitable values

$$[L = 2\pi(1.2)\text{ft.},\ A_2 \simeq 4\text{ft}^2,\ \kappa c_\ell = 200\ \text{ft}^2/\text{sec}]$$

we find

$$\eta_{21} \simeq 5\ \omega^{-\frac{1}{2}} \simeq 2\ f^{-\frac{1}{2}} \qquad (15.2)$$

15.3.2. Experimental Prediction #1

15.3.2.1 Description of the Experiment

An evaluation of the coupling loss factor may be obtained from the experimental data of Manning. Because of the complexity of the structural properties of the ring connector, an experimental measure of the coupling loss factor certainly is warranted. The ideal experiment would be conducted on the vehicle itself. This was not feasible in the experiments by Manning. A model of the instrument shelf mounted in a cylindrical rather than a conical shell was used.

In a vibration experiment of this type, one of the properties one would like to model accurately is the source impedance of the vehicle shell. This impedance depends in a complicated way on the geometric and material properties of the shell. The cylindrical shell used by Manning had the same surface density and bending wavespeed as the actual vehicle skin, and thus provided a realistic test model.

The model used by Manning is shown in Fig. 15.4. The steel shell has a diameter of 29 in. and thickness of 5/16 in. The instrument shelf is attached to the cylindrical shell by an L-shaped ring, a connection that is structurally similar to that used in the actual vehicle.

The experimental structure was excited by two 50 pound shakers located as shown in Fig. 15.4. Third octave bands of noise covering the frequency range 50 Hz to 10 kHz were used. No attempt was made to excite the fixture at the levels predicted during actual flights since the goal in these tests

was to obtain vibration levels on the instrument shelf relative to those on the cylindrical shell.

Acceleration levels measured in one-third octave bands were measured at a number of points on the fixture. Three groups of measurement positions were used: on the instrument shelf, on the shell at the point of connection to the shelf, and in the reverberant field of the shell, that is, away from the ends, the connector, and the shakers. All levels were measured relative to a single reference acceleration level measured at the ring connector. The data is shown in Figs. 15.5, 15.6, and 15.7. Figs. 15.5 and 15.6 show the variation of vibration level in the reverberant field of the shell and on the ring connector, respectively. Fig. 15.7 shows the transmissibility from the test shell to various points on the instrument shelf. The transmissibility gives the acceleration level at a point on the shelf relative to the average acceleration level in the reverberant field of the test shell.

15.3.2.2 Determination of η_{12} From the Data (Model #1)

In this paragraph we discuss how estimates of the coupling loss factor may be obtained from the vibration data based on model #1, the equivalent plate model. As we shall see, although the data is useful, it is insufficient for an accurate prediction of the coupling loss factor without some further assumptions. Educated guesses are necessary for some parameters. The interpretation of the data based on the equivalent plate model is expected to provide reasonable estimates only at high frequencies.

We consider here a two component system, the skin and the shelf, with only one system, the skin, being directly excited. Eq. (14.3.6) applies to the relative total energies of each system in this situation.

$$E_{2,tot} = E_{1,tot} \frac{\eta_{12}}{\eta_{12} + \eta_{21}} , \qquad (15.3)$$

where 1 and 2 refer to the skin and to the shelf, respectively. We have also the symmetry relation

$$N_1\eta_{12} = N_2\eta_{21}. \tag{15.4}$$

In the tests discussed above the transmissibility was expressed in terms of the average acceleration levels of the skin and of the shelf. In terms of these levels, Eq. (15.3) may be written

$$\frac{M_2\langle a_2^2\rangle}{M_1\langle a_1^2\rangle} = \frac{N_2}{N_1}\ \frac{\eta_{21}}{\eta_2 + \eta_{21}}, \tag{15.5}$$

or

$$\eta_{21} = \eta_2\ \left(\frac{N_2M_1\ \langle a_1^2\rangle}{N_1M_2\ \langle a_2^2\rangle} - 1\right)^{-1} \tag{15.6}$$

Eq. 15.6 gives an estimate of η_{21} provided that the quantities on the right hand side are known. Now, $\langle a_1^2\rangle/\langle a_2^2\rangle$ has been measured, M_1 and N_1 are known quite accurately, and M_2 may be estimated with reasonable accuracy. We have seen that N_2 is not easy to estimate, and η_2 was not measured.

The test data thus does not seem particularly useful for determining the coupling loss factor. However, several comments on this attempted evaluation can be made:

1. While η_{21} may not be directly evaluated in this case, the data obtained on the transmissibility may still be used in our SEA approach to predict vibration levels on the actual instrument shelf. We shall discuss this evaluation later.

2. This type of test, while on occasion the only possible way of obtaining a value of the coupling loss factor, can be inherently inaccurate. We note in

particular the case of very small η_2 ($\eta_2 << \eta_{21}$). In this case, equipartition of energy among the modes of the shelf and the skin occurs. η_{21} does not control the relative levels in this case, and so, the response values are quite insensitive to the value of η_{21}.

3. The above comments notwithstanding, we may, with suitable assumptions (sometimes guesses!) evaluate η_{21} if it proves necessary to do so. It is instructive to do so here in order to compare the values obtained with our theoretical predictions.

The following table gives some representative values of the numbers of modes in third octave bands for the text fixture skin, and for the equivalent plate representing the shelf (see Paragraph 15.2.2).

TABLE 15.1

MODE COUNTS FOR SHELL AND SHELF STRUCTURES

1/3 Octave Band Center Frequency Hz	$N_1 = n_1\Delta\omega$	$N_2 = n_2\Delta\omega$	N_1/N_2
125	.8	.3	2.6
250	2	.6	3
500	6	1.2	5
1,000	18	2.3	8
2,000	64	4.6	14
4,000	109	9.2	12
8,000	208	18.4	11

For the values chosen in our model we have $M_1/M_2 \simeq 4$. The data from Ref. 1 provides values of $\langle a_1^2\rangle/\langle a_2^2\rangle$. Since this

ratio always corresponds to at least 10 dB in the frequency range of interest, Eq. (15.6) may be approximated to

$$\eta_{21} \simeq \eta_2 \frac{N_1 M_2 \langle a_2^2 \rangle}{N_2 M_1 \langle a_1^2 \rangle} \tag{15.7}$$

or

$$10 \log \eta_{21} \sim 10 \log \eta_2 + T + 10 \log N_1/N_2 - 6 \tag{15.8}$$

where T represents the transmissibility to be obtained from Fig. 15.7.

A comparison of the predictions obtained from Eqs. (15.2) and (15.8) is shown in Table 15.2.

TABLE 15.2

VALUES OF COUPLING LOSS FACTOR

1/3 Octave Band Hz	Eq. 15.2 $10 \log \eta_{21}$	Eq. 15.8 $10 \log \eta_{21}/\eta_2$
125	- 7.5	- 11
250	- 9	- 19
500	- 10.5	- 23
1000	- 12	- 27
2000	- 13.5	- 7
4000	- 15	- 5
8000	- 16.5	- 8

For a relatively well damped shelf, a guess of $\eta_2 \sim 0.1$ would be realistic. Even with this large value, the two estimates differ by up to 15 dB at frequencies below 2000 Hz.

Several factors contribute to this discrepancy. Perhaps the most drastic assumption is that of the multi-modal nature of the response of the instrument shelf in all bands. This feature enters into both estimates. We note, however, that at frequencies above 1000 Hz where there are indeed a number of modes in each frequency band the agreement between the two estimates (with $\eta_2 = 0.1$) is reasonable. The equivalent plate model may thus be appropriate in the 2, 4 and 8 kHz bands.

15.3.3 Alternate Prediction of η_{21}

15.3.3.1 Theoretical Prediction #2 (low frequencies, 100 to 1000 Hz)

Our previous assumption of the multimodal nature of the response of the instrument shelf proved to be unrealistic at low frequencies, particularly for the frequency bands where we know from experimental data that the shelf response is not multimodal. A more realistic low frequency model is as follows: In each frequency band of interest, we assume that the shelf can be treated as a lumped parameter system with one degree of freedom, that is, as a single resonator. Assume that the resonator is free to vibrate along the axial direction of the vehicle, and is caused to vibrate by moment arms attached to the skin of the vehicle. A diagram of this model for the test fixture in Fig. 15.4 is shown in Fig. 15.8.

This model clearly predicts motion of the shelf in the axial direction only. Now, from the data of Manning we may note the following: at lower and middle frequencies, the reverberant field acceleration level of the cylinder is typically 20 dB higher than the average level at the ring connector, showing that the ring has a considerable stiffening effect as far as transverse motion of the shell is concerned. We are thus perhaps justified in considering only the moment transmitted by the L-shaped ring connector. We may subsequently estimate the acceleration levels in the cross-sectional plane by equating them to those at the ring connector.

This is an overestimate, however, as one can see from paragraph 15.3.3.3.

Because of the axial symmetry of our model, we may treat the shell as a beam of thickness h and width $2\pi a$, acted on by a concentrated moment. Fig. 15.8a shows a schematic drawing of the model. We assume that a value of η_{21} can be obtained by considering the power input to an infinite beam when the instrument shelf is excited by a force F. From Fig. 15.8b we see that the power supplied to the undamped resonator representing the shelf is all transferred to the beam, so that power balance requires that

$$\Pi_{in} = \omega \eta_{21} \quad E_{2,tot} \tag{15.9}$$

where $E_{2,tot}$ is the total energy of the oscillator (shelf). The input impedance for the force F is

$$Z_{tot} = i\,\omega\, M_2 + i\,\frac{K}{\omega} + \frac{Z_{beam}}{k^2 a^2} \quad ,$$

where

$$Z_{beam} = 2E\,\frac{I}{\omega}\,k^3(1-i)$$

is the point input impedance for an infinite beam (Section II, see also Ref. 4Q). It follows from equation 15.9 that

$$\eta_{21} = R_e(Z_{tot})/\omega M_2$$

$$= \frac{1}{2\pi}\,\frac{M_1}{M_2}\,\left(\frac{\kappa c_\ell}{\omega}\right)^{\frac{3}{2}}\,\frac{1}{a^3} \quad .$$

For the values of the parameters used by Manning, this result predicts a value for the coupling loss factor of

$$\eta_{21} \simeq 20\ f^{-\frac{3}{2}} \tag{15.10}$$

and hence

$$\eta_{12} \sim 20\ f^{-\frac{3}{2}}\ (n_1 \Delta\omega) \tag{15.11}$$

where $(n_1 \Delta\omega)$ is the number of resonant skin modes in the frequency band.

15.3.3.2 Experimental Prediction #2

The vibration data can also be interpreted in terms of this second model. We merely replace equation 15.6 by the similar equation

$$\eta_{21} = \eta_2 \left(\frac{M_2 \langle a_1^2 \rangle}{n_1 \Delta\omega M_2 \langle a_2^2 \rangle} - 1 \right)^{-1} \tag{15.12}$$

where $\langle a_2^2 \rangle$ now refers to only the axial acceleration of the shelf.

We note that if an approximation similar to that leading to equation (15.8) is made, the two models while predicting different values of η_{21} for a given frequency band predict the same value of η_{12} for that band.

15.3.3.3 Transverse Vibration of Shelf for Modal #2

Our low frequency model predicts only vibration in the axial direction. It was suggested above that an overestimate could be obtained by equating the shelf vibration levels in the direction perpendicular to the vehicle axis to the vibration

levels on the skin at the ring connector.

Values of the vibration level at the ring connector can be obtained by allowing the mass in Fig. 15.8(b) to move transversely. For only transverse motion we find the coupling loss factor (by the same method as in paragraph 15.3.3.2 to be

$$\eta_{21} \sim 4 f^{-\frac{1}{2}} . \qquad (15.13)$$

15.3.3.4 Comparison of Coupling Loss Factor Predictions

The theoretical and experimental predictions of η_{12} are compared in Fig. 15.9. We have estimated possible values of the shelf loss factor η_2 as shown. The experimental predictions are based on the chosen values of η_2 (the data available in fact predicts only (10 $\log \eta_{12}/\eta_2$).

We have used extremely simple models for our theoretical predictions. Nevertheless, the agreement between theory and experiment is fair. In particular, the difference in the low and high frequency behaviour is readily seen.

This fairly successful use of crude models of complicated structures demonstrates the strength of SEA. Although, for example, our lumped-mass-on-a-beam model seems very different from the actual reentry vehicle, the two systems are sufficiently similar that useful results can be obtained on a statistical basis by treating both systems as two members of the same ensemble of similar systems. We require merely that such gross parameters as, for example, the total mass be preserved.

15.3.3.5 Summary of Couping Loss Factor Values

It remains for us to choose appropriate values of η_{12} and η_{21} for each frequency range from among the many predictions just discussed. Fig. 15.9 indicates that there is a change in the apparent behavior at low and high frequencies. We therefore propose using the low frequency model for frequencies at and below 1000 Hz, and the high frequencies at and above 2000 Hz.

If purely theoretical predictions are required, then η_{12} and η_{21} are given as follows:

$f_o \leq 1000$Hz:

$$\eta_{21} = 20\, f^{-\frac{3}{2}} \tag{15.10}$$

$$\eta_{12} = \frac{1}{n_1 \Delta\omega}\, \eta_{21} \tag{15.14}$$

$f_o \geq 2000$Hz:

$$\eta_{21} = 2\, f^{-\frac{1}{2}} \tag{15.2}$$

$$\eta_{12} = \frac{N_1}{N_2}\, \eta_{21} \tag{15.15}$$

The change-over frequency point has been chosen in fact from comparisons with experiments. However, a theoretical basis may be given for this changeover if we say that the high frequency model applies when there are more than two resonant modes of the shelf in a third-octave band.

Because of the complexity of the fixture, we expect our experimental predictions to be more accurate than the purely theoretical predictions. It follows that the best approach is to use values of 10 log (η_{12}/η_2) obtained from Fig. 15.8 with corresponding values of 10 log (η_{21}/η_2) obtained by using Eqs. (15.14) and (15.15) in the appropriate frequency range.

15.4 Prediction of the Vehicle Skin Vibration Levels.

In this paragraph we discuss the response of a conical shell to a turbulent-boundary-layer pressure field. The prediction is taken from Manning's work. For completeness, and since Manning's work is not available, we have included below some results of his work. This work together with the mean square pressure levels shown in Fig. 15.11 can be used to predict the actual acceleration levels of the vehicle shell.

15.4.1 Response of a Conical Shell to a Turbulent Boundary Layer (TBL) Pressure Field

15.4.1.1 General Outline of the Calculation

Fig. 15.10a indicates an important feature of a TBL pressure field. At a frequency ω, the fluctuating wall pressure possesses wave number components k_x that are very nearly equal to ω/U_c, U_c being the mean convection velocity of the pressure field. At frequency ω, a section S of the cone at radius a [Fig. 15.10b] accepts power from the pressure field, if there is a local vibration pattern on section S that is resonant at frequency ω and also has a local wavenumber component $k_x = \omega/U_c$. Such a wavenumber vector at resonance is shown by a heavy dot in Fig. 15.10a. (If the frequency ω is lower than the local ring frequency c_ℓ/a for section S, two such wavenumber vectors may be possible.

From the known results for a cylindrical shell, we can calculate this wavenumber vector, as well as the associated power input from the pressure field to section S(see Ref. 42). Also, from the calculated value fo the wavenumber component k corresponding to the heavy dot in Fig. 15.10a and from the known radius a at section S, we determine the number n of the cone mode to which this particular resonant motion over the section S belongs

$$n = k_\theta a \qquad (15.16)$$

The spatial extent of this parent mode is also easily determined. If $k_\theta a/k_p a_2 < 1$, Case I of paragraph 15.2.3.1 applies and the parent mode extends over the entire surface of the cone. Otherwise, Case II applies. The non-zero region of the parent mode for Case II is sketched in Fig. 15.10(a). The radius a_o at the boundary AB of this region is determined from the conditions:

$$\frac{k_\theta a}{k_p a_o} = 1. \qquad (15.17)$$

Now we assume that the power transmitted by the pressure field to the section S is retained entirely by the parent mode and is manifested as uniform coherent vibration of this mode.

This procedure then enables us to estimate the average mean-squared acceleration (in any given frequency band), over the extent of the parent mode, that results from the interaction between the TBL pressure field and the section S. By making the assumption that there is negligible coherence between vibration of different modes, we obtain the total acceleration-level at a particular location on the cone surface (in a frequency band) by merely summing up contributions from all the sections S of the conical shell.

The cone vibration would be contributed partly by modes that exclude the smaller end of the cone from their vibration patterns. The larger end of the cone, however, is always included. In other words, the power accepted by the various cone sections from the TBL pressure field is distributed in a preferential direction: namely, towards the larger end of the cone. Consequently, the vibration levels on the cone surface are expected to increase from the smaller to the larger end of the cone.

15.4.1.2 Response Estimate for the Conical Shell

15.4.1.2.1 Structural Model

The conical shell is modeled as an isotropic conical

shell 110 in. long, with maximum and minimum diameters of 6.4 and 39 in. The surface mass density is taken to be 15 lb/ft^2. Based on the experimentally determined values of the bending wave speeds in the two layered and multi-layered sample bars, we take the quantity κc_ℓ to be 90 ft^2/sec. The longitudinal wave speed c_ℓ by itself enters in the description of the extensional or membrane stress-controlled vibration. We assume c_ℓ to be 10,000 ft/sec. The chosen values of κ and c_ℓ are then consistent for a shell thickness of about 3/8 in. The structural loss factor η_1 is taken to have a value of 0.025 at all frequencies. This estimate is based on the value of η_1 deduced at 2000 Hz from shock transmission studies.

15.4.1.2.2 Flow Model

The free stream velocity U of the flow is taken to be 21,000 ft/sec. The mean convection velocity U_c of the TBL pressure field is taken as 0.6 U. The dynamic head q is 50 atm, and the root-mean-square pressure fluctuation p_h on the cone surface is 0.02 q. The boundary layer displacement thickness is taken to increase linearly from the smaller end to the larger end of the cone, with a mean value of 0.2 in. This choice is equivalent to taking the displacement thickness $\delta^* = 0.0026x$, x being the distance along the generator from the cone vortex. The frequency spectrum of the fluctuating pressure at any location is assumed to scale with the Strouhal number $f\delta^*/U_\infty$ where U_∞ is the free stream flow speed. The pressure spectrum at the mid-section of the cone is shown in Fig. 15.11 . The coherence is expressed in a compact way by the wavenumber spectrum $\phi_3(k_\theta)$ in the circumferential direction. The following form is chosen for this spectrum at frequency ω

$$\phi_3(k_\theta) = \frac{L_3}{2}\left(1 + (k_\theta L_3)^2\right)^{-\frac{3}{2}} \qquad (15.18)$$

with

$$L_3 = 2\delta^*\left(1 + \left(\frac{2\omega\delta^*}{U_c}\right)^2\right)^{-\frac{1}{2}} .$$

15.4.1.2.3 Results

The calculation procedure of paragraph 15.4.1.1 was carried out with the division of the conical shell into seven sections of equal axial length. The acceleration-response spectra at the two extreme sections and at the middle section are shown in Fig. 15.12. Mass-law response is also indicated. These spectra are normalized with respect to the pressure spectrum at the midsection as also shown in Fig. 15.11. The acceleration levels in all frequency bands are seen to increase from the smaller to the larger end. From Fig. 15.11 the pressure spectrum increases monotonically with frequency in the frequency range indicated.

Since the pressure spectrum is assumed to scale on the local Strouhal number $f\,\delta^*/U_\infty$ and since the thickness δ^* increases from the smaller to the larger end of the cone, the pressure levels increase in any frequency band below the spectral maximum. This behavior tends to accentuate the difference in the acceleration levels on the different sections of the cone. The essential mechanism, however, still is the restricted extent of the vibration patterns of the cone modes.

An explanation of the peaks in acceleration spectra for the mid-section and the smaller end shown in Fig. 15.12 is of interest. Consider first the acceleration response of a cylindrical shell that is excited by a TBL pressure field. Below the cylinder ring frequency $c_\ell/2\pi a$ where a is the cylinder radius, a significant portion of vibration is contributed by the membrane-stress-controlled modes. We denote this type of vibration by MV. This MV contributions is maximum near the ring frequency and drops sharply at higher frequencies. This is because membrane stresses cease to be effective above the ring frequency.

For the cone response under consideration, the cone section near the larger end has a local ring frequency of about 1000 Hz. The power input from the TBL pressure field to the MV of this section is maximum at its ring frequency. Also, the MV is associated with relatively small values of the modal number n. Furthermore, the modes involving the MV extend over the entire surface of the cone. Thus, the maximum power input at 1000 Hz to the MV near the larger end of the cone is manifested as vibration on the entire cone surface. Let us recall that the pressure levels in all frequency bands are maximum near the large end of the cone. Hence, this power input forms a significant portion of the total power input

to the cone around 1000 Hz. Since the vibration level increases from the smaller to the larger end of the cone, the presence or absence of the power input to the MV near the larger end causes the greatest relative change in the vibration level at the smaller end and the minimum relative change in the level at the larger end. The sharpness of the peaks in acceleration spectra at 1000 Hz depends on the magnitude of the fractional change in the response. Fig. 5.13 presents the response estimates based on two alternate calculation procedures that involves assumptions that are relatively less realistic. For the acceleration spectrum marked A, the structural and the flow models are the same as those for the results of Fig. 5.12; however, the assumption of paragraph 15.4.1.1 (that each mode retains all the power fed into it by the TBL pressure field) is now replaced with the more naive assumption that the total power input to the structure in any frequency band is distributed uniformly over the structural surface, yielding a uniform acceleration level everywhere on the structure. A third procedure could be based on the assumption that the modes with resonance frequencies within a particular frequency band share the power (fed into them by the pressure field in the same frequency band) among each other in such a way that the time-averaged energy of each mode is the same. While this assumption is more realistic, it is not used here because it would entail complicated calculations. It is interesting to note that the above three assumptions yield identical estimates of vibration for a rectangular flat plate or for a cylinder shell, whereas they yield three distinct estimate for a conical shell.

Acceleration spectrum B in Fig. 15.13 pertains to the estimated response of a cylindrical shell that has the thickness and the material properties of the structural model and a radius which is the average of the radii of the two ends, $(a_1 + a_2)/2$. The TBL pressure field is taken to have the same properties everywhere on the cylinder as those assumed for the midsection of the structural model. This estimate B is the simplest to obtain and is seen to lie within the range of the acceleration spectra of Fig. 15.12. Therefore, the response of an equivalent cylinder seems to be useful in yielding an approximate first-order estimate for the response of a conical shell.

15.4.2 Empirical Prediction of Acceleration Levels

A commonly used empirical prediction scheme is that of Franken [41]. This approach is not really valid here, however, for two reasons. First, although vehicle diameter is included in the Franken prediction scheme, the diameter of the reentry vehicle is so very much smaller than the diameters of the vehicles on which Franken took his data that doubts must be raised about the validity of the extrapolation. Second, Franken's measurements were taken with acoustic rather than TBL excitation. The predicted relative acceleration levels based on Franken's scheme are shown in Fig. 15.14. In view of the above caveats, the agreement with the prediction of Fig. 15.13 is surprisingly reasonable at high frequencies.

15.4.3 Power Input to the Shell

In SEA vibration predictions it is sometimes more useful to consider the basic input parameter for the problem to be the power input to part of the system rather than the acceleration level of part of the system. The use of one or the other of these quantities is discussed in the next paragraphs.

The power input to the shell has been computer in the approach described in paragraph 15.4.1, although specific results are not given. It may arise, however, that acceleration levels are predicted directly, as in the Franken approach. The total power input to the shell can be found from the acceleration levels by using the relationship

$$\Pi_{in} = \omega \eta_1 \quad E_{1,tot} = \frac{\eta_1 M_1}{\omega} \quad \langle a_1^2 \rangle \qquad (15.19)$$

In this equation η_1 is the effective loss factor of the structure. The other parameter values are $M_1 = 15$ lbs/ft^2 and $\eta_1 = 0.025$. Values of the input power if required may thus be computed directly from the predicted values of the mean square acceleration $\langle a_1^2 \rangle$.

15.5 Vibration Levels of the Instrument Shelf

We are now in a position to use our SEA model of the reentry vehicle to predict the vibration levels on the instrument shelf. The various parameters required for the SEA model have been discussed above. We shall discuss below three ways of using these parameters to predict the vibration levels.

Our goal in the present problem is to predict vibration levels of the instrument shelf within the reentry vehicle when we are given information about the excitation field acting on the skin of the vehicle. Our approach is to predict first either the vibration levels of the skin itself or to predict the power input of the skin from the turbulent boundary layer. Implicit in both these predictions is the neglect of the interior structure of the vehicle on the skin vibration. This effect shows up in two ways: First, as an additional mass and stiffness which may alter the modal resonance frequencies, and second, as an additional path for the loss of energy. The latter effect can be viewed either as an increase in loss factor as far as the skin is concerned, or as a coupling loss factor as far as the relative vibration levels of the internal structure and the skin are concerned.

The power input in a frequency band to a multimodal structure depends on the total mass of the structure and (if we consider only resonant response) on the number of resonant modes in the band. We remember that modal densities are additive, and for shell-like structures at high frequencies tend to be proportional to the surface of the structure. The addition, say, of a stiffener to a shell thus does not greatly affect the modal density. It follows that the total power input to the structure also does not change very much.

On the other hand, the stiffener may be such that it provides energy flow path to other parts of the system. Thus, effective loss factor of the part being considered may increase. As the total energy of the system in a frequency band is inversely proportional to the loss factor (for constant input power) the vibration levels on the structure would decrease. Very often, the coupling between structures is weak. The coupling now has a negligible effect on the vibration of the directly excited structure; both power input and vibration levels remain approximately unchanged.

15.5.1 Prediction Based on Skin Acceleration Level

In this Section, we give SEA predictions on the instrument shelf vibration levels based on:

1. prediction of the acceleration levels of the skin;

2. prediction of the power input to the skin, and

3. direct use of the experimental data.

If we assume that the loss factor used by Manning is the effective loss factor of the vehicle skin and internal structure, then the values of the skin vibration levels predicted in the reference are the appropriate levels to use. In terms of these predictions the instrument shelf vibration level is given by

$$\langle a_2^2 \rangle = \frac{M_1}{M_2} \langle a_1^2 \rangle \frac{\eta_{12}}{\eta_2 + \eta_{21}} \qquad (15.20)$$

The subscripts 1 and 2 refer to the vehicle skin and shelf, respectively. The appropriate values of η_{12} and η_{21} can be used as discussed in paragraph 15.3. Of course, when equations such as (15.14) and (15.15) are used, the parameter η_1 now refers to the modal density of the conical shell (paragraph 15.2). Values of the acceleration level $\langle a_1^2 \rangle$ are obtained from Figs. 15.11 and 15.13. Typical results are discussed in paragraph 15.5.4.

15.5.2 Prediction Based on Input Power

The input power Π_{in} for a turbulent boundary layer can be found from Section I of this report and from Ref. 37. We then have

$$\Pi_{in} = \omega\eta_1 E_{1,tot} + \omega\eta_{12} E_{1,tot} - \omega\eta_{21} E_{2,tot} \qquad (15.21)$$

and

$$E_{2,tot} = E_{1,tot} \frac{\eta_{12}}{\eta_2 + \eta_{21}} . \qquad (15.22)$$

From these equations we find

$$E_{1,tot} = \frac{M_1}{\omega^2} \langle a_1^2 \rangle = \Pi_{in} (\omega \eta_1 + \frac{\omega \eta_2 \eta_{12}}{\eta_2 + \eta_{21}})^{-1} . \qquad (15.23)$$

Typical values of the parameters have been given.

A comparison of Eq. (15.23) and (15.19) shows the effect that the internal structure has on the skin vibration. We see immediately that if the coupling loss factors are small, Eqs. (15.23) and (15.19) give approximately the same result. When this is so, then the prediction of paragraphs 15.6.1 and 15.6.2 will be the same. We emphasize, however, that when the coupling is strong, Eqs. (15.23) and (15.22) should be used to predict the vibration levels.

As a final comment on the difference between the two approaches just outlined we note the following: If decay measurements are taken on the skin alone a value of η_1 is obtained. If the internal structure is then put in place and further decay measurements taken, an effective loss factor for the skin of

$$\eta_1 + \frac{\eta_2 \eta_{12}}{\eta_2 + \eta_{21}} \qquad (15.24)$$

is obtained. The correct approach thus clearly depends on the experimental configuration used.

15.5.3 Prediction from the Experimental Data

We have discussed methods of obtaining values of the

coupling loss factors from Manning's experimental data at some length, even though we noted that these values were not required explicitly as direct vibration predictions are possible. The Manning experiments were performed on a fixture as similar as possible to the actual vehicle. When estimating η_{21}, the coupling loss factor from shelf to skin, we have seen that the skin can be treated approximately as an infinite structure. As discussed in earlier parts of this report, the use of the infinite structure approximation is a common one in obtaining some SEA parameters. It follows that (to this approximation) the value of η_{21} is the same for the test fixture as for the actual vehicle. On the other hand, values of η_{12} will be different since the modal density of the test fixture and the actual vehicle are different.

If we suppose that the skin acceleration levels on the actual vehicle have been predicted, we can then make an estimate of the shelf vibration levels. Two equations such as (15.22) can be written, one describing the test fixture, and one describing the actual vehicle. Values of η_2 and η_{21} are the same for each equation. It follows by simple substitution that

$$\frac{E_{2,tot}}{E_{1,tot}} = \frac{n_1}{n_2} \frac{\tilde{E}_{2,tot}}{\tilde{E}_{1,tot}} ,$$

where the variables with a tilde refer to the test fixture, and those with no tilde to the actual vehicle. The equation can be written

$$\frac{\langle a_2^2 \rangle}{\langle a_1^2 \rangle} = \frac{\tilde{n}_1 M_1}{n_1 M_1} \frac{\langle \tilde{a}_2^2 \rangle}{\langle \tilde{a}_1^2 \rangle} \qquad (15.25)$$

Thus values of the shelf acceleration $\langle a_2^2 \rangle$ relative to the predicted vehicle skin acceleration level $\langle a_1^2 \rangle$ can be found directly in terms of the transmissibility ratio $\langle \tilde{a}_2^2 \rangle / \langle \tilde{a}_1^2 \rangle$ found in the experiment. The parameters n_1 and M_1

and $\tilde{n}_3$ and $\tilde{M}_3$ are the modal density and total mass of the skin in the vehicle, and in the test fixture, respectively. Typical values are discussed below.

15.5.4 Results

Some predictions for the mean square acceleration level on the instrument shelf in the vehicle are presented in this section. We note first that as the coupling loss factors are small, predictions based on paragraphs 15.5.1 and 15.5.2 will be the same. A number of different predictions are possible since in some cases a number of different values have been predicted for each parameter. Some representative predictions are shown in Fig. 15.15.

Curve A of Fig. 15.15 is obtained from purely theoretical considerations. Values of the coupling loss factors used for the low and high frequency models are summarized in paragraph 15.3.3.5. We have used the equivalent cylinder prediction of the skin acceleration level with $\eta_1 = 0.025$ as shown in Fig. 15.13. The estimated values of η_2 are shown in Fig. 15.9. This curve would be obtained by the prediction schemes of both paragraphs 15.5.1 and 15.5.2 above.

Curve B of Fig. 15.15 shows the prediction obtained directly from the data by the method described in paragraph 15.5.3.

15.5.5 Other Vibration Parameters

Fig. 15.15 shows predictions of the acceleration levels of the upper instrument shelf of the vehicle. Other vibration parameters can be obtained directly by the methods of Chapter 7.

15.6 Confidence Limits

The predictions discussed so far are mean values of the vibration parameters, the mean being obtained from an ensemble of similar systems. As discussed in earlier parts of this report, it is of interest to obtain measures of the deviation

of a realized response from the mean. This can be done in terms of the standard deviation from the mean square response.

The four major effects producing a variance in response have been discussed in paragraph 4.2 of Part I. We emphasize that all four effects are features of the SEA model we have chosen, and not the actual system under study. Thus, in the present problem the confidence estimates give no indication of how accurately our SEA model describes the vibration of the actual vehicle. What the confidence limits do tell us is the range of vibration of the response we might expect to measure if a physical replica of our SEA model were constructed. However, if data taken on the actual vehicle falls within the predicted high confidence (say 80%) limits, this is an indication that our SEA modeling is, at least, adequate.

We shall restrict attention here to "bracketting" confidence limits for broad band excitation. We have predicted above the mean square acceleration levels in third octave bands of the upper instrument shelf, $\langle a_2^2 \rangle$. We first estimate the variance in this response. Eq. (4.2.13) of Part I gives the ratio of variance to mean square response as

$$\frac{\sigma_2^2}{\langle a_2^2 \rangle} = [n_1 n_2 \frac{\pi}{2} (\omega\eta_1 + \omega\eta_2)\Delta\omega]^{-1} \left(\frac{\langle \psi_1^4 \rangle^2}{\langle \psi_1^2 \rangle^2}\right) \left(\frac{\langle \psi_2^4 \rangle}{\langle \psi_2^3 \rangle^2}\right)^2 .$$

The spatial response factors corresponding to our low and high frequency models are as follows:

$$\frac{\langle \psi_1^4 \rangle}{\langle \psi_1^2 \rangle^2} = 9/4 \qquad \text{all } f_o$$

$$\frac{\langle \psi_2^4 \rangle}{\langle \psi_2^2 \rangle^2} = \begin{cases} 3/2 & f_o \leq 1000 \text{ Hz} \\ 9/4 & f_o \geq 2000 \text{ Hz} \end{cases}$$

The appropriate values of $N_1 + N_2$ have been discussed above (for example $n_2\Delta\omega=1$ for frequencies less than 1000 Hz). Values of the variance are shown in Fig. 15.16.

Confidence limits based on the variance can be obtained from Fig. 4.9 of Part I. The 80% limits for the theoretical prediction given in Fig. 15.15 are shown in Fig. 15.17. The limits tend to bracket the measured values except in the highest frequency band.

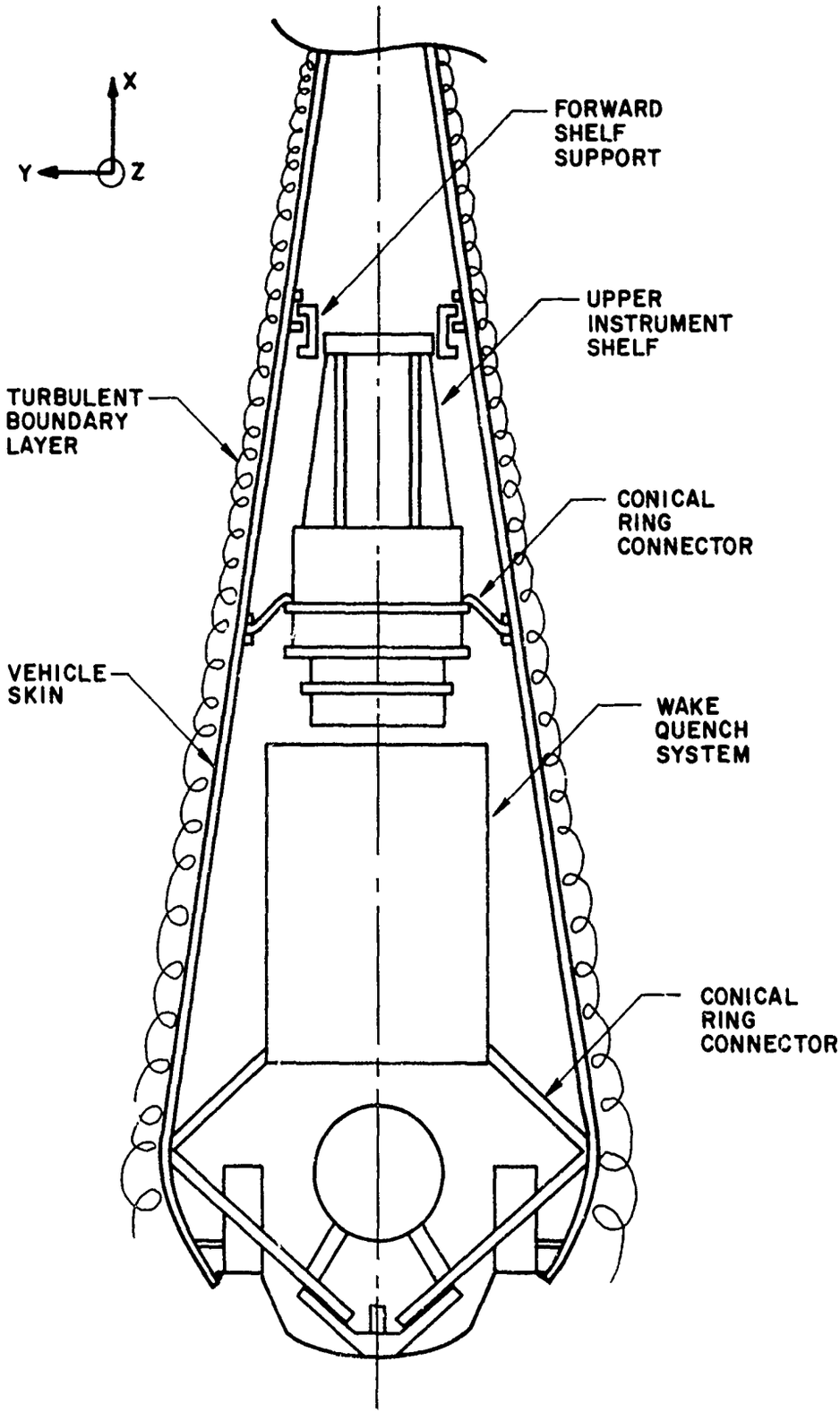

FIG. 15.1

REENTRY VEHICLE

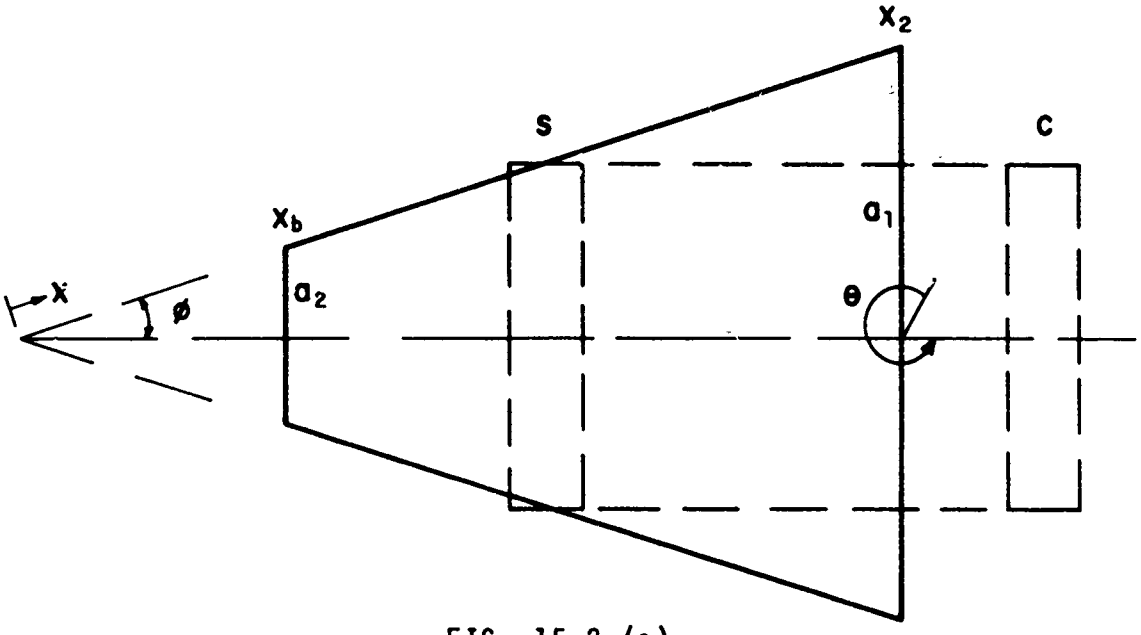

FIG. 15.2 (a)

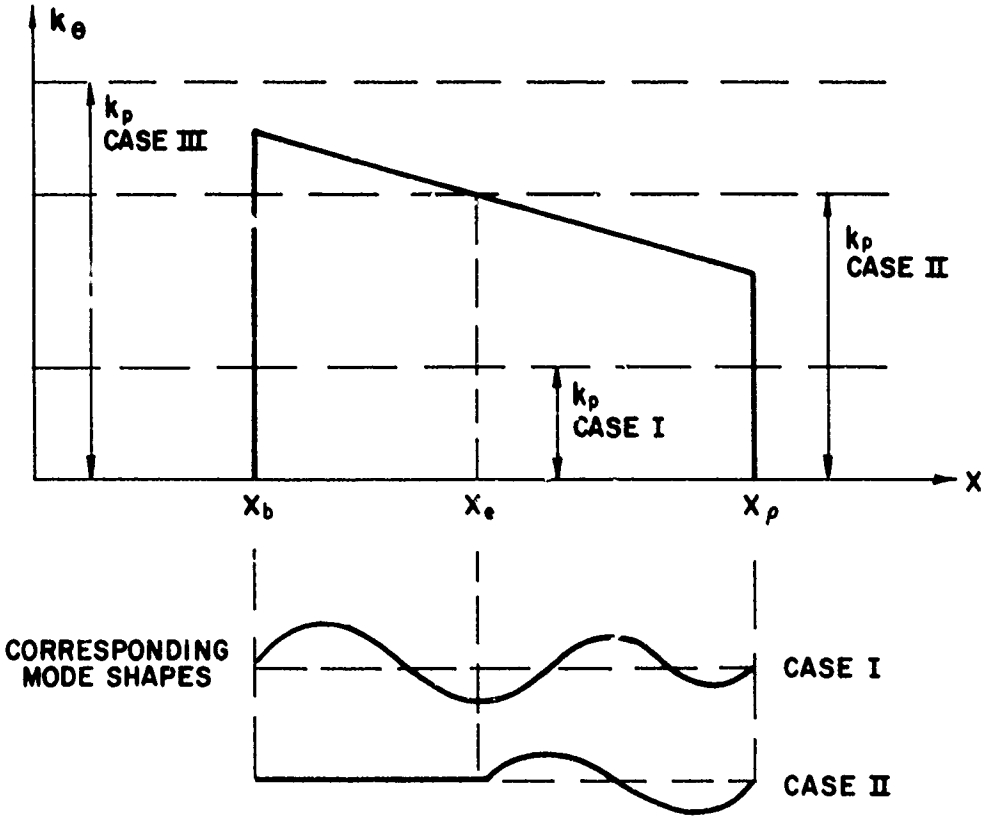

FIG. 15.2 (b)

A TRUNCATED CONICAL SHELL SHOWING (a) GEOMETRY WITH EQUIVALENT CYLINDER SECTION AND (b) WAVENUMBERS AND MODE SHAPES FOR VARIOUS CASES

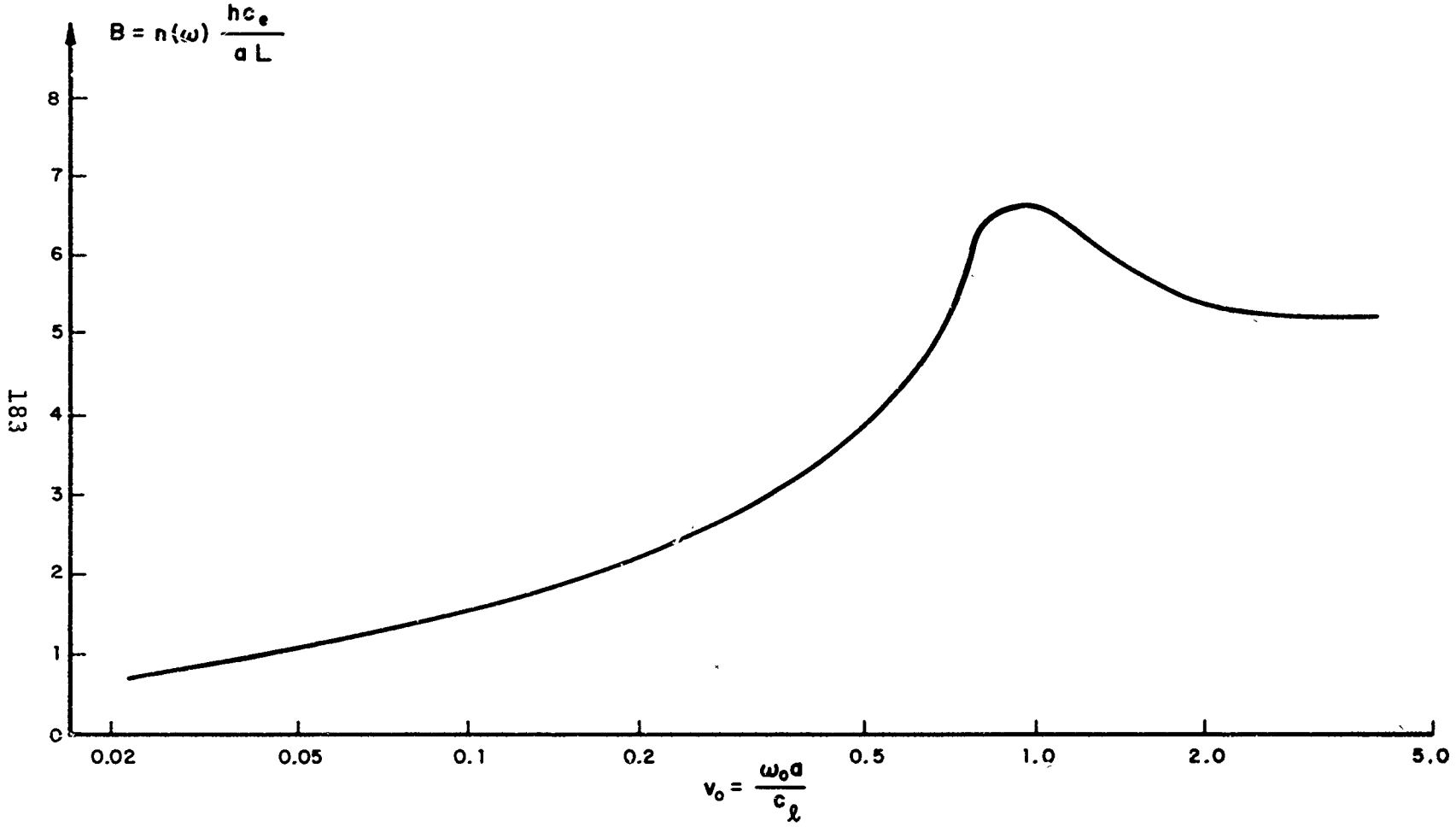

FIG. 15.3

MODAL DENSITY OF CIRCULAR CYLINDER

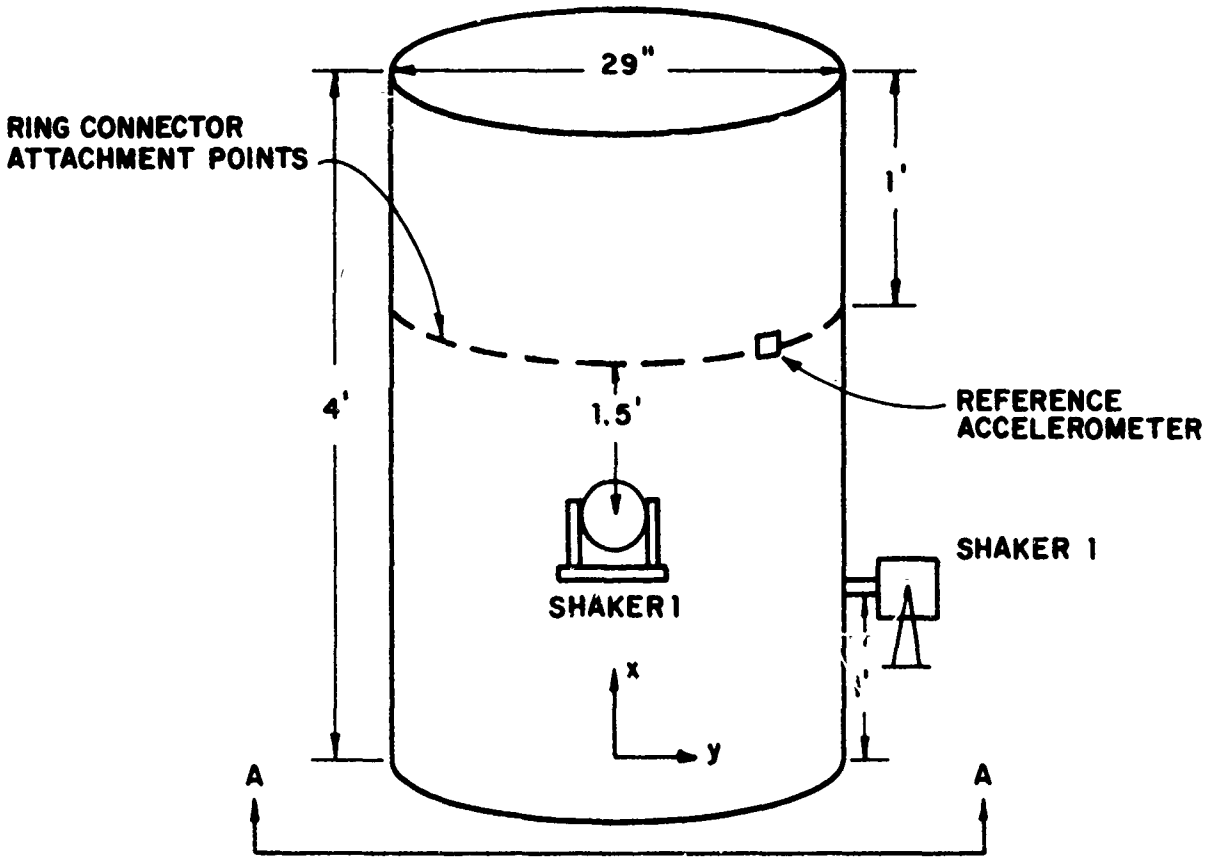

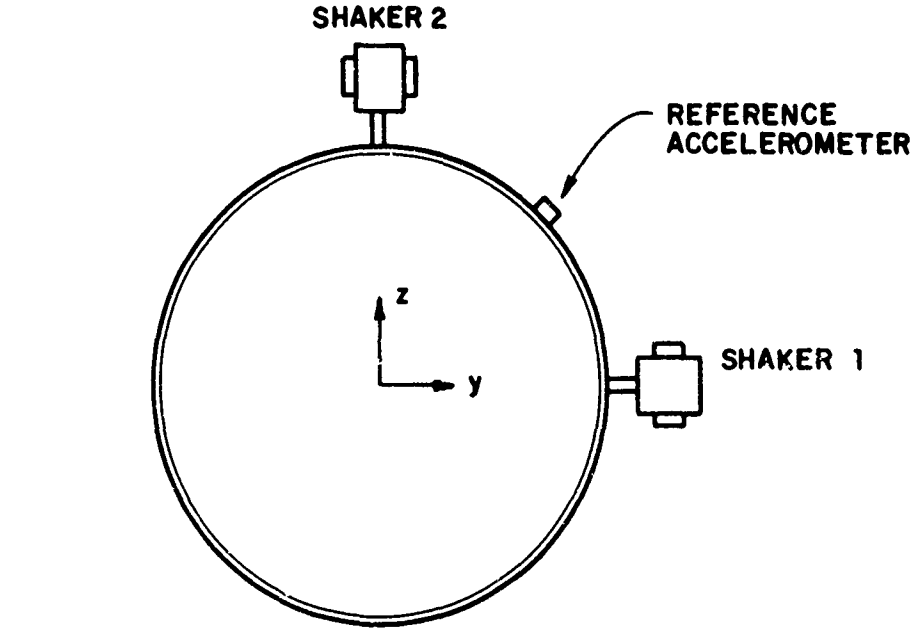

SECTION AA

FIG. 15.4

CYLINDRICAL SHELL TEST FIXTURE

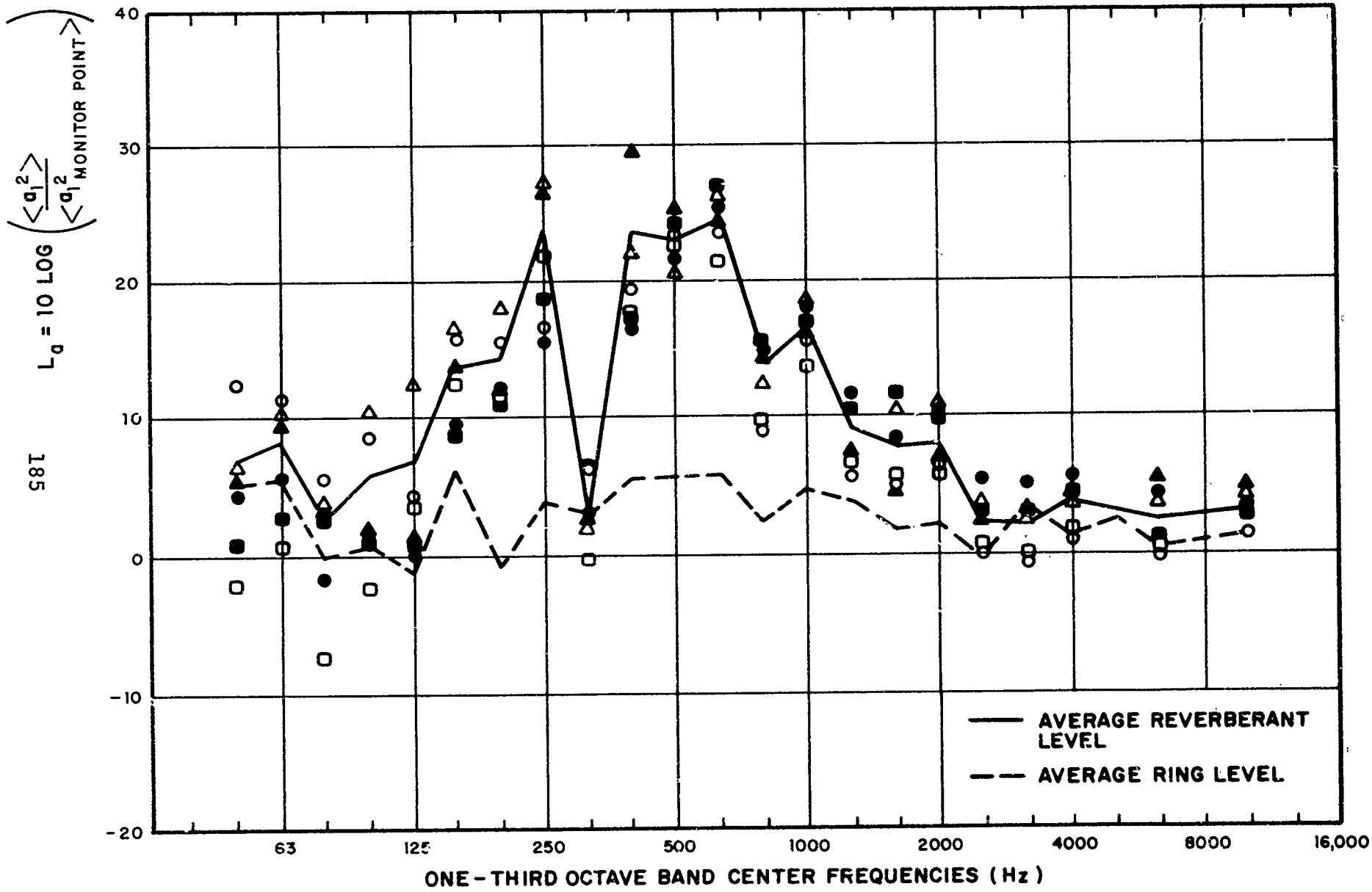

FIG. 15.5

VARIATION OF VIBRATION LEVEL IN REVERBERANT FIELD OF FIXTURE

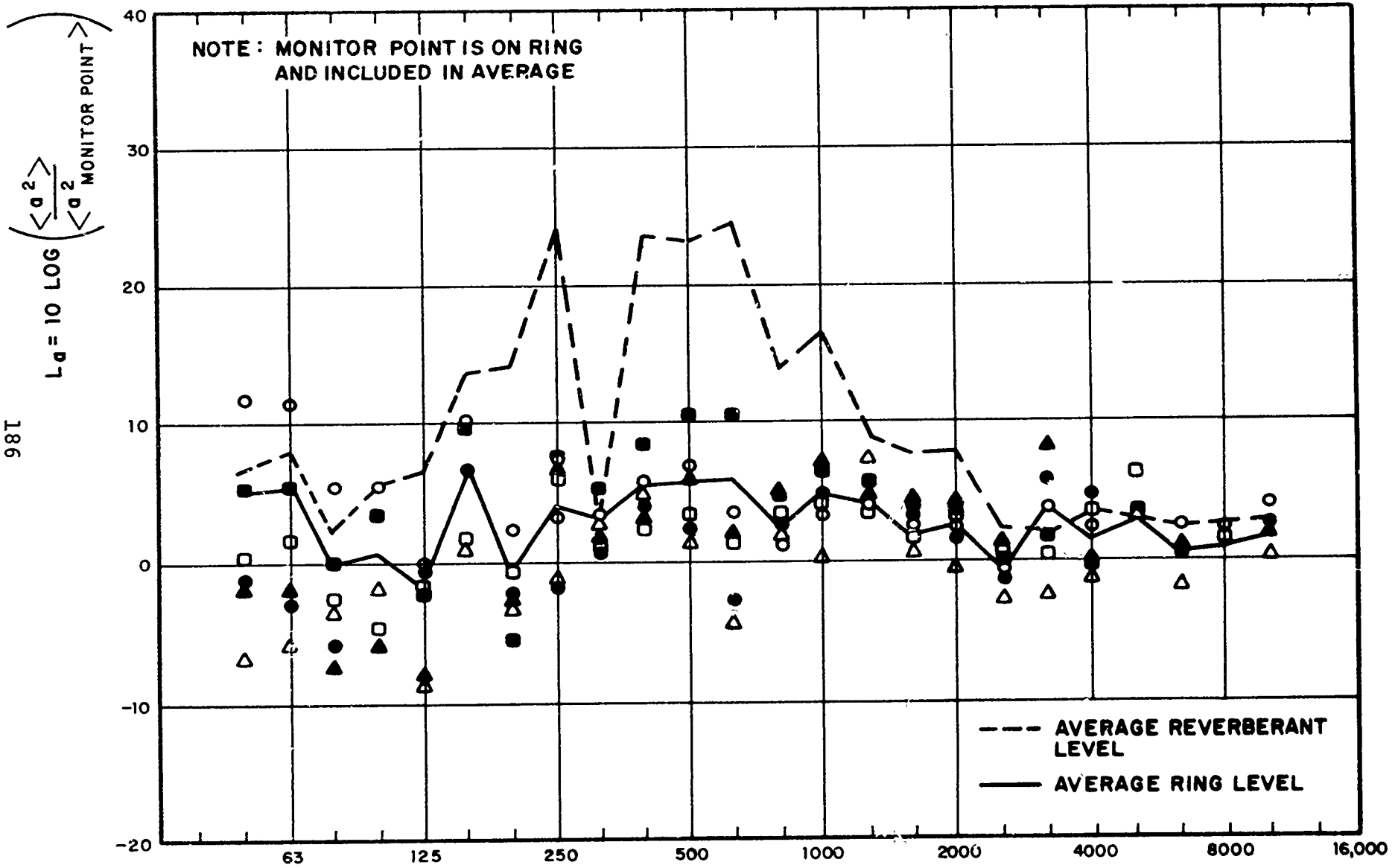

FIG. 15.6

VARIATION OF VIBRATION LEVEL ON RING CONNECTOR

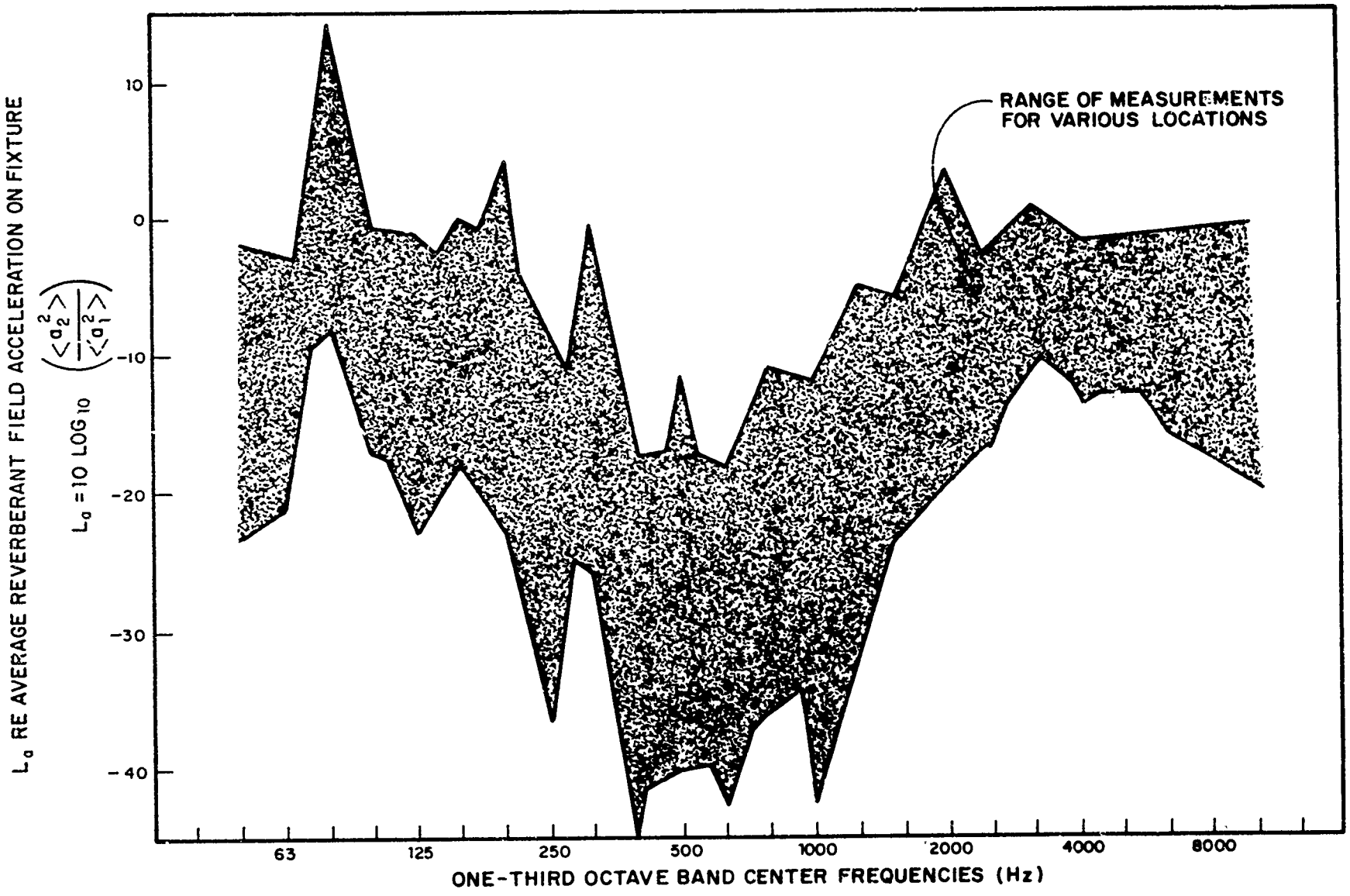

FIG. 15.7 TRANSMISSIBILTY FROM THE TEST FIXTURE TO THE INSTRUMENT SHELF

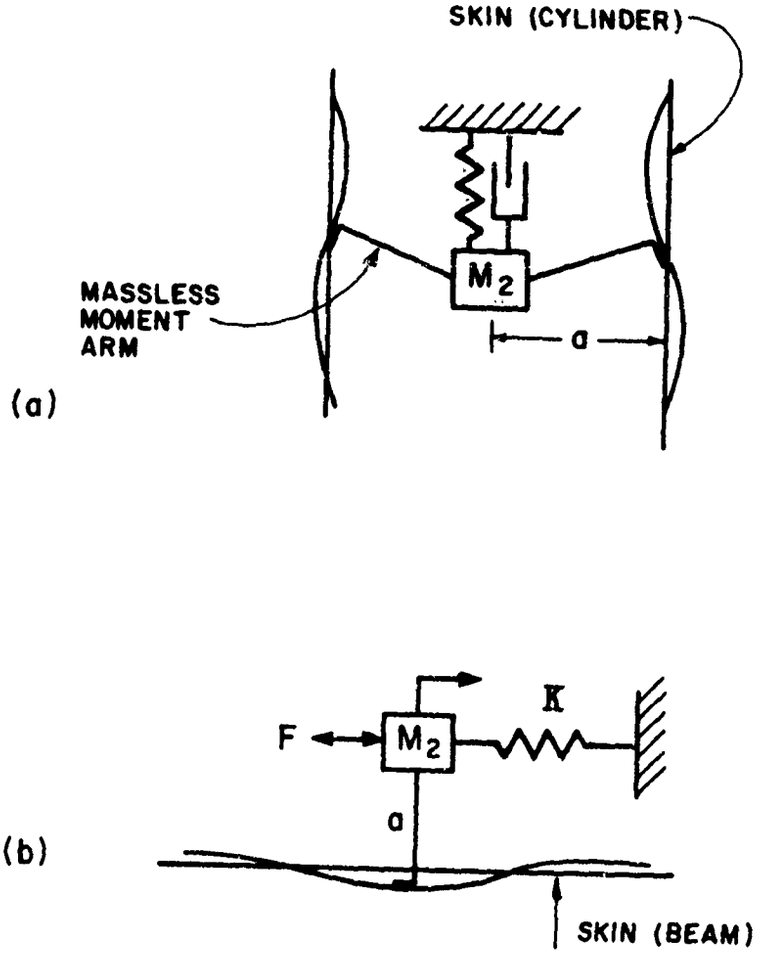

FIG. 15.8

LUMPED PARAMETER MODEL OF SHELF

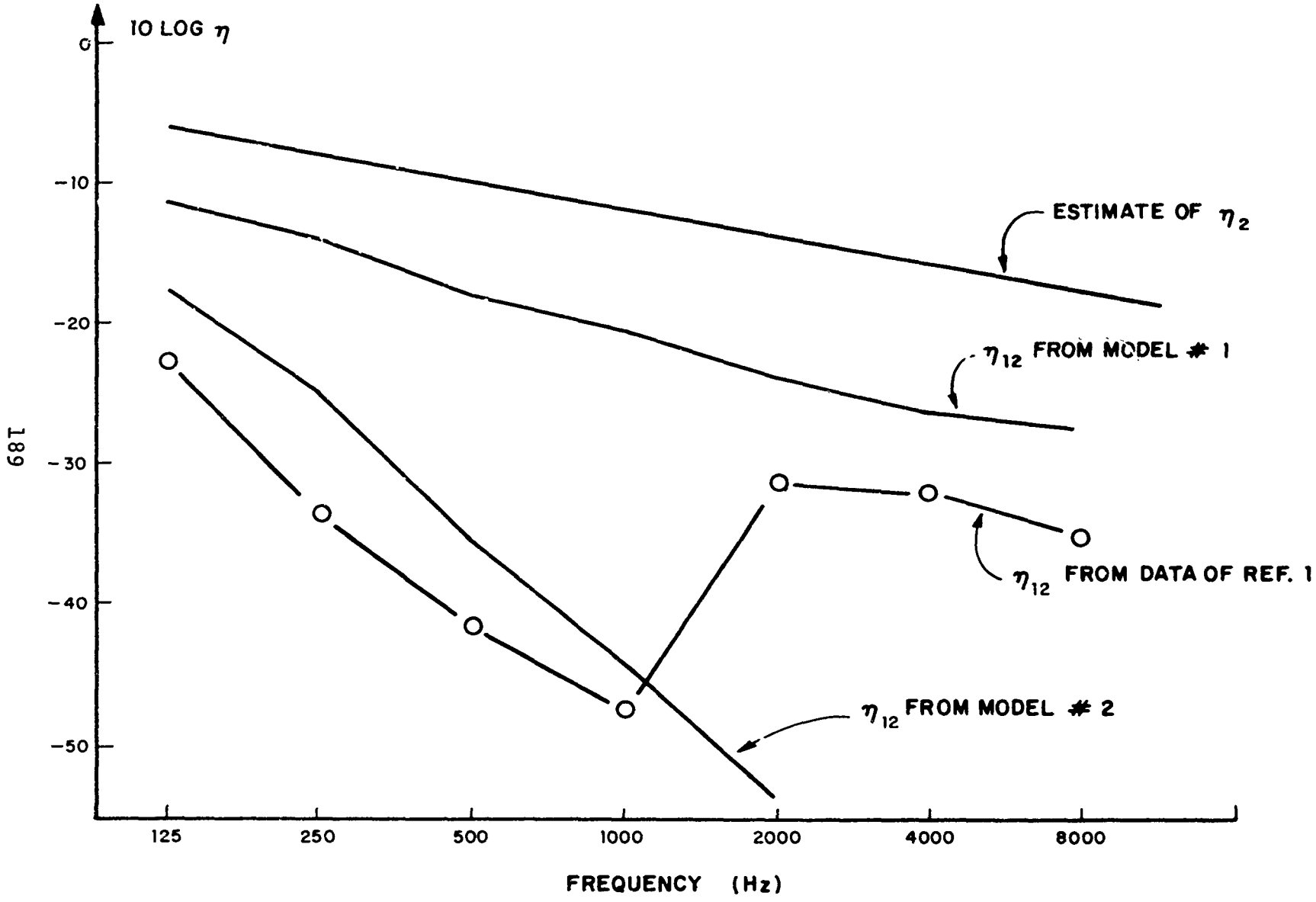

FIG. 15.9

COMPARISON OF PREDICTIONS OF η_{12}

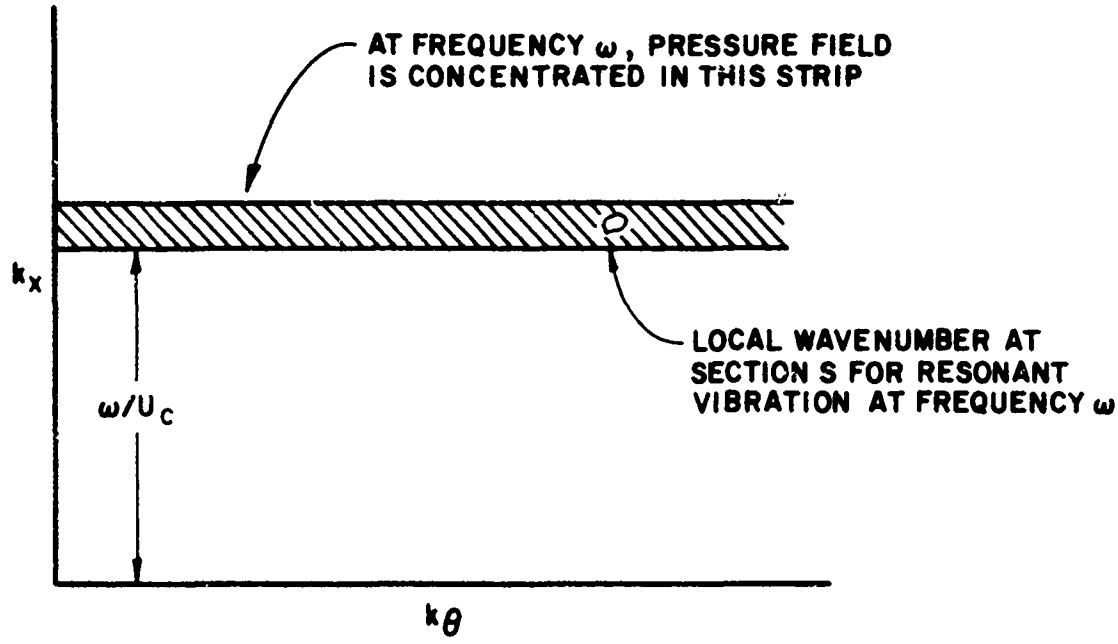

(a) (k_x, k_θ) PLANE

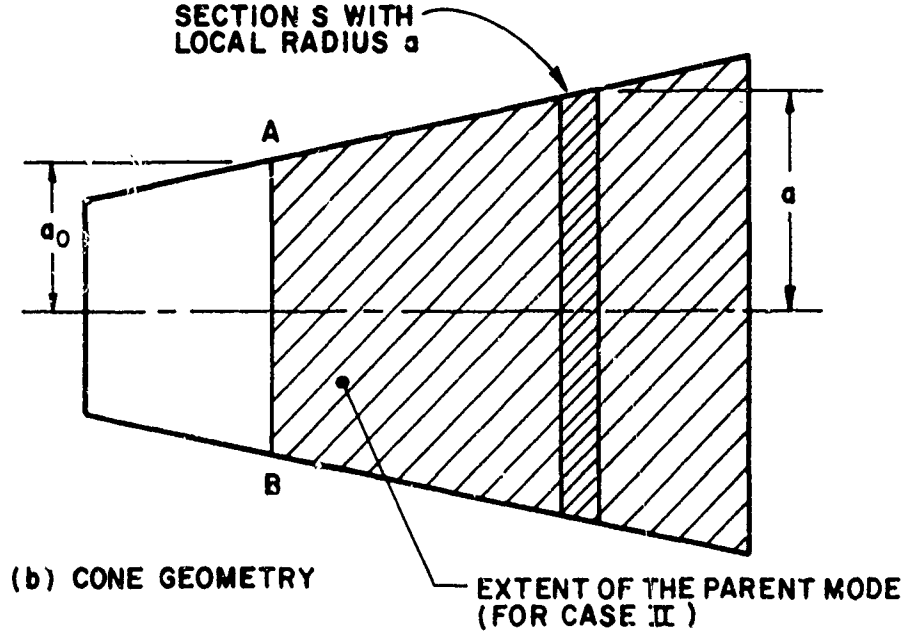

(b) CONE GEOMETRY

FIG. 15.10

REPRESENTATION IN THE WAVENUMBER PLANE OF THE TBL PRESSURE FIELD

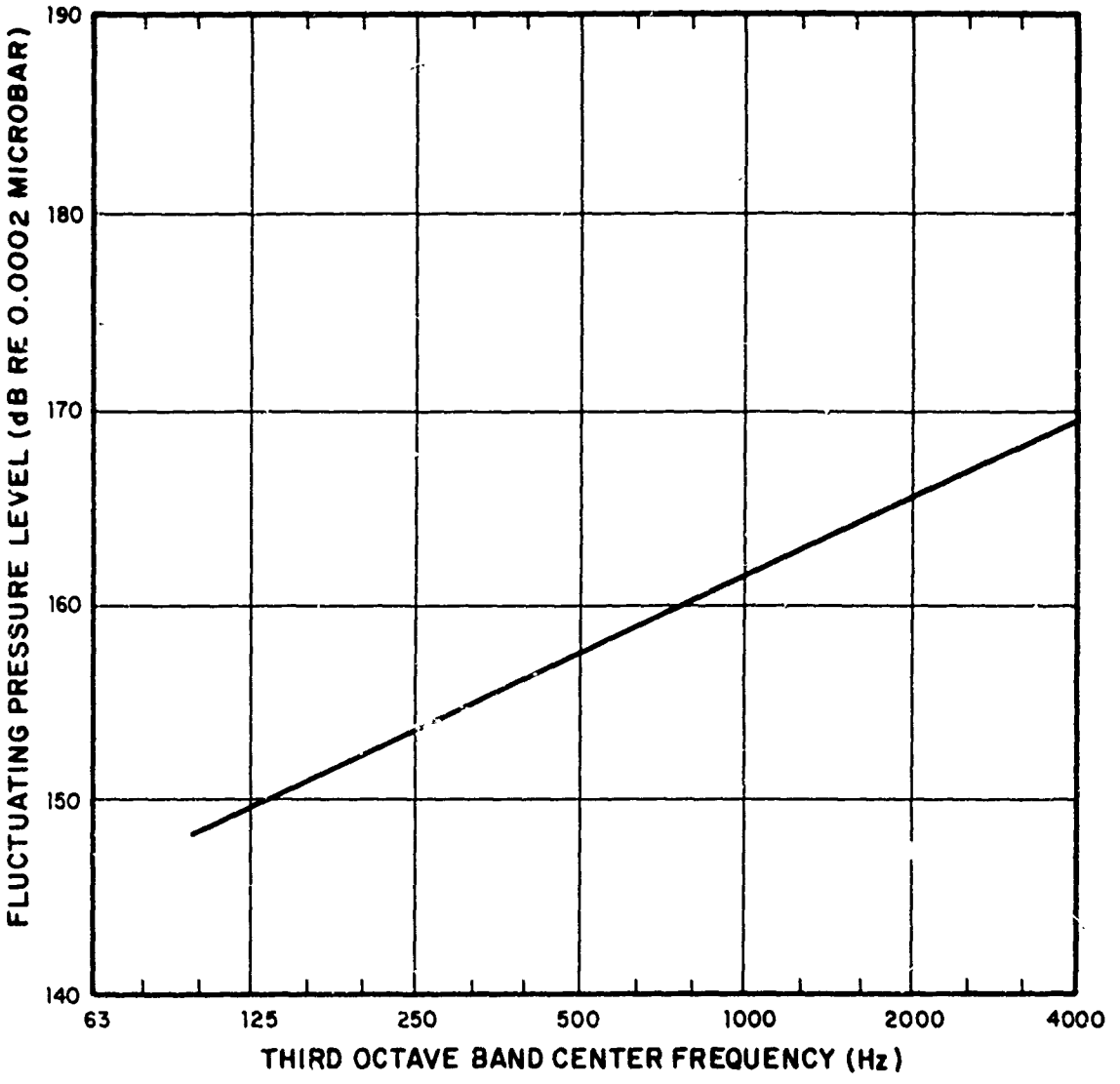

FIG. 15.11

ESTIMATED TBL PRESSURE SPECTRUM AT THE MID-SECTION OF THE CONICAL SHELL

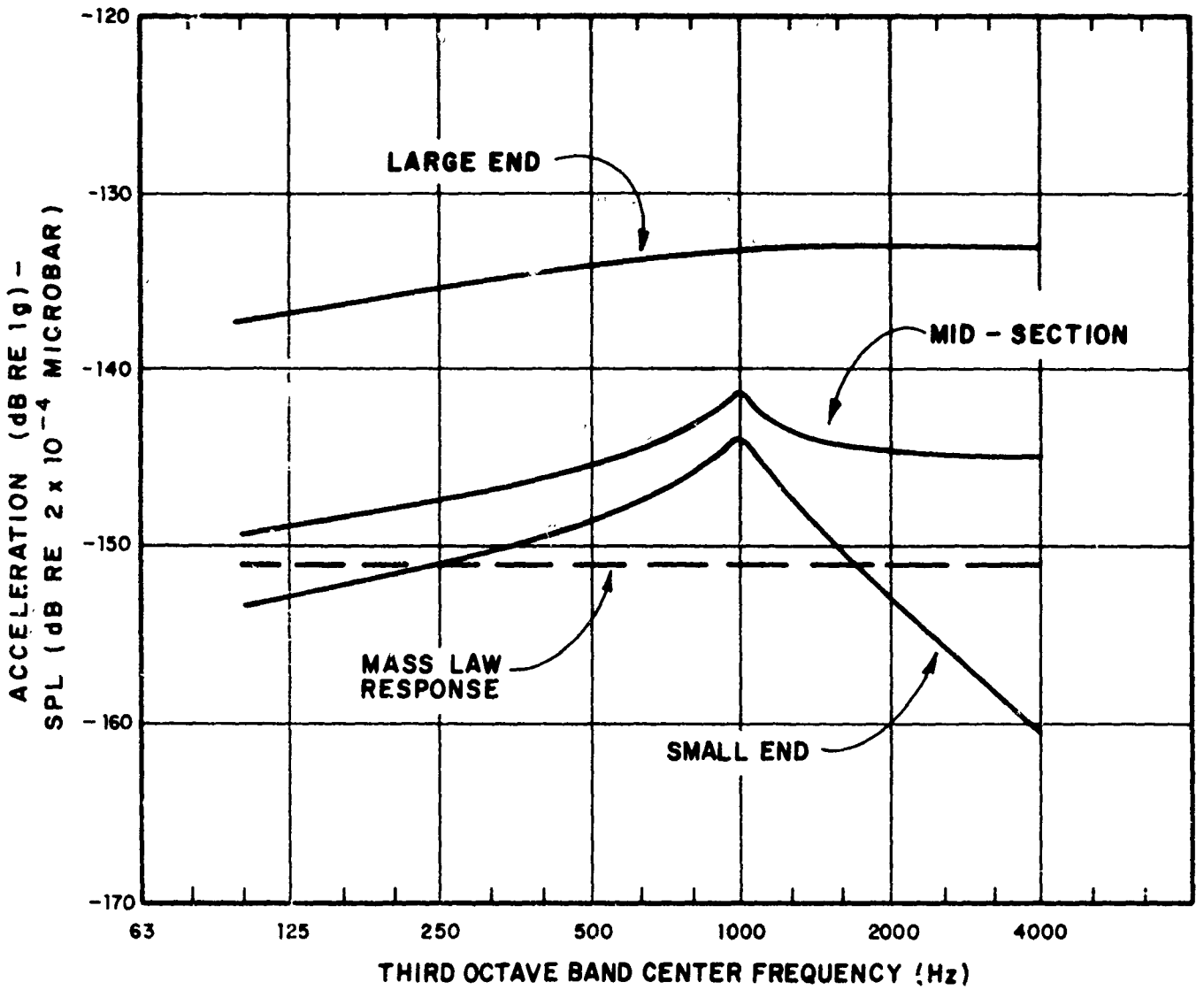

FIG. 15.12

ESTIMATED RESPONSE OF THE
CONICAL SHELL TO TBL PRESSURE FIELD

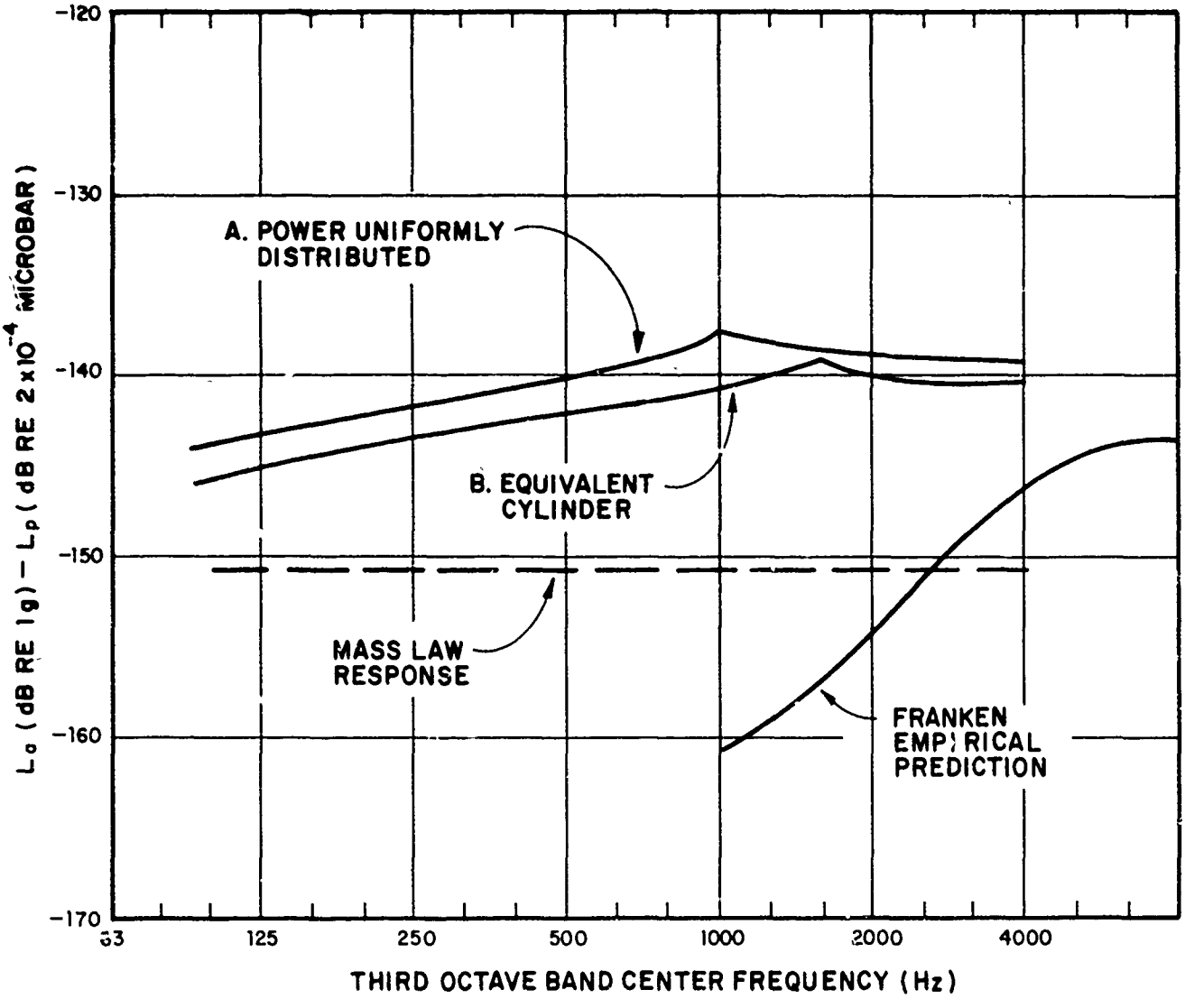

FIG. 15.13

ALTERNATE ESTIMATES OF RESPONSE OF THE CONICAL SHELL, THE TBL PRESSURE FIELD

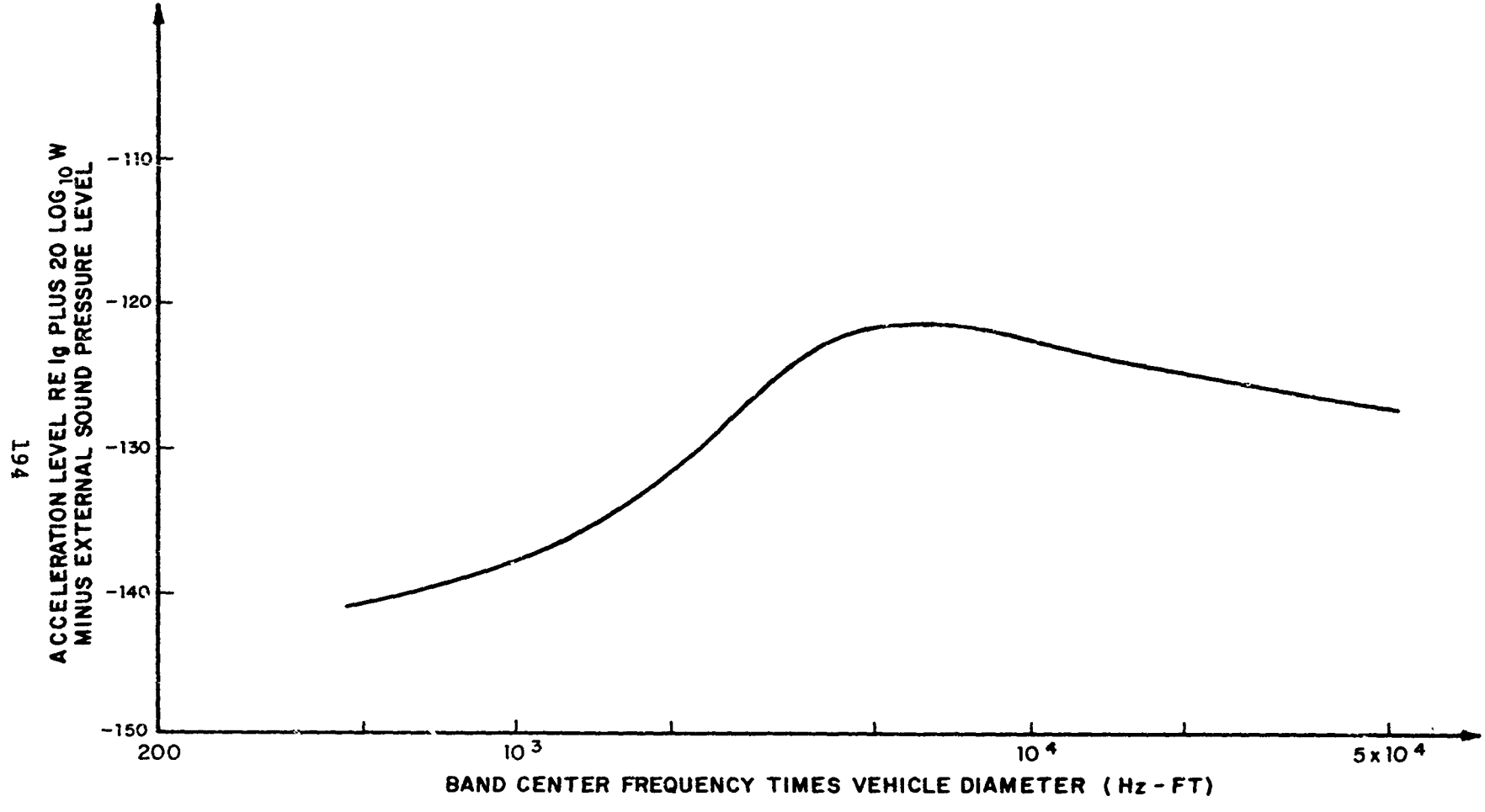

FIG. 15.14

FRANKEN PREDICTION SCHEME

(FROM REF. 47)

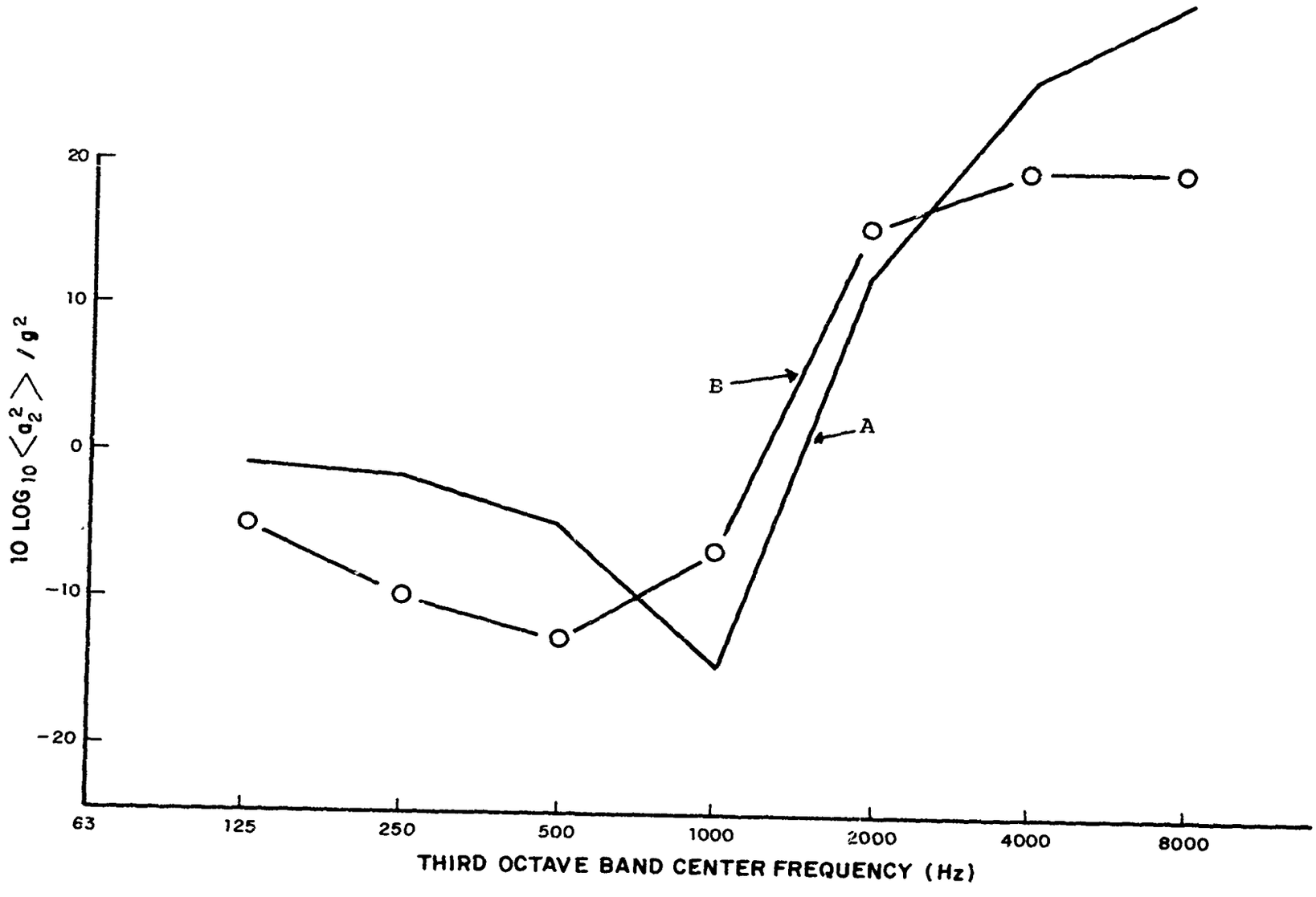

FIG. 15.15

PREDICTION OF VEHICLE SHELF VIBRATION LEVEL

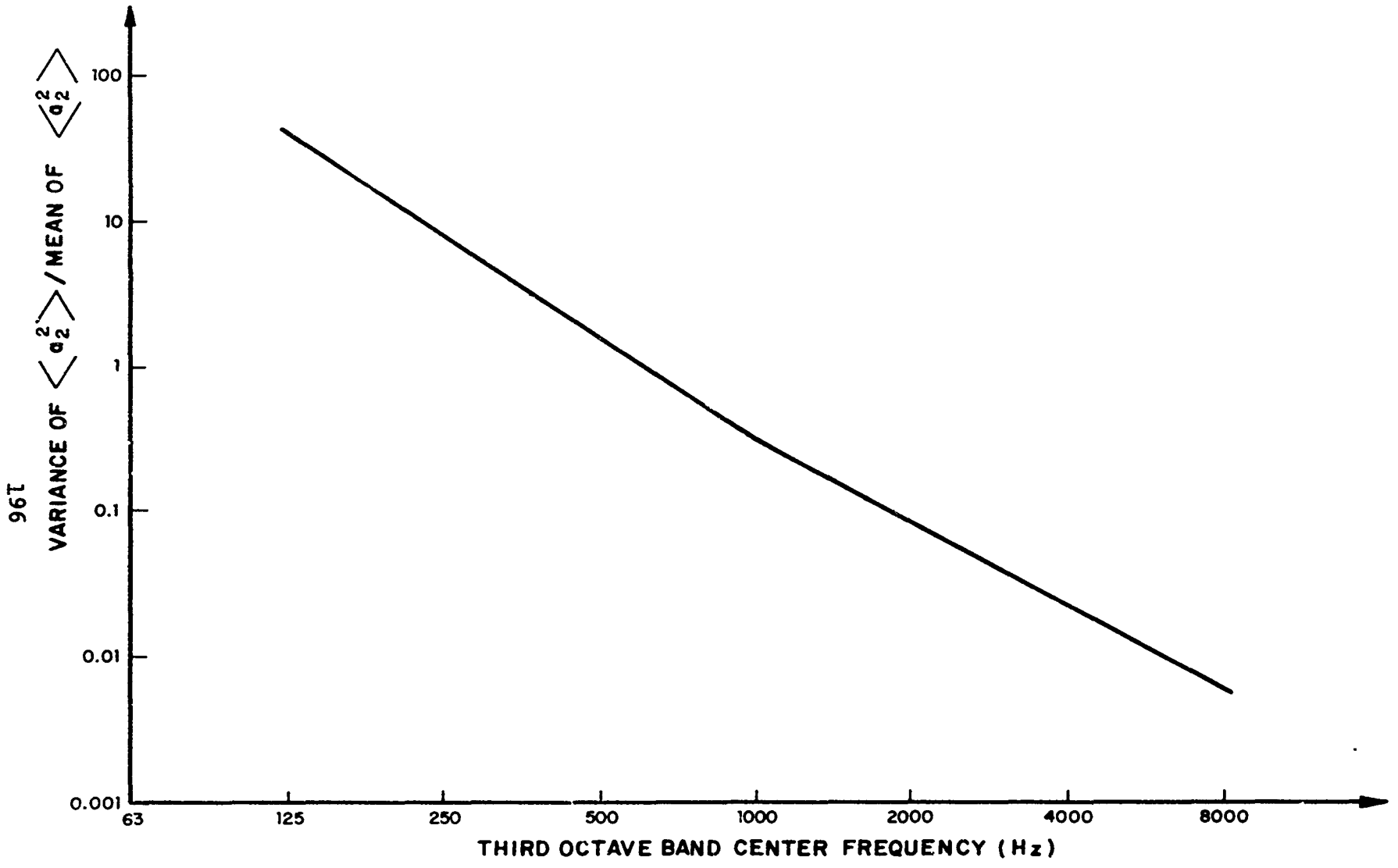

FIG. 15.16

VARIANCE OF $\langle a_2^2 \rangle$

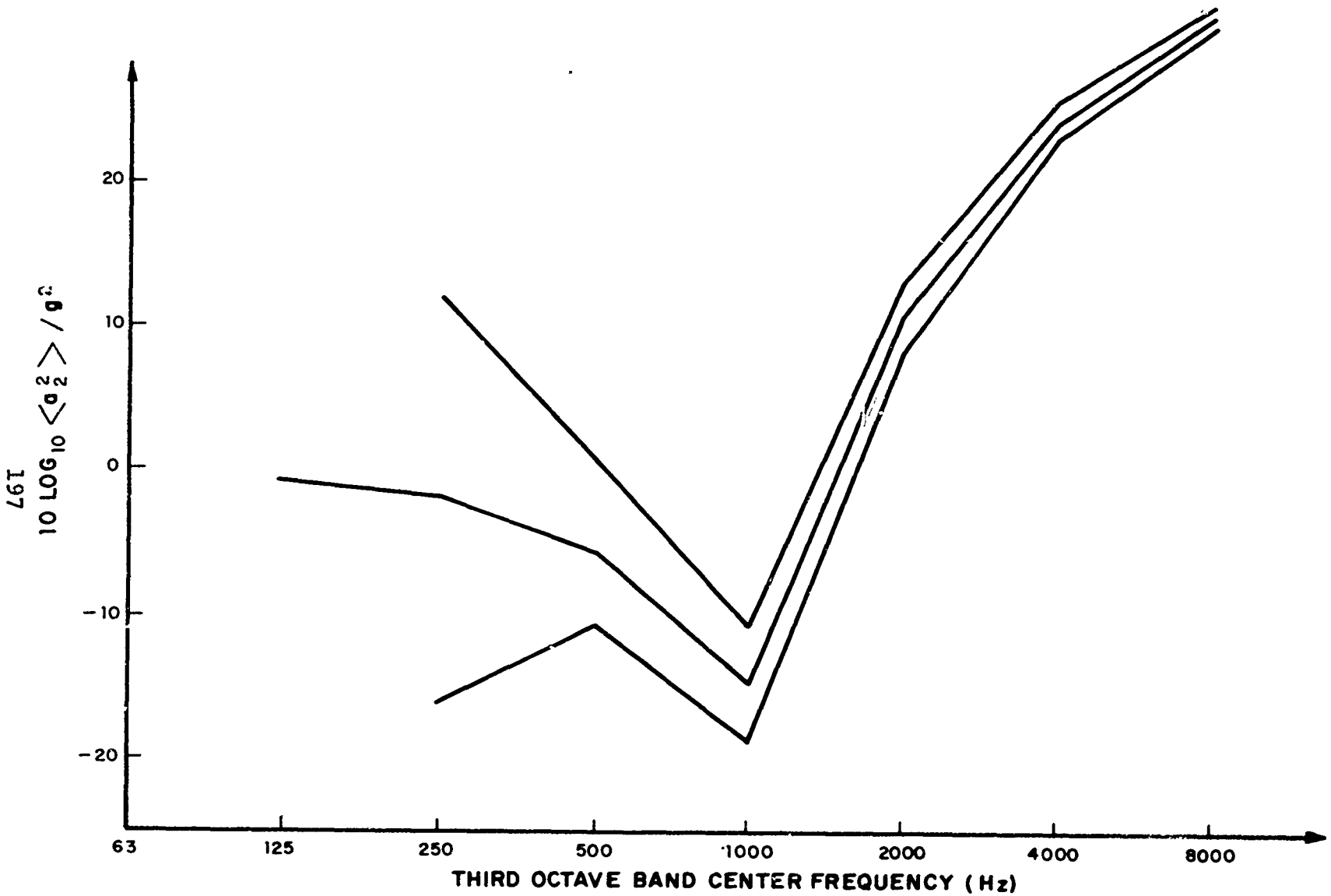

FIG. 15.17

80% CONFIDENCE LIMITS FOR MEAN OF $\langle a_2^2 \rangle$

REFERENCES

1. E. E. Ungar, et al., "A Guide for Predicting the Vibrations of Fighter Aircraft in the Preliminary Design Stage", Tech. Report AFFDL-TR-71-63, April 1973.

2. P. T. Mahaffey and K. W. Smith, "A Method for Predicting Environmental Vibration Levels in Jet-Powered Vehicles" Shock and Vibration Bulletin, No. 28, Pt. 4, pp 1-14 (1960).

3. P. A. Franken, "Sound-Induced Vibrations of Cylindrical Vehicles," J. Acoust. Soc. Am., 34, 453-454 (1962).

4. R. W. White, D. J. Bozich and K. McK. Eldred, "Empirical Correlation of Excitation Environment and Structural Parameters with Flight Vehicle Vibration Response," AFFDL-TR-64-160, Dec. 1964.

5. E. A. Guillemin, Introductory Circuit Theory, Ch. 5, John Wiley and Sons, New York, 1953.

6. R. Lyon, "What Good is Statistical Energy Analysis, Anyway?" Shock and Vibration Digest, Vol. 2, No. 6, pp. 1-9 (June, 1970).

7. J. E. Manning, "A Theoretical and Experimental Model-Study of the Sound-Induced Vibration Transmitted to a Shroud-Enclosed Spacecraft". BBN Report 1891, submitted May 1, 1970 to NASA. Work Performed Under Contract NAS5-10302, and submitted to: NASA Goddard Space Flight Center, Greenbelt, Maryland.

8. P. Kopff, "Note A Mr. Absi" - L.V.B. (Centre Experimental de recherches et d'etudes du batiment et des travaux publics) - September, 1972.

9. E. E. Ungar and K. S. Lee, "Considerations in the Design of Supports for Panels in Fatigue Tests," Tech. Rept. AFFDL-TR-67-86, September 1967.

10. R. H. Lyon, "Statistical Analysis of Power Injection and Response in Structures and Rooms" J. Acoust. Soc. Am., Vol. 45, No. 3, pp. 545-565 (1969).

11. R. H. Lyon and E. E. Eichler, "Random Vibrations of Connected Structures," J. Acoust. Soc. Am. 36, pp. 1344-1354 (1964).

12. F. V. Hunt, "Stress and Strain Limits on the Attainable Velocity in Mechanical Vibration", J. Acoust. Soc. Am., Vol. 32, No. 9, pp 1123-1128 (1960).

13. E. E. Ungar, "Maximum Stresses in Beams and Plates Vibrating at Resonance", J. Eng. Ind. Vol. 84, No. 1 pp 149-155 (February 1962).

14. R. J. Roark, Formulas for Stress and Strain, McGraw-Hill Book Co. (1954).

15. R. H. Lyon, "Boundary Layer Noise Response Simulation with a Sound Field", Chapter 10 of Acoustical Fatigue in Aerospace Structures, Ed. by W. J. Trapp and D. M. Forney (Syracuse University Press, Syracuse, New York, 1965).

16. Schroeder, M. R. "The Statistical Parameters of the Frequency Response Curves of Large Rooms" Acustica 4, Beiheft 2, 594, 1954.

17. Lazan, B. J., "Damping of Materials and Members in Structural Mechanics" Pergamon Press Ltd., Oxford, London, 1968.

18. Snowdon, J. C. "Vibration and Shock in Damped Mechanical Systems" John Wiley & Sons, Inc., New York (1968).

19. Mead, D. J., "The Damping Stiffness and Fatigue Properties of Joints and Configurations Representative of Aircraft Structures", in WADC-Univ. of Minn. Conference on Acoustic Fatigue, edited by W. J. Trapp and D. M. Forney, Jr. [WADC TR 59-676 (March 1961)].

20. Maidanik, G. "Energy Dissipation Assoc. with Gas-Pumping in Structural Joints, J. Acoust. Soc. Am., Nov. 1966, Vol. 40, p. 1064.

21. Ungar, E. E., "A Guide to Designing Highly Damped Structures .... Using Layers of Viscoelastic Material" Machine Design, February 14, 1963, p. 162-168.

22. Szechenyi, E. "Modal Densities and Radiation Efficiencies of Unstiffened Cylinders Using Statistical Methods", J. Sound Vib. 19, No. 7, pp. 65-81 (1971).

23. Wilkinson, J. P. D., "Modal Densities of Certain Shallow Structural Elements", J. Acoust. Soc. Am. 43, No. 2 pp. 245-251 (February 1968).

24. Erdelyi, A., et al., Higher Transcendental Functions, Vol. 2 (McGraw-Hill Book Co., Inc., New York, 1953) p. 313 (March 1971).

25. Pierce, A. D. "Physical Interpretation of the WKB or Eckonal Approximation for Waves and Vibrations in Inhomogeneous Beams and Plates", J. Acoust. Soc. Am. 48, No. 1 (Pt. 2) pp. 275-284 (July 1970).

26. Gemogenova, O. A., "Formalism of Geometrical Optics for Flexural Waves" J. Acoust. Soc. Am. 49, No. 3 (Pt. 2) pp 776-780.

27. Berendt, Raymond D.; Winzer, George E.; Burroughs, Courtney B., "A Guide to Airborne, Impact and Structure-Borne Noise-Control in Multi-Family Dwellings" U. S. Department of Housing and Urban Development, Washington, D. C., September, 1967.

28. Crocker, M. J. and Battarcharya, M. C. and Price, A. J., "Sound and Vibration Transmission through Panels and Tie-Beams Using Statistical Energy Analysis" Jour. of Eng. Ind., Trans. ASME Vol. 93, Series B No. 3, August 1971.

29. Beranek, L. L., Noise and Vibration Control, (McGraw-Hill Book Co., New York 1971) p. 283.

30. This result from a report by J. E. Manning is similar in form to a result by L. Cremer, Akustische Zeitschrift, Vol. 7, p. 81 (1942).

31. Maidanik, G.,"Response of Ribbed Panels to Reverberant Acoustic Fields", J. Acoust. Soc. Am. 34 (6) p. 809, (1962).

32. Fahy, F. J. "Vibration of Containing Structures by Sound in the Contained Fluid" J. Sound Vib. (1969) 10 (3) pp 490-512.

33. Fahy, F. J. "Response of a Cylinder to Random Sound to Contained Fluid", J. Sound Vib., (1970) 13 (2) pp 171-194.

34. Lyon, R. H. and Eichler, E., "Random Vibration of Connected Structures", J. Acoust. Soc. Am., Vol. 36, No. 7, pp 1344-1354, July 1964.

35. Heckl, M. "Wave Propagation in Beam-Plate Systems" J. Acoust. Soc. Am., Vol. 33, No. 5, p. 640-651.

36. Ungar, Eric E.; Koronaios, Nicholas; and Manning, J. E., "Application of Statistical Energy Analysis to Vibrations of Multi-Panel Structures", AFFDL-TR-67-79, August 1967.

37. Cremer, L.; Heckl, M.; and Ungar, E., Structure-Borne Sound, (Stringer, New York, 1973) p. 281.

38. See reference number 1.

39. See reference number 7. Also, see page 37, reference 43.

40. Heckl, M. A., "Compendium of Impedance Formulas", BBN Report #774 (1961). Work performed under NONR 2322 (00); see also Chapter 4 of reference 37.

41. Franken, P. A., "Sound-Induced Vibrations of Cylindrical Vehicles," J. Acoust. Soc. Am. 34, p. 453 (1962).

42. Chandiramani, K. L., et al., "Structural Response to Inflight Acoustic and Aerondynamic Environments", BBN Report #1417, (1966). NAS 8-20026, NASA George C. Marshall Space Flight Center, Huntsville, Alabama.

43. R. H. Lyon, Random Noise and Vibration in Space Vehicles. Shock and Vibration Information Center, U. S. Dept. of Defense, SVM-1 (1967).